MOLECULAR CHARACTERIZATION AND THERAPY OF ACYL-COA DEHYDROGENASE DEFICIENCIES

by

Olivia Marie D'Annibale

BS Biology, Penn State Behrend, 2016

Master of Public Health, University of Pittsburgh, 2018

Submitted to the Graduate Faculty of the

Graduate School of Public Health in partial fulfillment

of the requirements for the degree of

Doctor of Philosophy

University of Pittsburgh

2022

UNIVERSITY OF PITTSBURGH

GRADUATE SCHOOL OF PUBLIC HEALTH

This dissertation was presented

by

Olivia Marie D'Annibale

It was defended on

February 23, 2022

and approved by

Eric S. Goetzman, Ph.D., Associate Professor, Pediatrics, School of Medicine, University of Pittsburgh

Al-Walid Mohsen, Ph.D., Research Professor of Pediatrics, School of Medicine, School of Public Health, University of Pittsburgh

Ryan Minster, Ph.D., Associate Professor, Human Genetics, School of Public Health, University of Pittsburgh

Zsolt Urban, Ph.D., Associate Professor, Human Genetics, School of Public Health, University of Pittsburgh

Dissertation Director: Jerry Vockley, M.D., Ph.D., Professor of Pediatrics, School of Medicine, Professor, School of Public Health, University of Pittsburgh

MOLECULAR CHARACTERIZATION AND THERAPY OF ACYL-COA DEHYDROGENASE DEFICIENCIES

Olivia Marie D'Annibale, PhD

University of Pittsburgh, 2022

Acyl-CoA dehydrogenase (ACAD) deficiencies are autosomal recessive inborn errors of metabolism together affecting 1/50,000 babies born in the United States. Isovaleric academia (IVA) is caused by genetic defects in isovaleryl-CoA dehydrogenase (IVDH) catalyzing the third step in the leucine (Leu) degradation pathway resulting from mutations in the isovaleryl-CoA dehydrogenase (*IVD*). Very long-chain acyl-CoA dehydrogenase (VLCAD) catalyzes the initial step of β-oxidation of fatty acids with carbon length chain of 14 to 22 and its deficiency results from biallelic mutations in *ACADVL*. Both deficiencies are detected through tandem mass spectrometry as part of newborn screening (NBS) and confirmed via DNA sequencing of *IVD* or *ACADVL*. However, the identification of variants of unknown significance (VUS) leads to uncertainty in patient diagnosis and treatment. Therapy for both disorders is dietary based, but most patients still experience episodes of metabolic decompensation triggered by physiological stress with significant morbidity and mortality.

Using CRISPR/Cas9 technology, I generated *IVD* and *ACADVL* null HEK293T cell lines to examine VUS pathogenicity. Cell lines contained no IVDH or VLCAD protein or enzyme activity, respectively. Expression plasmids containing VUSs were synthesized and transfected null cells assayed with a high through-put system with results comparing favorably to those obtained with patient fibroblasts.

I examined peroxisome proliferator activated delta receptor (PPARδ) activators as a treatment for VLCADD, predicted to improve the expression of *ACADVL*. Functional studies in patient cells indeed demonstrated an improvement in bioenergetics in some cell lines, confirming a potential for therapy, but indicating the need for a personalized medicine approach based on patient genotype.

NBS has been designated as one of the top public health successes of the 20th century, and has continued to expand in the past two decades to include more than 50 disorders. However, techniques to confirm the diagnosis in screen positive babies has lagged. VUS pathogenicity confirmation provides a major public health benefit to the newborn screening community. In addition, targeting therapeutics to specific genetic disease variants will maximize public health outcomes of NBS. The technologies utilized here are generalizable to many IEMs and will improve the testing and treatment of affected babies identified by NBS.

Table of Contents

List of Tables

List of Figures

Preface

First and foremost, I would like to thank my mentor, Dr. Jerry Vockley, for his endless support and encouragement in guiding me through my graduate career. I am grateful for his knowledge, willingness to teach, and great sense of humor. He has taught me so much about how to approach a problem, acquire funding, and passion for science. I am grateful for the Vockley school of public speaking, and the amount of time he has taken to not only work on my writing, but presentation skills. I could not have asked for a better mentor and am so grateful for his constant wisdom and jokes.

It truly takes a village to raise a PhD student. The members of the Vockley laboratory and the entire Genetic and Genomic Medicine division on the fifth floor of Rangos Research Center, have been an incredibly support system through the years. I could not have asked for a better group of scientists to spend my formative PhD years with. I am especially grateful to Dr. Lina Ghaloul-Gonzalez and Dr. Dwi Utami Kemaladewi for their incredible mentorship and support. I want to thank Dr. Yu Leng Phua for his constant advice, wisdom, and positive outlook. Thank you to Dr. Erik Koppes for his constant insight into the world of PCR and encouragement. My deepest gratitude to Dr. Yuxun Zhang for his ETF supply and jokes along with Dr. Bharathi Sivakama, Dr. Shakuntala Basu, Dr. Kaitlyn Bloom, Paige Heiman, and Anuradha Karunanidhi for their constant support, laughter, and help in the lab.

I also want to thank my thesis committee members: Dr. Eric Goetzman, Dr. Ryan Minster, Dr. Al-Walid Mohsen, and Dr. Zsolt Urban. Their thoughtful comments, insight, and mentorship have been invaluable and helped in the progress of my dissertation project. I would also like to thank the Graduate School of Public Health and the Department of Human Genetics for providing

an opportunity to pursue not only my masters of public health genomics, but a PhD. I am grateful to Dr. Andrea Durst and Dr. Beth Roman for their guidance and academic advisement over the years. I am especially grateful to Dr. Candace Kammerer, for being my academic advisor, masters essay advisor, mentor and friend the past six years.

There are not enough words to describe how grateful and thankful I am for the support and love of my parents, Mark and Kathy D'Annibale. I would not be the person I am without them and their willingness to help, answer phone calls, and drive down to Pittsburgh for just a two-hour visit. I am forever grateful for their constant encouragement for my love of science, starting from the second grade science fair. My brother, Jarrod D'Annibale, who is a constant support and can always make me laugh. I am grateful for my grandparents, John and Diane D'Annibale and Carl and Anna Rogala, who have been so encouraging and for my grandfather who constantly calls my cell cultures "pets." My family members who are too many to list here, but have been supportive and encouraging at every family function. I am especially thankful for Lexi Schmidt who has not only made going into lab everyday enjoyable, but is truly my person and soul sister. All of my friends I have met in Pittsburgh and along the way, I am forever grateful for the phone calls, text messages, snapchats, and memes sent to me to keep my spirits high. I am constantly amazed by the support system around me and has been invaluable in my graduate career.

1.0 INTRODUCTION

1.1 BRANCHED CHAIN AMINO ACID CATABOLISM

Branched chain amino acids (BCAA) have an aliphatic side-chain with a branch (a central carbon atom bound to three or more carbon atoms), and include leucine, isoleucine, and valine (Leu, Ilu, and Val, respectively) [1, 2]. BCAAs can be synthesized in plants but not in mammals, making them dependent on dietary sources. When dietary BCAAs are in excess, or are released from protein stores in the body, they are catabolized through a partially shared pathway. The first two reaction steps are common to Leu, Ile, and Val: branched-chain-amino-acid aminotransferase (BKAT) and branched-chain α-keto acid dehydrogenase (BCKDH) (Fig. 1) [3]. BKAT catalyzes the reversible transfer of the BCAA amino group to α-ketoglutarate to form glutamate and the corresponding branched-chain keto acids (BCKAs): α-ketoisocaproate (KIC, ketoleucine), α-keto-β-methylvalerate (KMV, ketoisoleucine), and α-ketoisovalerate (KIV, ketovaline) [3]. Glutamate then acts as an amino group source to form alanine from pyruvate or as a substrate for ammonia detoxification to glutamine [3]. Glutamine, alanine, and most of the BCKAs are released from the muscle into the blood [3].

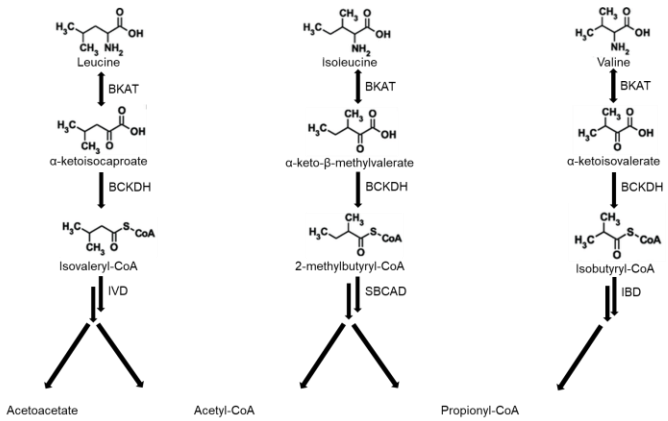

Figure 1. The proximal portion of the BCAA catabolic pathways.

The initial steps in Leu, Ile, and Val are catabolized through two shared enzymes: BKAT and BCKDH. Separate enzymes are subsequently utilized for the next catabolic step. End products are acetoacetate, acetyl-CoA, and propionyl-CoA.

BCKDH is the second enzyme in the BCAA catabolism pathway and is a multienzyme complex located on the inner surface of the mitochondrial membrane [3]. BCKDH catalyzes the irreversible decarboxylation of the BCKA to the corresponding branched-chain acyl-CoA esters [2-ketoisocaproic (KIC), 2-keto-3methylvaleric (KMV), and 2-ketoisovaleric acids (KIV) from Leu, Ile, and Val respectively] [3]. It is regulated through a phosphorylation-dephosphorylation mechanism, with phosphorylation leading to inactivation of the enzyme [3]. Following the BCKDH reaction, the pathways for each BCAA diverge, catalyzed by a unique acyl-CoA dehydrogenases (ACAD). Isovaleryl-, short branched chain-, and isobutyryl-CoAs (IVD, SBCAD, and IBD) for Leu, Ile, and Val, respectively. The ACAD enzymatic products are further catabolized through three separate pathways to end products of acetyl-CoA and acetoacetate (Leu), propionyl-CoA (Val), and acetyl-CoA plus propionyl-CoA (Ile) [3]. Overall, approximately 90% of the propionyl-CoA generated from amino acids originates from Ile [4].

1.2 MITOCHONDRIAL FATTY ACID OXIDATION

Mitochondrial fatty acid oxidation (FAO) catabolizes fatty acid molecules, typically to generate energy during times of fasting or physiologic stress [5]. A fatty acid is a carboxylic acid with a aliphatic chain that can be saturated or unsaturated [1]. Most fatty acids contain an even number of carbon atoms in their alpha-backbone, and are identified based on the number of carbons. For example, palmitate is a straight chain, saturated fatty acid containing 16 alpha-backbone carbons (often referred informally as "C16").

Long chain fatty acids enter cells via protein fatty acid transporters on the cell surface concurrent with or followed by addition of a CoA group by a fatty acyl-CoA synthase (FACS) to generate an acyl-CoA [5, 6]. Medium chain fatty acids are similarly activated to acyl-CoAs in the cytoplasm and appear to enter mitochondria directly without the use of carrier proteins [5, 6]. However, long chain acyl-CoAs are imported into the mitochondria through a three-step process known as the carnitine cycle. Carnitine palmitoyl transferase 1 (CPT1) conjugates the long-chain acyl group to carnitine generating an acylcarnitine, which is transported by the carnitine-acylcarnitine translocase (CACT) across the inner mitochondrial membrane in exchange for free carnitine [5, 6]. The acyl group is released into the mitochondrial matrix as acyl-CoA by carnitine palmitoyl transferase 2 (CPT2). The acyl-CoA then enters the fatty acid β-oxidation cycle, a series of four enzymatic steps that results in the production of the two carbon acetyl-CoA, one NADH, and one $FADH_2$, regenerating an acyl-CoA that is two carbons shorter [5-7]. Very long chain acyl-CoA dehydrogenase (VLCAD), another ACAD, catalyzes dehydrogenation of long-chain acyl-CoA substrates with a 12-22 carbon backbone to their enoyl-CoA product with reduction of the electron transfer flavoprotein (ETF) [5, 6, 8]. Reduced ETF is reoxidized by its redox partner, the electron transfer flavoprotein dehydrogenase (ETFDH), which then utilizes oxidized coenzyme

Q10 to finally transfer the reducing equivalents to the electron transport chain (ETC) complex III [5, 6, 8].

All of the activities of long chain fatty acid oxidation occur in a macromolecular enzyme complex that interacts with the ETC to optimize catalytic efficiency. Long-chain enoyl-CoAs from VLCAD are channeled in turn to the enoyl-CoA reductase subunit of the mitochondrial trifunctional protein (TFP), the long-chain 3-hydroxyacyl-CoA dehydrogenase (LCHAD), and the long chain ketoacyl-CoA thiolase [5, 6, 8]. TFP contains two subunits: alpha and beta. The alpha subunit contains the ECH and LCHAD activity and the beta subunit has the thiolase activity. The enoyl CoA hydratase oxidizes the double bond between the alpha and beta carbons generated by the ACAD reaction resulting in addition of a hydroxyl group to the beta carbon and a proton to the alpha carbon [6, 7]. The LCHAD subunit of TFP utilizes NAD^+ as an electron acceptor and directly interacts with the mitochondrial matrix NADH-binding domain of complex I. The reducing equivalents from NADH are transported through the membrane electron channel of complex I to complex III, oxidizing co-enzyme Q to generate QH_2 in the Q-binding domain of complex III [5, 6, 8]. ETFDH physically interacts with ETC complex III, facilitating transfer of its electrons to Coenzyme Q [5, 6, 8]. Following release by long chain ketoacyl-CoA thiolase, acetyl-CoA can enter the tricarboxylic acid (TCA) cycle or serve as substrate for ketone body (acetoacetate/3-hydroxybutyrate) synthesis [5, 6]. The thiolase reaction also generates a two carbon shorter acyl-CoA that can then undergo another round of fatty acid oxidation [6, 7]. The ETC creates a proton gradient across the IMM, which is used by complex V to make ATP, thus completing the steps of oxidative phosphorylation (OXPHOS) [5, 6]. Medium and short chain acyl-CoAs utilize chain length isozymes for fatty acid oxidation, including medium- and short-chain acyl CoA dehydrogenases, (MCAD, and SCAD), respectively [7] [6, 8]. A third matrix ACAD, long-chain

acyl-CoA dehydrogenase (LCAD) can also utilize long, straight chain substrates, but uniquely utilizes branched chain substrates that originate from the catabolism of complex lipids. LCHAD oxidizes the beta carbon to produce a molecule of NADH [6, 7].

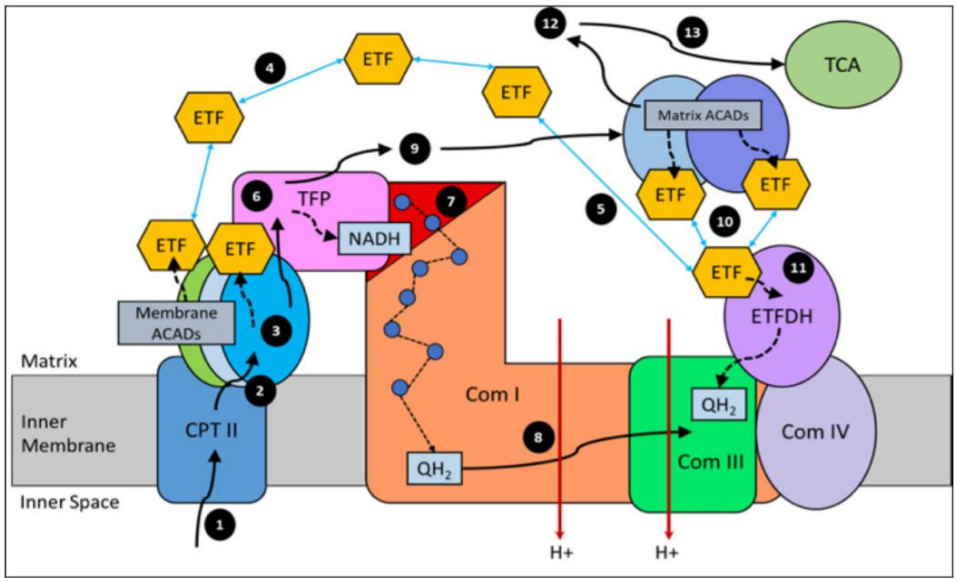

Figure 2. Schematic of the fatty acid oxidation supercomplex.

Adapted from Wang et al 2019, cartoon of the interaction of the enzymes of fatty acid oxidation and the electron transport chain interact to facilitate the breakdown of long-chain acylcarnitines generating acetyl-CoA for the TCA cycle or ketone body production [8]. Steps 1-3: long-chain acyl-CoA substrates transferred as acylcarnitines from the intermembrane space, and converted into acyl-CoA by CPTII, for use as a substrate by VLCAD. VLCAD converts the long-chain acyl-CoA substrate to its enoyl-CoA and reduces ETF. Steps 4-5: VLCAD releases ETF into the mitochondrial matrix where it finds its redox partner, ETFDH, and shuttles QH2 to Complex III. Steps 6-7: the long-chain enoyl-CoAs channel to TFP, which produces one molecule of acetyl-CoA and an acyl-CoA that is two carbons shorter. As the acyl-CoAs become shorter, they are released into the matrix. Step 8: In complex I, NADH is oxidized through iron-sulfur clusters to generate QH2 and transported through the membrane electron channel of Complex I to Complex III. Steps 9 and 10: medium- and short-chain acyl-CoA substrates produced by TFP are transferred to the matrix ACADS, MCAD and SCAD. ETF Is reduced again and released to ETFDH. The remaining FAO reactions are catalyzed by monofunctional enzymes that are weakly associated with the complex. Step 11:

ETFDH oxidizes reduced ETF by reducing CoQ to QH2 and QH2 is channeled to Complex III. Steps 12 and 13: acetyl-CoA can enter the TCA cycle.

1.3 ACYL-COA DEHYDROGENASES

The acyl-coenzyme A dehydrogenases (ACADs) are a class of enzymes that catalyze the α,β-dehydrogenation of acyl-CoA substrates in FAO and BCAA (among others) catabolism in mitochondria, resulting in the introduction of a trans double-bond between C2 (α) and C3 (β) of the acyl-CoA thioester substrate [9]. An active site glutamate acts as the catalytic base, attacking the acyl moiety α-carbon proton to initiate the enzymatic reaction, whereas the β-carbon hydrogen is transferred to the flavin adenine dinucleotide (FAD) as a cofactor as a hydride [1, 9]. There are nine mitochondrial ACADs involved in the fatty acid and branched chain amino acid oxidation pathways, and two of ACADs unknown function: ACAD10 and ACAD11 [9, 10]. The five FAO ACADs are short chain acyl-CoA dehydrogenase (SCAD), medium chain acyl-CoA dehydrogenase (MCAD), long chain acyl-CoA dehydrogenase (LCAD), very long-chain acyl-CoA dehydrogenase (VLCAD), and ACAD9. The four branched chain amino acid oxidation pathways are isovaleryl-CoA dehydrogenase (IVD; i3VD), glutaryl-CoA dehydrogenase (GCD), isobutryl-CoA dehydrogenase (IBD, ACAD8), and short/branched chain acyl-CoA dehydrogenase (SBCAD, i2VD). VLCAD participates in fatty acid oxidation with maximal activity towards substrates of 12-22 carbon in length [9]. Isovaleryl-CoA dehydrogenase (IVD) catalyzes the third step in leucine catabolism. In addition to a common enzyme mechanism, the ACADs share a conserved amino acid sequence and tertiary structures. All of the mitochondrial matrix ACADs have similar structures [9, 10]. The most studied ACAD is MCAD. MCAD is a homotetramer

composed of a dimer of dimers with each monomer containing one catalytic site (Fig. 3) [9-12]. In MCAD the catalytic base is Glu376 and a mutation Glu376Asp results in 5% MCAD activity compared to wildtype [13]. The structure of IVD has also been elucidated and is a homotetramer similar to MCAD [11, 14, 15]. However, IVD's catalytic residue is Glu254 and approaches substrate from the opposite side of its binding pocket.

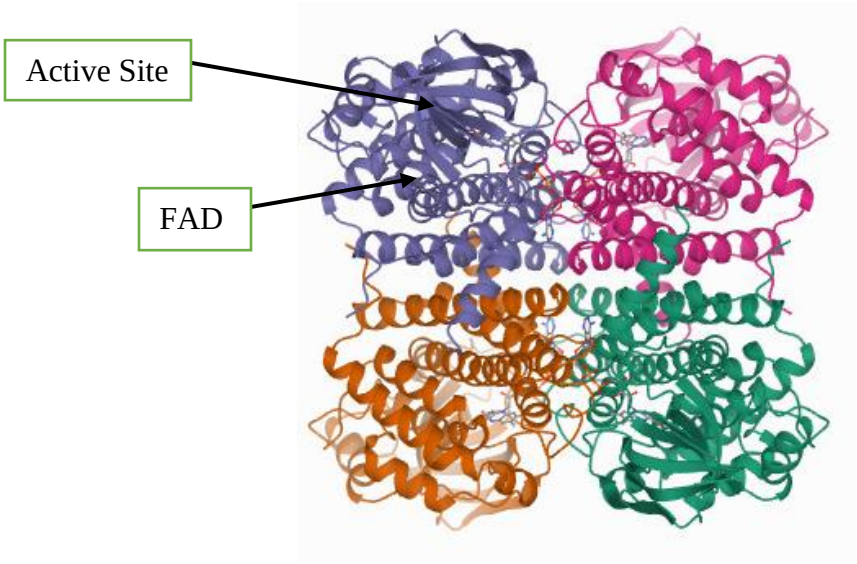

Figure 3. Medium chain acyl-CoA dehydrogenase enzyme crystal structure.

Adapted from Kim et al 1993, MCAD structure generated from X-ray crystallography of pig MCAD is similar to structure of human MCAD and other human ACADs containing 4 monomers and 4 active sites. Each color represents one monomer [12].

In contrast to the matrix ACADs, ACAD9 and VLCAD are homodimers with the former being a complex I assembly factor and the latter associating with the inner mitochondrial membrane. The VLCAD crystal structure has been determined and Glu-422 is the catalytic residue [16]. ACAD9 and VLCAD share 65% amino acid similarity and molecular modeling has revealed the catalytic Glu residue is conserved at position 426 in ACAD9 [17, 18].

Mutations in all the ACAD genes, except LCAD, have been described as causing inborn errors of metabolism in their respective pathways [11, 19, 20]. *ACADVL* and *IVD* gene mutations lead to VLCAD deficiency and isovaleric acidemia, respectively.

1.4 ISOVALERIC ACIDEMIA (IVA)

Isovaleryl-CoA dehydrogenase (IVD; EC 1.3.8.4) catalyzes the conversion of isovaleryl-CoA to 3-methylcrotonyl-CoA in Leu catabolism with transfer of electrons from the reduced enzyme to the electron transfer flavoprotein (ETF). Isovaleric acidemia (IVA), the first organic acidemia described in humans, is caused by biallelic mutations in the *IVD* gene [21-23]. It has an incidence of 1:280,000 individuals diagnosed after onset of symptoms, but a birth prevalence of 1:100,000 newborns when diagnosed via newborn screening [24]. A common variant, c.941C>T (p.Ala282Val) identified by newborn screening appears to reduce enzyme activity *in vitro* but does not cause clinical disease in humans [25]. Symptoms in unscreened individuals develop in infancy about 50% of the time and include vomiting, decreased levels of consciousness, seizures, hypothermia, dehydration, acidosis and a characteristic odor of "sweaty feet", leading to coma and death if unrecognized [21, 26]. Chronically, mild to moderate mental disabilities are common [23, 26].

With the advent of tandem mass spectrometry based newborn screening, most IVA patients are identified before they show signs of symptoms. Newborn screening is performed ideally after the first oral or enteral feeding at about 24 hours of life [27]. It is performed via a heal prick and blood is collected on Guthrie paper [27-30]. Samples are then analyzed via MS/MS between 24 and 72 hours after collection. Results are generated and reports are distributed to a newborn's

primary care physician by day 7 of life [27]. If a positive screen is detected, the primary care physician and the designated Metabolic Center is contacted for confirmatory DNA sequencing. Specifically, IVA is detected by an elevation in C5-carnitine which is indicative of isovaleric acid [25, 31-34]. Follow-up confirmational sequencing of the *IVD* gene is performed to confirm diagnosis in addition to repeating the acylcarnitine analysis. IVA patients identified through newborn screening have a much better outcome than if diagnosed symptomatically; however, the need for treatment and monitoring to prevent acute episodes of metabolic crisis remains [31].

1.4.1 Treatment of IVA

Current treatment for IVA involves restriction of foods high in protein including dairy products, meat, fish, eggs, legumes, and nuts, often with a requirement for leucine restricted medical foods to meet overall protein requirements for growth or health maintenance [35, 36]. Additionally, medications that can conjugate isovaleric acid and reduce systemic toxicity have been used, including glycine (150-250 mg/kg per day) and/or L-carnitine (100 mg/kg per day) [31]. All of these measures date to the original description of the disease and remain the mainstay of treatment, with no new therapies developed since [37]. Even with adherence to diet and supplementation, patients still experience decompensation under certain conditions.

1.4.2 Mutations in *IVD*

Mutations in the genes encoding for BCAA enzymes have been described and reported to cause inborn errors of metabolism. Over 300 mutations have been documented in *IVD* in the ClinVar database search in February 2022, exhibiting a wide range of type and phenotypic

severity, but many of uncertain significance. Genotype/phenotype correlations have not been completely explored in IVA. However, patients with two null mutations in *IVD* typically result in more severe phenotype including seizures, decreased levels of consciousness, dehydration, acidosis, leading to coma and death if untreated, while patients with missense mutations tend to have a milder phenotype [20, 25, 31, 38]. A common mutation in *IVD*, c.941T>C (p.Ala282Val), is detected in half of newborns with IVA identified through newborn screening and has been associated with mild or asymptomatic disease [25].

Several studies have determined *IVD* mutation pathogenicity and severity. Mohsen et al 1998 performed functional studies on IVA patient fibroblasts and overexpression of *IVD* cDNAs in E. coli [20]. While all the mutations examined were missense mutations, stability modeling and IVD enzyme activity measurements revealed the mutations having 13-60% stability and undetectable to 19% IVD activity compared to control [20]. The common mutation in *IVD*, c.941T>C (p.Ala282Val), was determined to have 50% stability and 19% IVD activity via expression studies [20]. This was consistent with the mild or asymptomatic clinical phenotype, as the mutant IVD is relatively stable and active within the cells [20, 25].

However, not all point mutations lead to a single amino acid change, several *IVD* point mutations are splice site mutations can result in the skipping of exon 2, and unstable *IVD* mRNA in exon 4 or exon 8 of IVD [39]. Another functional study performed on a Korean population of IVA patients containing two novel splice site mutations, an insertion in intron 1 and a deletion in intron 4, resulting in unstable *IVD* mRNA and no IVD enzyme activity [40]. These studies confirm the need to perform functional studies on *IVD* variants to determine pathogenicity and develop effective IVA patient-personalized treatments.

1.5 VERY LONG-CHAIN ACYL-COA DEHYDROGRENASE (VLCAD) DEFICIENCY

Very long-chain fatty acid (VLCAD) deficiency is an autosomal recessive disorder caused by mutations in *ACADVL* gene [41]. The frequency of VLCADD is about 1:30,000 to 1:100,000 live births [29, 33]. Symptoms of VLCADD include hypoglycemia, recurrent rhabdomyolysis, myopathy, hepatopathy, and cardiomyopathy which may present in infancy or later in childhood or adolescence [42]. VLCADD is detected through newborn screening with elevations of C14:2, C14:1, C16, and C18:1 acylcarnitines [33, 43]. Similar to IVA, VLCADD is confirmed with DNA sequencing of the *ACADVL* gene after a positive newborn screen [27].

1.5.1 Treatment of VLCAD Deficiency

Treatment options for VLCADD are limited and have historically involved restricting dietary long chain fat intake, and supplementation with medium chain triglycerides (MCT) that can bypass the block in long chain FAO [44-47]. However, MCT preparations typically contain a mixture of 8-12 carbon fats that do not provide the odd chain substrates necessary to replenish the succinate in the TCA cycle that becomes depleted in VLCADD [47-54]. Triheptanoin, a triglyceride of heptanoate, provides acetyl-CoA and propionyl-CoA, which is converted to succinyl-CoA to the TCA cycle [47]. It has completed Phase 2-3 clinical trials that have shown it to eliminate the hypoglycemia mediated by TCA cycle depletion and greatly reduce cardiomyopathy in these patients [46, 47]. It was approved by the FDA for the treatment of long chain fatty acid oxidation disorders in 2019 [53, 54]. However, recurrent rhabdomyolysis and, to a lesser extent, cardiomyopathy remain a problem especially during times of physiologic stress

such as intercurrent illness or extended periods of exercise [45]. Thus, additional therapies remain a priority.

1.5.2 Mutations in *ACADVL*

Mutations in all the genes encoding the FAO enzymes that result in inborn errors of FAO metabolism have been described, except LCAD deficiency. Over 900 mutations have been documented in *ACADVL* in a ClinVar database search in February 2022, exhibiting a wide range of type and associated clinical severity, but many of unknown significance. There is a genotype/phenotype correlation in VLCAD deficiency. Patients with deletions, duplications, or insertions in *ACADVL* resulting in a null mutation tend to have severe VLCAD deficiency characterized by cardiomyopathy, hepatomegaly, and recurrent episodes of metabolic decomposition typically triggered by fasting, vomiting, and fever, while those with missense mutations can have a milder phenotype [42, 55-57]. The *ACADVL* common mutation, c.848T>C (p.Val283Ala), has been associated with mild disease with onset of symptoms, typically recurrent rhabdomyolysis, in adolescence or adulthood [55, 58].

Each patient has a different combination of mutations that results in a phenotypic variability. Thus, multiple treatment approaches are necessary. Functional studies on both VLCADD patient fibroblasts identified through newborn screening found no detectable VLCAD enzyme activity for multiple base duplications, deletions, and splice site mutations [55]. Expression studies of missense mutations followed by VLCAD activity measurements, protein, and mutant modeling, confirmed that missense mutations from VLCADD patients were pathogenic, consistent with clinical findings and patient symptoms [55]. VLCADD fibroblasts had decreased mitochondrial respiratory chain function and ATP production, impaired oxygen

consumption and overall increase in reactive oxygen species [56]. However, VLCADD fibroblasts containing null mutations had worse cellular bioenergetics compared to fibroblasts containing missense mutations [56]. *ACADVL* mutation severity also correlated to VLCADD fibroblast response to antioxidant treatment with less severe missense mutations with residual VLCAD enzyme activity responding better than those with severe duplication or deletion mutations [56]. Treatment of various VLCADD fibroblasts with bezafibrate, a hypolipidemic drug increased in VLCAD amount and activity for missense mutations associated with a mild phenotype [59]. In contrast, bezafibrate treatment was not effective for fibroblasts from severely affected patients containing null mutations [59].

Collectively, these studies suggest that *ACADVL* mutation needs to be considered in determining appropriate treatments for each patient. While genotypic-phenotype correlations are difficult to establish, they are crucial for patients identified through newborn screening [57]. DNA sequencing and functional studies have determined that homozygous null mutations in *ACADVL* lead to no VLCAD enzyme activity and consequent severe phenotypes. While various missense mutations often require functional studies to determine pathogenicity and onset of the disease in infancy or adolescence [57]. Thus, a mutation-specific treatment approach is necessary for VLCAD deficiency.

1.6 REGULATION OF FATTY ACID OXIDATION BY THE PEROXISOME PROLIFERATOR-ACTIVATED RECEPTOR

A new therapeutic option considered for VLCAD deficiency is utilizing peroxisome proliferator-activated receptor (PPAR) agonists to upregulate FAO genes, including *ACADVL*.

Peroxisomes are organelles that perform H_2O_2-based respiration, fatty acid β-oxidation, and cholesterol metabolism [60]. PPARs were originally identified as inducing peroxisome proliferation in rat liver; however, this does not occur in humans [61]. Rather PPARs in humans are nuclear receptors that regulate of fatty acid β-oxidation, lipid metabolism, inflammation, cellular growth, and differentiation [62-66]. There are three classes of PPARs: PPARα, PPARγ, and PPARβ/δ. PPARα reduces triglyceride level and regulates energy homeostasis [60, 67]. PPARγ enhances glucose metabolism and insulin sensitization [60, 67, 68]. PPARδ is an activator of oxidative metabolism and is broadly expressed, responding to polyunsaturated fatty acids, dexamethasone, and eicosanoids [62, 69-72] (Fig. 4). These ligands bind to PPAR, which in turn binds to the retinoid X receptor (RXR) to create a PPAR-RXR heterodimeric complex. This complex then interacts with the peroxisome proliferator response element (PPRE) located in the promoter region of target genes, activating downstream gene expression [73]. In the absence of a ligand, the PPAR-RXR heterodimer is associated with a multicomponent corepressor complex containing histone deacetylase activity that maintains the chromatin in a condensed, inactivate state [73].

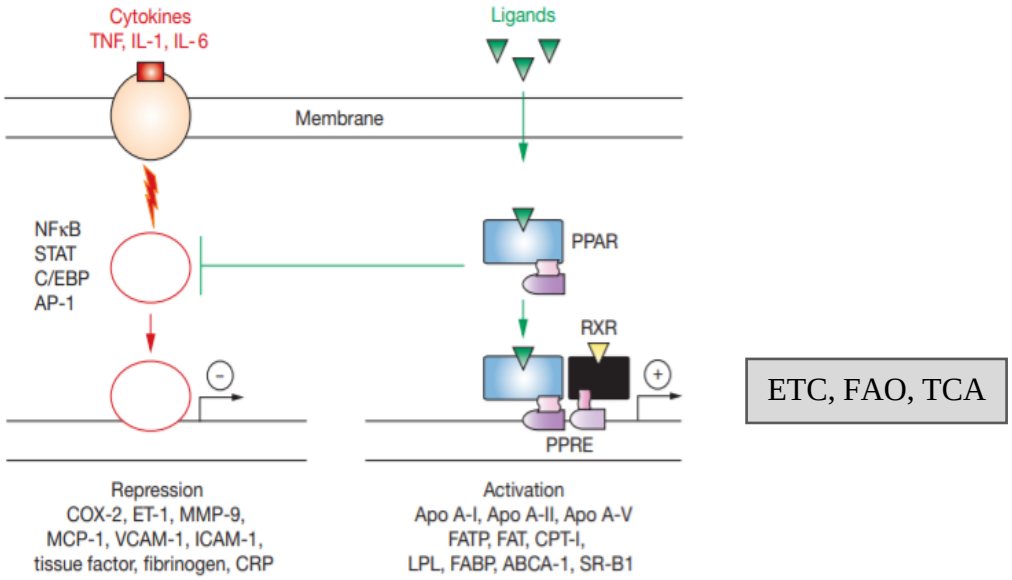

Figure 4. Mechanistic overview of the peroxisome proliferator-activated receptor (PPAR).

Adapted from Gervois et al 2007, PPARs are activated by ligand binding. The activated PPAR binds to the RXR complex which binds to the promoter region of the fatty acid β-oxidation transcription factor. This activates transcription and mRNA production and translation of fatty acid β-oxidation enzymes. [73]

Previous studies of PPARδ agonists have shown that they can mediate improvement in energy related diseases such as diabetes and obesity, as well as regulate lipid metabolism. For example, treatment of moderately obese men with dyslipidemia with placebo or PPARδ agonists resulted in a decrease in fasting and postprandial plasma triglycerides, LDL cholesterol, apoB and reduction in liver fat content and urinary isoprostanes (the marker of whole-body oxidative stress) [74]. Treatment of insulin-resistant middle-aged obese rhesus monkeys with the PPARδ agonist GW501516 led to a dose-dependent rise in serum high density lipoprotein cholesterol while lowering the levels of low density lipoprotein cholesterol, fasting triglycerides, and fasting insulin [75]. Genetically obese mice containing homozygous mutations in the Leptin (*Lep*) gene (known as ob/ob mice) have unregulated eating and resultant obesity. Ob/ob mice treated with GW501516 exhibited reduced plasma glucose and blood insulin levels [69]. Similarly, genetically predisposed obese *ob/ob* mice treated with a PPARδ agonist showed a decrease in lipid accumulation, while

PPARδ-deficient mice had greater weight gain on a high-fat diet compared to wild type animals [66]. *Db/db* mice are homozygous for the leptin receptor (Lepr) which results in a similar phenotype to the *ob/ob* mice [76]. Natural herbs such as bavachinin (a pan-PPAR agonist) from the glucose-lowering *Psoralea corylifolia* herb and ginger (a PPARδ agonist) have been reported to reduce the rate of obesity in the obese *db/db* mice and protect from diet induced obesity [76, 77].

Bezafibrate is a pan-PPAR agonist used to treat hyperlipidemia as it increases high density (HDL) cholesterol levels but decreases total and LDL cholesterol levels [78]. Since PPARs can increase fatty acid β-oxidation, there has been interest in repurposing bezafibrate as a treatment for fatty acid oxidation disorders. In an *in vitro* study, VLCADD fibroblast cell lines treated with two versions of bezafibrate demonstrated a 3-fold increase in palmitate oxidation with an increase in VLCAD mRNA, protein, and enzyme activity. RT-PCR also showed an increased expression of other genes encoding proteins in the β-oxidation pathway [79]. Similarly, treatment of CPT2 deficient human myoblast cells with bezafibrate, and the PPARδ agonist GWδ 0742 led to an increase in *CPT1-B* and *CPT2* mRNA levels with increased CPT2 activity, while GWα 7647, a PPARα agonist, had minimal effect [80]. Treatment with bezafibrate of fibroblasts from 26 patients with mitochondrial fatty acid oxidation trifunctional protein (MTP) deficiency with various mutations led to improved cellular palmitate oxidation in 6 of 26 cell lines [81]. However, in a small clinical trial in patients with VLCAD or CPT2 deficiency, bezafibrate failed to improve cardiac function or whole-body fatty acid oxidation [82]. One possibility for this dichotomy is the limited PPARδ effect of bezafibrate.

While PPARs has been shown to upregulate the expression of FAO genes, some data also suggest an effect on the genes involved in BCAA catabolism. PPARγ (functionally related to

PPARδ) deleted mice have been shown to have reduced BCAA catabolism [83]. Here, mice containing an adipocyte specific deletion of one *PPARG* copy had increased BCAA serum levels and reduced mRNA expression of BCAT2 and BCKDH, the proximal steps in the BCAA catabolism pathway [83]. This study suggests that without normal PPARγ activity, the two proximal steps in BCAA are impaired. Since PPARδ agonists have shown an effect in FAOD fibroblasts as described above, PPARδ might also have an effect on BCAA catabolism, though this has not been explored.

1.7 NEWBORN SCREENING

IVA and VLCAD deficiency are detected via tandem mass spectrometry during newborn screening (NBS) in the United States. NBS is a public health program that screens newborns for conditions that are treatable but not apparent before the onset of symptoms [30, 84-86]. Most NBS is performed on blood collected on filter paper by a heel prick a few days after birth with subsequent, biochemical, immunologic, or molecular testing at a centralized lab [86]. The first condition screened for by NBS was phenylketonuria (PKU). PKU, or phenylalanine hydroxylase (PAH) deficiency, is an autosomal recessive inborn error of metabolism that results from biallelic mutations in *PAH* [87]. Untreated PKU results in severe intellectual disability, behavior problems, seizures, microcephaly, musty body odor, and decreased skin and hair pigmentation [28, 87]. Early treatment with dietary restriction of phenylalanine (Phe) prevents the devastating neurologic consequences of this disease [28, 87-89] With diet adherence and monitoring, symptoms of PKU can be avoided. In the 1960s Robert Guthrie developed a high throughput method to detect PKU using a bacterial inhibition assay (BIA) performed on blood collected shortly after birth [28, 90,

91]. It has since been replaced with tandem mass spectrometry, which can measure numerous clinically relevant metabolites in addition to Phe levels with a single, rapid assay [86]. Secondary testing by sequential liquid chromatography with MS/MS further improves NBS specificity for many disorders [32]. Newborn screening programs in the US are regulated at the State level, but the United States Health Resources & Services Administration (HRSA) has developed a Recommended Uniform Screen Panel (RUSP) that provides evidence based recommendation to states that suggests diseases suggested for NBS [86]. The RUSP currently includes 35 primary conditions and 26 secondary conditions identified via tandem mass spectrometry, hemoglobin electrophoresis, immunodetection, and molecular testing, along with point of care screening for hearing loss and cyanotic congenital cardiac disease [86].

1.7.1 Challenges of Newborn Screening and Variants of Uncertian Significance

Follow up genetic diagnosis by molecular analysis and/or functional studies is necessary to confirm a diagnosis suggested by NBS. IVA and VLCAD deficiency are confirmed via DNA sequencing and *de novo* variants often have functional studies performed to determine pathogenicity. Since DNA sequencing is more available clinically and usually faster, it has become the *de facto* norm for NBS follow up. However, sequencing-based methods often identify variants of uncertain significance (VUS) in the relevant gene, though the frequency varies among disorders [92]. VUSs are typically point mutations as the American College of Medical Genetics (ACMG) criteria automatically classifies new deletion/insertions/duplications as likely pathogenic, especially of large stretches of DNA [93]. The presence of a VUS(s) makes a firm genetic diagnosis impossible without additional functional testing, significantly delay final diagnoses and complicating treatment decisions [92, 94]. High throughput functional assays that leverage a

common testing platform are particularly well suited for implementation in a clinical setting; however, no such options currently exist for most inborn errors of metabolism, leaving a high unmet need.

1.8 GENETIC DATABASES

When a new variant is identified in NBS for IVA and VLCAD deficiency, a genetic database is referenced to determine if the variant has been reported before. Genetic databases are a system of collecting and organizing genetic information. There are many different genetic databases containing different information including nucleic acid sequences, protein sequences, single nucleotide polymorphisms (SNPs), and model organism genomes. Each database has different inclusion criteria and no one database contains all of the information needed for genetic analysis and assessment. Frequently used databases include dbSNP, Entrez Gene, and the University of California Santa Cruz (UCSC) Genome Browser. dbSNP database is a collection of SNP information including SNP frequency and pathogenicity [95, 96]. Entrez Gene is a compilation genome information including gene name, location, products, markers, phenotypes, homologs, and links to additional databases [97, 98]. The UCSC Genome Browser allows for visualization of genetic data and genome annotation in addition to comparison of genomes of over 105 species [99-101]. Each genetic database has its benefits and pit falls, but collectively are tools to learn information about specific genes, variations within those genes, and implication on phenotype.

ClinVar is a genetic database that is freely accessible and reports relationships between human variants and phenotype [102-104]. These variants are submitted by clinicians and affiliated

organizations based on patient sequencing and clinical data. Each ClinVar entry contains information about the submitter, variation, associated phenotype, interpretation (pathogenic, likely pathogenic, VUS, likely benign, and benign), and evidence [102]. ClinVar also has a five star ranking system of the variants based on the amount of evidence, type of evidence, and if conflicting evidence on the variant is present. ClinVar follows the ACMG guidelines for classifying variants defined in the previous section [102, 104].

ClinVar and genetic databases are the most useful when they are routinely updated. ClinVar is updated weekly, and monthly reports are generated for users [104]. This is especially important in NBS to allow for proper identification of variants and pathogenicity status. If and when VUSs are reclassified, depends on the data available and the resources to update the database in a timely and appropriate manner.

1.9 CRISPR/CAS9 TECHNOLOGY

While prokaryotic expression systems have been used to determine *IVD* and *ACADVL* variant pathogenicity, a mammalian expression system is ideal since it contains all mechanisms needed for post-translational modification not found in *E. coli*. There are several methods for gene editing with clustered interspaced short palindromic repeats/CRISPR-associated-9 technology (CRISPR/Cas9) being the most effective and commonly used. CRISPR originated from the microbial adaptive immune system. Bacteria recognize CRISPR segments in foreign DNA via Cas nucleases and cleave the foreign DNA. Modified for genome editing, CRISPR/Cas technology uses RNA-guided nucleases to cleave defined target genetic elements [105]. Cas9, the most common of the Cas nucleases, recognizes CRISPR segments and cleaves near the protospacer

adjacent motif (PAM) sequence [105]. CRISPR/Cas recognizes the protospacer adjacent motif (PAM) sequence and introduces DNA double-strand breaks (DSBs), normally repaired by via non-homologous end-joining (NHEJ). NHEJ is a process that introduces small insertions or deletions (indels) at the repair junction by inserting or deleting random nucleotides to repair the double stranded break [106]. The Cas9 nuclease specificity is determined by a guide RNA (gRNA), a 20-nucleotide sequence, and binds to the PAM site and adjacent nucleotides. The target DNA must precede a 5'-NGG PAM sequence in the system derived from *Streptococcus pyogenes* [105].

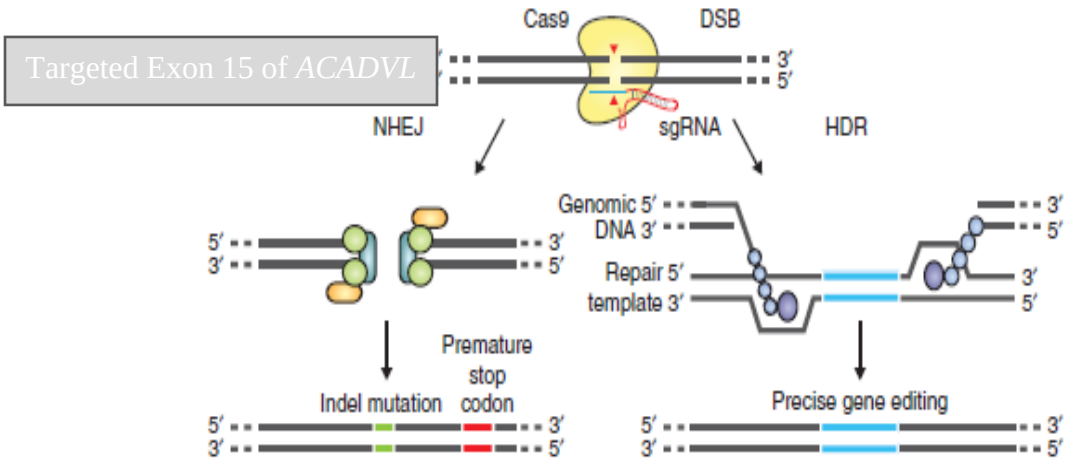

Figure 5. CRISPR/Cas mechanism for targeting DNA, cleavage, and repair.

Adapted from Yoshimi et al 2016, Cas9 creates a double stranded break in the gRNA targeted DNA. This break is repaired by non-homologous end-joining (NHEJ) or homology directed repair (HDR) using a single-stranded oligodeoxynucleotide (SSODN) template [106]. Here we targeted exon 15 of *ACADVL*, to delete the catalytic site of VLCAD to produce a null enzyme.

Homology directed repair (HDR) can perform more specific editing compared to NHEJ **(**Fig. 5**)** [105]. A single-stranded oligodeoxynucleotide (SSODN) is introduced in conjunction with the Cas9 nuclease and gRNA to introduce a specific point mutation within the genome. The

SSODN donor template works in combination with the engineered nucleases for efficient targeted insertion of small DNA fragments or point mutations [105, 106]. The gRNA binds to the PAM site and directs Cas9 to cleave the DNA. The SSODN acts as a repair template, complementary to the target DNA region, to direct the cell's DNA repair machinery what nucleotides to insert [107]. This process allows efficient generation of animal model such as a genetic model containing a specific point mutation.

1.10 PUBLIC HEALTH SIGNIFICANCE

Inborn errors of metabolism (IEMs) are individually rare genetic disorders but in combination represent a significant newborn health risk, affecting approximately 0.2-0.3% of live births [108]. IVA occurs in 1:100,000 to 1:250,000 live births and collectively the organic acidemias affect 1:20,00 live births [24, 109]. VLCADD occurs in about 1:30,000 to 1:100,000 live births, and collectively, FAO disorders affect 1:5,000 to 10,000 live births [29, 33]. IEMs are typically identified through newborn screening (NBS) and early intervention such as diet modification and supplementation improve patient outcomes [30, 33]. NBS has been identified as one of the top 10 public health initiatives of the 20th century. However, identification of disease without addressing therapy falls short of the maximum public health outcome. Additionally, NBS results are typically confirmed with confirmatory DNA sequencing, often resulting in identification of at least one VUS [32, 92]. The lack of confirmation of pathogenic mutation can lead to difficulty in determining treatment plans for patients.

This project addresses two problems in developing proper treatment plans for IEM patients identified through NBS. First, to develop a high throughput screening method for VUSs to

determine pathogenicity via functional studies. Second to test a new treatment method for VLCADD. Both use technologies that may be generalizable to many IEMs and provide better outcomes for affected babies identified by newborn screening.

1.11 HYPOTHESIS AND SPECIFIC AIMS

Acyl-CoA dehydrogenase deficiencies are autosomal recessive inborn errors of metabolism resulting from mutations in one of multiple acyl-CoA dehydrogenases. Collectively, they affect ~10,000 babies born in the United States. Isovaleric academia (IVA) is a defect in the leucine (Leu) catabolic pathway caused by mutations in the isovaleryl-CoA dehydrogenase gene (*IVD*). IVD catalyzes the conversion of isovaleryl-CoA to 3-methylcrotonyl-CoA with transfer of electrons from IVD to the electron transfer flavoprotein (ETF) [21-23]. Very long-chain acyl-CoA dehydrogenase (VLCAD) catalyzes the initial intra-matrix step of mitochondrial beta-oxidation of long-chain fatty acids (carbon length chain of 12 to 20 [41, 110]. Its deficiency is caused by biallelic mutations in the *ACADVL* gene. Both defects are detected by newborn screening in the US with tandem mass spectrometry of dried blood spots and typically confirmed via sequencing [92]. However, sequencing often identifies variants of uncertain significance (VUS), leading to uncertainty in diagnosis and development of treatment plans for patients. Currently, the therapy for each disorder is dietary, based on leucine restriction for the former and a low long chain fat diet and medium chain triglyceride (MCT) or triheptanoin supplementation and for the latter. In addition, carnitine and/or glycine supplementation provides some benefit [35, 36]. However, even with adherence to these measures, patients still experience episodes of metabolic decompensation with significant morbidity and mortality [25, 111].

Here, I developed two models to determine pathogenicity of VUSs in *IVD* and *ACADVL*, and explored a new therapeutic compound for VLCAD deficiency. I generated two independent HEK293T null models for *ACADVL* and *IVD* to perform functional studies to determine VUS pathogenicity. I examined the use of peroxisome proliferator activated delta receptor (PPARδ) activators for VLCAD deficiency.

1.11.1 Specific Aim 1: Develop and Characterize an *IVD* NULL HEK293T Model to Allow for Rapid Analysis of Variants of Uncertain Significance

IVA is detected through tandem mass spectrometry through newborn screening and confirmed by follow up sequencing of the *IVD* gene. Sequencing often identifies variants of uncertain significance (VUS) which leads to uncertainty in diagnosis and need for treatment. I hypothesized that partial deletion of *IVD* in a HEK293T cell line using CRISPR/Cas9 technology would provide an *IVD* null HEK293T cell line suitable for use in subsequent expression studies. I further hypothesized that this *IVD* null HEK293T model could be utilized in a high throughput assays system with transfection of *IVD* variants and subsequent functional studies to determine variant pathogenicity.

1.11.2 Specific Aim 2: Develop and Characterize and *ACADVL* NULL HEK293T Model to Allow for Rapid Anaylsis of Variants of Uncertain Significance

As in IVA, VLCADD has a high rate of VUS during follow up sequencing after newborn screening via tandem mass spectrometry. I hypothesized that deleting exon 15, the catalytic site of *ACADVL*, also using CRISPR/Cas9 technology in a HEK293T cell line, would generate an

ACADVL null cell line that could be used to assess pathogenicity of VUSs in a high throughput fashion.

1.11.3 Specific Aim 3: Evaluate The Effectiveness of a PPARδ AGONIST as a Treatment for VLCAD Deficiency

PPARδ activators are a group of molecules that interact with this nuclear receptor and upregulate transcription of multiple genes involved in mitochondrial metabolism, including those for fatty acid β-oxidation (FAO), the mitochondrial electron transport chain (ETC), and the tricarboxylic acid (TCA) cycle. I hypothesized that treating FAO-deficient patient fibroblasts with a PPARδ agonist would increase cellular FAO protein content and enzyme activity, decrease toxic metabolites, and improve FAO flux through the metabolic pathway, thus improving oxygen consumption rates and ATP production.

2.0 DEVELOP AND CHARACTERIZE AN *IVD* NULL HEK293T MODEL TO ALLOW FOR RAPID ANALYSIS OF VARIANTS OF UNCERTAIN SIGNIFICANCE

This chapter has been published in Molecular Genetics and Metabolism. The article is reproduced here under license from Wiley with only minor formatting and non-scientific changes. The original article and supporting information are available online at https://doi.org/10.1016/j.ymgme.2021.08.012.

Olivia M. D'Annibale[1,2], Erik A. Koppes[1], Ahmad N. Alodaib[1,3], Catherine Kochersperger[1], Anuradha Karunanidhi[1], Al-Walid Mohsen[1,2], Jerry Vockley[1,2].

[1] Division of Genetic and Genomic Medicine, Department of Pediatrics, University of Pittsburgh School of Medicine, and UPMC Children's Hospital of Pittsburgh, Pittsburgh, PA 15224;

[2] Department of Human Genetics, University of Pittsburgh Graduate School of Public Health, Pittsburgh, PA 15261;

[3] Department of Clinical Genomics, Centre for Genomic Medicine, King Faisal Specialist Hospital and Research Centre, Riyadh, Saudi Arabia.

2.1 ABSTRACT

Introduction. Clinical standard of care for newborn screening (NBS) is acylcarnitine metabolites quantitation by tandem mass spectrometry (MS/MS) from dried blood spots. Follow

up sequencing often results in identification of one or more variant of uncertain significance (VUS). Isovaleric acidemia (IVA) is an autosomal recessive inborn error of metabolism caused by deficiency of isovaleryl-CoA dehydrogenase (IVDH) in the Leu catabolism pathway. Many *IVD* mutations are characterized as VUS complicating IVA clinical diagnoses and treatment. We present a novel platform approach to confirm the functional implication of genetic VUS identified in newborns with IVA applicable to multiple inborn errors of metabolism identified by newborn screening. **Methods.** An *IVD* null HEK293T cell culture model was generated by using a dual sgRNA CRISPR/Cas9 genome-editing strategy targeting *IVD* exons 2-3. Clonal cell lines were confirmed by a combination of genomic breakpoint sequencing and droplet digital PCR. The *IVD* null model had no IVDH antigen signal and 96% reduction in IVDH enzyme activity. The *IVD* null model was transfected with vectors containing control or variant *IVD* and functional assays were performed to determine variant pathogenicity. **Results.** c.149G>C (p.Arg50Pro; precursor numbering), c.986T>C (p.Met329Thr), and c.1010G>A (p.Arg337Gln), c.1179del394fs mutant proteins had reduced IVDH protein and activity. c.932C>T (p.Ala311Val), c.707C>T (p.Thr236Ile), and c.1232G>A (p.Arg411Gln) had stable IVDH protein, but no enzyme activity. c.521T>G (p.Val174Gly) had normal IVDH protein and activity. *IVD* variant transfection results confirmed results from IVA fibroblasts containing the same variants. **Conclusions.** We have developed an *IVD* null HEK293T cell line to allow rapid determination of VUS pathogenicity following identification of novel alleles by clinical sequencing following positive NBS results for suspected IVA. We suggest similar models can be generated via genome-editing for high throughput assessment of VUS function for a multitude of inborn errors of metabolism, and can ideally supplement NBS programs.

2.2 INTRODUCTION

The clinical standard of care for newborn screening (NBS) for many inborn errors of metabolism is quantitation of acylcarnitine metabolites by tandem mass spectrometry (MS/MS) from dried blood spots on Guthrie cards. Secondary testing by sequential liquid chromatography with MS/MS further improves NBS specificity for many disorders [32]. Follow up genetic diagnosis is recommended by molecular analysis and functional studies. Sequencing-based methods often result in identification of variants of unknown significance (VUS) in at least one allele, though the frequency varies among disorders [92]. When VUSs are present, a firm genetic diagnosis of an inborn errors of metabolism remains in question, as specific functional testing for the novel variants is often unavailable or difficult to obtain, and can lead to a significant delay of final diagnoses and treatment implementation [92, 94].

Isovaleric acidemia (IVA, OMIM #243500) is an autosomal recessive inborn error of metabolism of the leucine (Leu) catabolic pathway [21-23]. It results from biallelic mutations in the gene encoding isovaleryl-CoA dehydrogenase (IVDH, EC 1.3.8.4), leading to the accumulation of isovaleryl-CoA and its metabolites. Symptoms of untreated IVA can first appear during infancy, childhood or adolescence; and include characteristic sweaty foot odor, poor feeding, vomiting, seizures, and mental disabilities [21, 26, 31]. IVA is typically detected via MS/MS-based NBS and is marked by a characteristic increase of C5-carnitine [33, 85]. However, the C5-carnitine can represent isovaleryl- or 2-methylbutyryl-carnitine and genetic confirmation of the diagnosis is required. IVA patients are typically treated with a Leu restricted diet, and L-glycine and/or L-carnitine supplementation to replenish exhausted endogenous supply [31, 37, 112-115]. In a study of IVA patients identified by NBS in Germany and the United States of primarily Caucasian and Arabic ethnicities, a common *IVD* mutation 932C>T (p.Ala311Val) was

identified in nearly half of the individuals, and predicts a mild clinical presentation and no need for therapy [25, 31, 34]. However, there are a growing number of *IVD* variants across diverse ethnicities being reported with unknown functional effects. As of this writing, 107 VUSs in the *IVD* gene are reported in ClinVar, leading to uncertainty in the diagnosis and treatment in identified infants. Classification of these VUSs as pathogenic or benign is critical to appropriately define the need for treatment following NBS.

In this study, we describe a scalable approach to determine the functional significance of VUSs identified by NBS in a timely manner to facilitate better diagnostic and therapeutic outcomes. We present proof-of-concept of this system by examining the functional implication of VUSs identified in newborns with elevated C5-carnitine indicative of IVA. To implement the study of *IVD* variants, an *IVD* null HEK293T cell line was generated using CRISPR/Cas9 genome-editing. Expression of control or variant *IVD* cDNAs within the *IVD* null HEK293T line then allowed characterization of IVDH enzyme activity in cellular extracts. This model enables determination of pathogenicity of individual *IVD* VUSs, and is amendable for development as a high throughput platform for screening VUSs in other inborn errors of metabolism.

2.3 MATERIALS AND METHODS

Experiments were performed in accordance with the approved guidelines and regulations. Experimental human protocols were approved by the Institutional Review Board at the University of Pittsburgh, protocol 19030195.

2.3.1 Subjects

Patients were detected after abnormal NBS of elevated C5-carnitine consistent with IVA (Supplementary Table S1). Skin biopsies for fibroblast culture were performed on a clinical basis from infants and subsequent analysis was performed written informed consent from parents and/or legal guardians. Sequencing of *IVD* was performed on a clinical basis in a CLIA certified laboratory on IVA patients and parents to determine the presence of *IVD* mutations in trans. Control fibroblast cells were obtained from the American Type Culture Collection (ATCC.org).

2.3.2 Cell lines & culture

HEK293T (obtained from ATCC.org) and fibroblast cell lines were grown in Dulbecco's Modified Eagle Medium (DMEM; Corning Life Sciences, Manassas, VA) containing 4.5 g/L glucose and supplemented with 10% fetal bovine serum, 4 mM glutamine and 100 IU penicillin and 100 µg/mL streptomycin (Corning Life Sciences, Manassas, VA) at 37 °C in a 5% CO_2 humidified atmosphere.

2.3.3 CRISPR-Cas9 genome-editing

CRISPR sgRNAs targeting *IVD* repeat-masked intron 1 and intron 3 (Supplementary Table S2) were designed using the Crispor.org web application [116] with optimal residues at the protospacer adjacent motif (PAM) (5'-NGG-3') +1 and -4 positions and cloned into the *Bbs*I site of the pSpCas9(BB)-2A-GFP vector (PX458; Addgene #48138) [105]. HEK293T cells were seeded into 6-well plates and co-transfected with 1µg of each PX458 plasmid complexed with

Lipofectamine 3000 (Invitrogen) at a 1:3 plasmid to reagent ratio for 24 hours. Cells were disaggregated after 48 hours and flow sorted for GFP(+) single cells into 96-well plates. Colonies were grown for 2-3 weeks, scaled up to 24-well plates and DNA extracted using the DNeasy Blood and Tissue kit (Qiagen, Valencia, CA). PCR amplification of deletion or inversion breakpoints (Primers available in Supplemental Table 2) was performed was performed using Q5 high-fidelity polymerase (New England Biolabs). PCR products were gel extracted (Zymo Research, Irvine, CA) and either directly Sanger sequenced or cloned into pJet2.1 (ThermoFisher Scientific) and sequenced.

2.3.4 *IVD* cDNA analysis

IVA patient fibroblast and IVD variant plasmid transfected *IVD* KO HEK293T cell mRNA was isolated using a RNeasy Mini kit (Qiagen, Valencia, CA) with on column DNaseI digestion. First strand synthesis of complementary DNA (cDNA) from 500 ng of mRNA was performed using the Superscript Vilo IV Master Mix (Qiagen, Valencia, CA). Reverse transcription PCR (RT-PCR) of full-length and partial *IVD* cDNA regions was performed with Q5 DNA polymerase (New England Biolabs) and directly Sanger sequenced to identify sequence variants (Primers available in Supplementary Table S4).

2.3.5 Western blot

Fibroblasts and HEK293T cells were grown in T175 flasks to 90% confluence, harvested by trypsinization, pelleted, and stored at -80°C for western blot. Frozen pellets were treated with 50 µL of radioimmunoprecipitation assay (RIPA) buffer (Thermofisher Scientific) and 1X

Protease Inhibitor Cocktail (PI) (Roche, St Louis, MO) for 30 minutes on ice and centrifuged at 14,000 x g for 15 minutes at 4°C. Supernatants were collected and 25 µg of protein was loaded onto a 4 to 15% gradient Criterion precast SDS-PAGE gel (Biorad, Hercules, CA). Following electrophoresis, the gel was blotted onto a nitrocellulose membrane and incubated with mouse anti-IVD antibody (1:2000; Origene, Rockville, MD), then incubated with secondary goat anti-mouse-HRP antibody (1:3000, Biorad, Hercules, CA). Pierce ECL Western Blotting Substrate kit (Thermofisher Scientific) was used to visualize bands. Membranes were stripped and re-probed with mouse anti-glyceraldehyde 3-phosphate dehydrogenase (GAPDH; 1:25,000) monoclonal antibody (Abcam, Cambridge, MA) to verify equal loading.

2.3.6 ETF fluorescence reduction assay

The electron transfer flavoprotein (ETF) fluorescence reduction assay was performed using a Jasco FP-6300 spectrofluorometer (Easton, MD) with cuvette holder heated with circulating water at 32°C, as previously described [19, 117]. ETF was diluted 1200-fold into a buffer containing 50 mM Tris, pH 8.0, 5 mM EDTA and 50% glycerol, and 10 µl were used for each assay. The ETF concentration in the reaction mixture was 2 µM. 30 µM of isovaleryl-CoA lithium salt hydrate (iC5-CoA; Sigma-Aldrich Co., St. Louis, MO) or octanoyl-CoA lithium salt hydrate (C8-CoA; Sigma Aldrich Co.) were used to measure IVD and medium chain acyl-CoA dehydrogenase (MCAD) activity, respectively. Spectra Manager 2 software (Jasco, Inc.) was used to collect data and calculate reaction rate and Microsoft Excel was used to calculate kinetic parameters.

2.3.7 Digital droplet polymerase chain reaction (ddPCR)

Genomic DNA from HEK293T parental, control and *IVD* null clonal lines, and from patient fibroblasts was restriction digested with *XbaI* and diluted to a concentration of 18 ng/µl with 2 µl used as input per reaction. Multiplex probe-based ddPCR assays (Supplementary Table S3) were setup with FAM labeled Taqman probe PCR assays for *IVD* exons (1, 2, 3, 4, 9 or 12) and either HEX labeled Taqman probe PCR assays for reference loci either external (*RPP30*, *XIST*) or internal (*IVD* exon 4). The ratio of the target *IVD* exon to expected diploid reference gene was calculated based on the concentration of each (copies per µl) within a single reaction with a 95% confidence interval indicated by Poisson statistics [118].

2.3.8 *IVD* variant vector design and isolation

Control and variant *IVD* gene pcDNA3.1(+) mammalian expression vectors were constructed by BioMatik (Willmington, DE). ENST00000651168.1 IVD-215 was used in the vector construct. Mutations were introduced via site-directed mutagenesis. *IVD* pcDNA3.1(+) vectors were transformed into XL-1-Blue supercompetent Escherichia coli (E. coli) (Agilent Technologies, Santa Clara, CA) and grown in Luria-Bertani (LB) broth and 100 µg/mL ampicillin. Supercoiled plasmid DNA was prepared using a midi prep kit (Zymo Research, Irvine, CA).

2.3.9 Transfection of *IVD* mutant vectors

HEK293T *IVD* KO cells were seeded into 6-well plates or 10 cm^2 dishes and cotransfected with 2.5 or 15 µg of plasmid DNA, respectively, at 60% confluency using *Trans*IT X2 (Mirus Bio

LLC, Madison, WI). Cells were incubated for 48 hours and then harvested for western blotting and ETF reduction assay for IVDH protein presence and enzyme activity.

2.3.10 Computational Molecular Modeling

To examine the environment of residues and their interactions with others, a computer model of IVDH was visualized using a Silicon Graphics Fuel workstation (Mountain View, CA) and the *Insight* II 2005 software package, which included *Homology*/*Modeler*, and *Discover* modules and the atomic coordinates of monomers A and B of human IVDH (PDB: 1IVH) in the dimer form, as reference molecule [15]. An IVDH:ETF ternary complex was modeled using the MCAD complexed with the ETF (PDB: 1T9G), [119]. Using *Homology*, the known IVDH and MCAD structures were "Superimposed" by matching their secondary structures to examine the IVDH:ETF complex interactions and the possible effect on IVDH ETF interaction.

2.3.11 Statistics

Data are presented as mean ± standard deviation (SD) for replicates and analyzed using unpaired Students *t* test (Graphpad Version 7, graphpad.com). Statistical significance was considered $p < 0.05$.

2.4 RESULTS

2.4.1 CRISPR/Cas9 IVD gene editing

The *IVD* gene on human chromosome 15 contains 12 exons and encodes a 423 amino acid polypeptide [120]. Traditionally, the 30 amino acid mitochondrial targeting leader sequence has been removed from protein variant nomenclature [19, 31, 39, 121] but the full-length protein annotation is used in ClinVar. An in-frame ATG that is 9-nt upstream is annotated in alternate GENCODE transcript annotation gives the potential for an alternative translational initiator with a slightly larger product, but is poorly conserved and deviates from the consensus Kozak sequence [120, 121], and is not reflected in the ClinVar SNP annotation. In addition, alternative spliced products with either exon 2 skipping or an extended exon 2 associated with an alternate downstream UTR are annotated in the NCBI RefSeq database. Notably, *IVD* intron 1 splice acceptor mutations leading to constitutive exon 2 skipping is associated with IVA diagnoses [39].

To evaluate the function of variants of unknown significance identified through clinical sequencing we sought to create a robust method that would ultimately be amenable to analysis of variants in multiple genes as well as high throughput techniques. We first generated functional null mutations in *IVD* in HEK293T cells by targeting *IVD* exons 2-3 to recapitulate the murine $Ivd^{tm1b(EUCOMM)Hmgu}$ homozygous lethal null allele [122]. A dual CRISPR single guide (sgRNA) strategy [123] was implemented with a pair of sgRNAs designed to induce Cas9-nuclease mediated double-stranded DNA breaks (DSBs) *in cis* at *IVD* introns 1 and 3 to generate deletion or inversions of the intervening 847 bp sequence containing exons 2-3 (Fig. 6A). Genomic breakpoint PCR assays using primers flanking the sgRNA sites enabled the identification of genome-edited alleles (Figs. 6A-B; S1A-B). Vector-based CRISPR/Cas9 reagents for the expression of sgRNAs

and spCas9-P2A-GFP [105] were transfected into HEK293T cells and clonal lines were derived by isolation and expansion of single GFP-positive cells. We initially tested the efficiency of dual sgRNA targeting with four permutations of *IVD* sgRNAs in bulk transfected cells before selecting the most efficient pair for clonal derivatization. In our *IVD* CRISPR-Cas9 genome-editing screen 13 out of 21 HEK293T clonal lines amplified a deletion breakpoint PCR band (Figs. 6B and S1B, top panel). A similar, high frequency of inversion alleles was detected by proximal (11 of 21) and distal (12 of 21) inversion breakpoint PCR assays (Figs 6B and S1B, second panel). Further, as evidenced by the lack of amplification of intact sgRNA sites we identified potential homozygous genome-edited lines (Figs. 6B and S1B, bottom panel).

Confirmation of genomic deletion, inversion and sgRNA site PCRs by Sanger sequencing revealed the exact molecular composition of genome-edited alleles in 3 homozygous *IVD* null lines (4-3, 4-13 and 4-16) and two controls (4-11 and 4-20) (Figs. S2, S3 and S4). Sanger sequencing identified a single deletion-breakpoint and distal inversion allele in 4-3 (Figs. S1A, S2B) and subsequently the proximal inversion breakpoint was identified that contained a partial deletion of intron 1 (Fig. S3B). Clone 4-13 likewise had a single deletion-breakpoint (Fig. S2A) but on further PCR analysis also contained a second larger deletion allele spanning from exon1 into intron 3 (Fig. S4A). In contrast, clone 4-16 yielded a dual chromatograph for the deletion-breakpoint PCR indicating heterozygosity, and two alleles distinguished by a single nt were subsequently cloned and sequenced (Supplemental Figs. 2A and 2A). Sequencing of control line 4-11 revealed heterozygosity of alleles with small indels at each intronic CRISPR sgRNA site indicating two unique intact alleles (Figs. S2C-D and S2B-C). In contrast line 4-20 contained a single intact allele (Figs S2C-D).

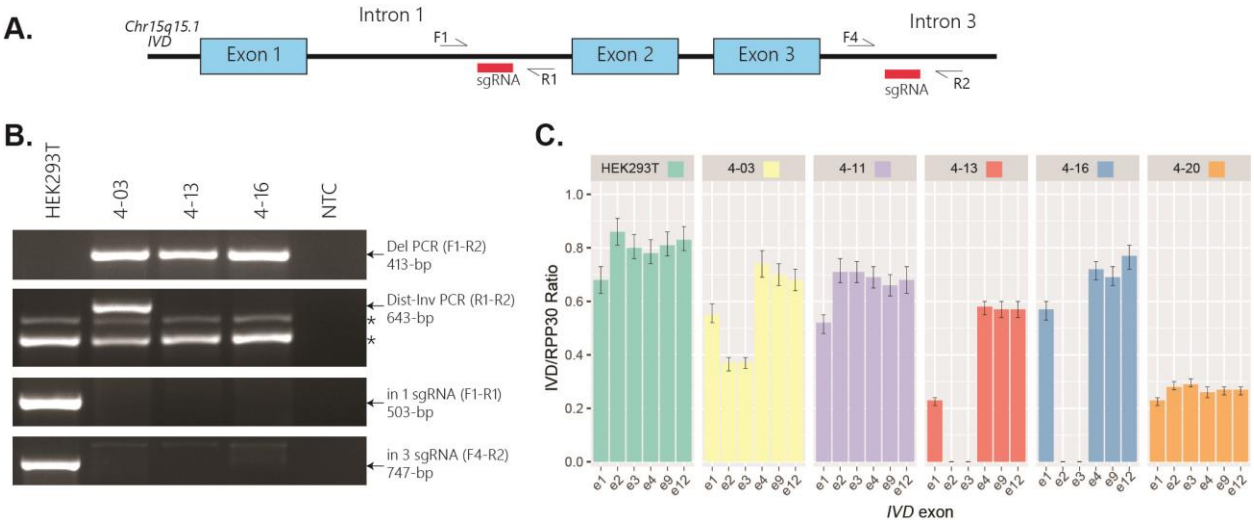

Figure 6. Targeted deletion of IVD exons 2-3 by using CRISPR/Cas9 genome-editing

(A)Location of sgRNA and genotyping primers used to generate and screen for *IVD* null alleles. Key: Blue box, *IVD* exons with intervening introns; pink rectangles, sgRNA intron 1 and 3 sites; directional arrows, genotyping primers. (B) Genotyping PCR assays identifying 3 *IVD* null clonal HEK293T lines through presence of deletion (top) and/or inversion (second from top) breakpoint-PCR bands and lack of intact sgRNA sites (bottom). * indicates non-specific band. (C) Genomic copy number of *IVD* as ascribed by the ratio of *IVD* to *RPP30* by ddPCR. Note that HEK293T is likely pseodotriploid for the RPP30 locus and that technical variability led to lower-than-expected exon 1 estimates. Bars represent absolute copy number ratio of *IVD* exons across the locus with Poisson distribution 95% confidence intervals.

Quantitative genomic copy number analysis across the *IVD* locus by droplet digital PCR (ddPCR) provided definitive proof of clonal *IVD* null HEK293T cell line genotypes (Fig. 6C). Parental HEK293T showed a ratio of *IVD* exons 1-12 to *RPP30*, an unlinked single copy locus on chr10 that was close to 0.8 reflective of a mixed population of pseudotriploid lineages as has been reported by cytogenetic studies [124, 125]. In contrast, the clonal lines had a ratio closer to 0.65 at intact exons suggesting a stable ratio of 2:3 indicative of diploid chr15 (*IVD*) and triploid chr10 (RPP30). Exons 2 and 3 show a clear reduction to heterozygous levels in 4-3 as the inversion allele

is still detected. In contrast the copy number of exons 2-3 in 4-13 and 4-16 are completely ablated, evidence of homozygous deletion. Heterozygosity is also observed in 4-13 exon 1 reflective of the larger deletion allele and across all exons in 4-20 indicative of aneuploidy. Similar results were observed in genomic copy number ddPCR assays using either XIST (known triploid locus in HEK293T), or by using *IVD* exon 4 as an internal reference (Fig S5). Deletion of exons 2-3 results in a frame shift deletion. Thus, we have identified and fully characterized genome editing events in three independent *IVD* null HEK293T clonal lines as well as a normal and haploid control.

2.4.2 Functional characterization of IVD null HEK293T cells

Western blotting was performed to determine the amount of IVDH protein present in the deleted HEK293 cell lines (Fig. 7A). Intact clonal line 4-11 had equivalent IVDH protein abundance compared to the parental lineage control, whereas aneuploid clone 4-20 had reduced IVDH protein levels. As expected, *IVD* null HEK293T clones 4-13, 4-16, and 4-3 had no detectable IVDH protein. IVDH and MCAD enzyme activity was assessed using the ETF fluorescence reduction assay (Fig. 7B-C). While 4-11 had the same level of activity as the parental HEK293T, clone 4-20 had partial activity and the three *IVD* null clones 4-3, 4-11 and 4-16 had minimal activity (Fig. 7B). There was no statistical difference in MCAD enzyme activity in control and all *IVD* deletion clones (Fig. 7C).

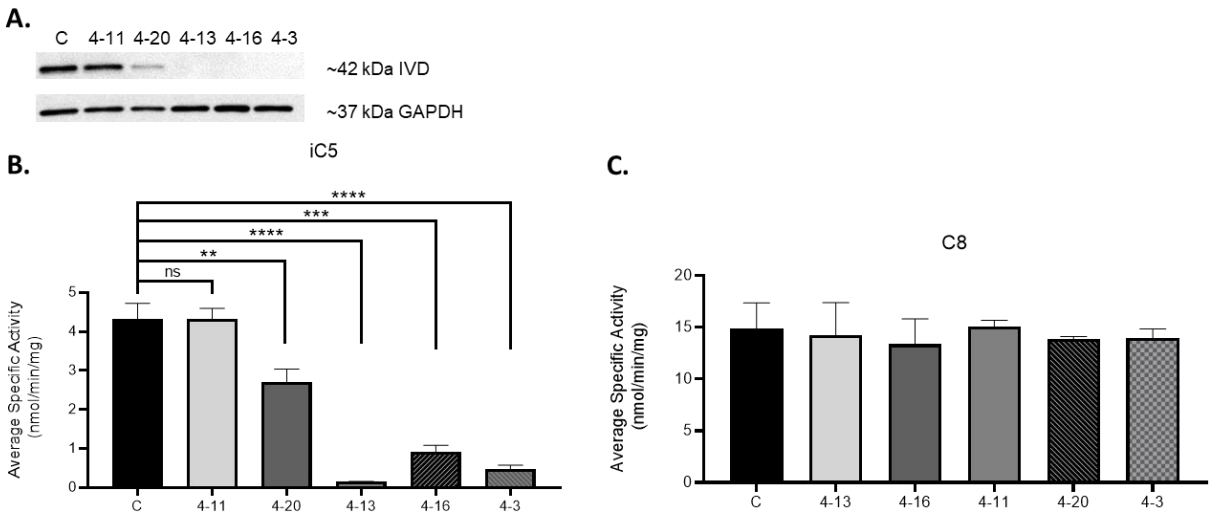

Figure 7. Protein and enzymatic activity of control and IVD null HEK293T lines.

(A) Western blot for IVDH confirms its absence in clonal lines 4-13, 4-16 and 4-3 and reduction in line 4-20. (B) Enzymatic activity of IVDH (isovaleryl-CoA as substrate) and (C) and MCAD (octanoyl-CoA as substrate). IVDH activity assays were done in triplicates and octanoyl-CoA assays were done in duplicates. Means and standard deviations were calculated. Data were analyzed using paired T-test. ****p<0.0001, *** p<0.001, **p<0.01, ns = no statistical difference.

2.4.3 Genetic and functional validation of variants of uncertain significance in IVA patient fibroblasts

Fibroblasts from four IVA patients containing clinically determined mutations and VUSs were analyzed for IVDH activity using the ETF fluorescent reduction assay (Table 1). Genetic mutations were confirmed at the mRNA level through Sanger sequencing of RT-PCR products (Fig. S6). All variants were detected at heterozygous levels in the sequence chromatograph except for c.1232G>A (p.Arg411Gln) in FB909, which was homozygous. To rule out changes in *IVD* copy number in the IVA patients we utilized ddPCR and found the locus to be diploid across the entire gene (Fig S7).

Additionally, functional analysis revealed that all four patient fibroblast lines had reduced IVDH protein presence in cell lysates (Fig. 8A) and reduced IVDH enzyme activity compared to control (Fig. 8B), consistent with clinically defined IVA. While FB825 and FB827 also had reduced MCAD activity compared to the concurrent control (Fig. 8C); it was within the range that we have observed in other control fibroblast lines.

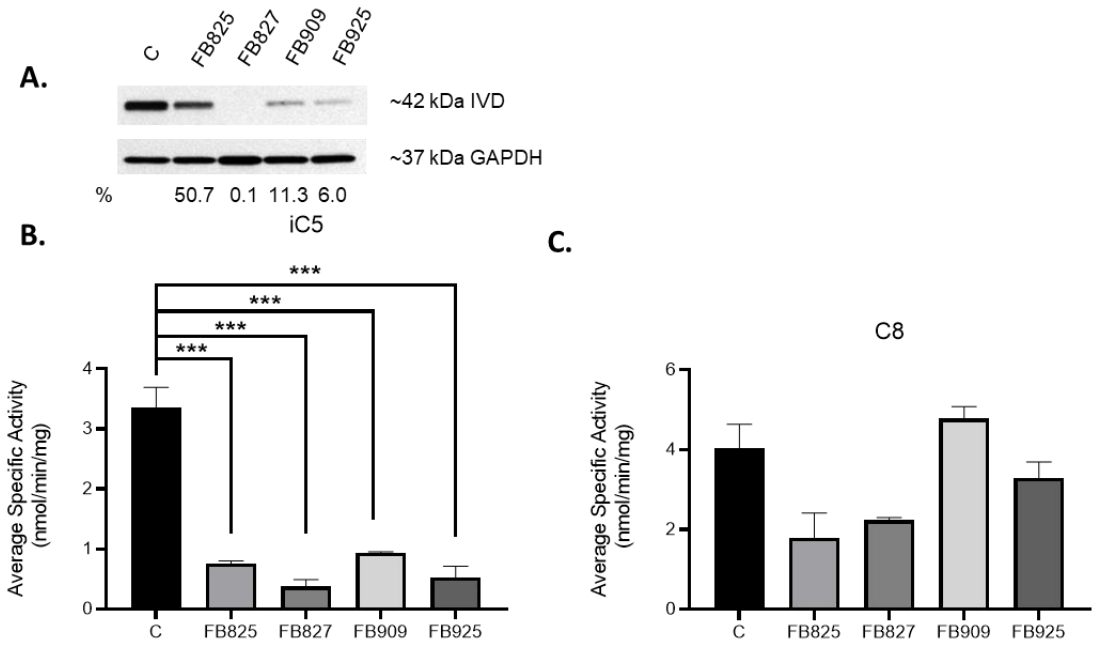

Figure 8. Protein expression and enzymatic activity assays for IVA patient-derived fibroblasts.

(A) Western blot of IVA patient and control fibroblasts for detection of IVDH and GAPDH (B) Enzymatic activity assay for IVDH (isovaleryl-CoA as substrate). (C) Enzymatic ETF assay for MCAD (octanoyl-CoA substrate). IVDH activity assays were done in triplicates and octanoyl-CoA assays were done in duplicates. Means and standard deviations were calculated. Data were analyzed using unpaired T-test. ***$p<0.001$.

2.4.4 Functional analysis of individual VUS alleles in HEK293T IVD null lines

To evaluate the effect of *IVD* VUS alleles we evaluated protein expression and enzymatic activity in *IVD* null HEK293T cells that were transfected with vectors driving expression of normal consensus *IVD* cDNA or *IVD* cDNA containing individual mutations from variants identified in IVA patients (Table 1, Fig. 9). Abundant IVD protein levels were observed with expression of control, c.521T>G (p.Val174Gly), c.932C>T (p.Ala311Val), c.707C>T (p.Thr236Ile), and c.1232G>A (p.Arg411Gln) cDNAs (Fig. 4A). In contrast, IVDH protein was hardly observed with expression of c.149G>C (p.Arg50Pro), c.986T>C (p.Met329Thr), c.1010G>A (p.Arg337Gln) and c.1179del (p.Leu394fs) cDNAs (Fig. 9A). To confirm that the lack of IVDH was due to unstable protein and not lack of expression from the plasmid, RT-PCR was performed on transfected IVD KO HEK293T cells. All transfected cells had *IVD* mRNA confirming expression was expressing the *IVD* gene properly (Fig. 9D). *GPI* was used as an internal control and had no change in mRNA expression in untransfected or transfected cells (Fig. 9D). Expression of the control cDNA in *IVD* null HEK293T cells led to dramatic increase in IVDH activity (Fig. 9B). While expression of c.521T>G (p.Val174Gly) *IVD* cDNA partially rescued enzymatic activity, all other tested mutations showed little or no enzyme activity. Expression of the common c.932C>T (p.Ala311Val) variant had 12% of the control plasmid, consistent with previous expression studies of this variant [20]. MCAD activity was unperturbed by transfection of either control or variant *IVD* cDNAs (Fig. 9C).

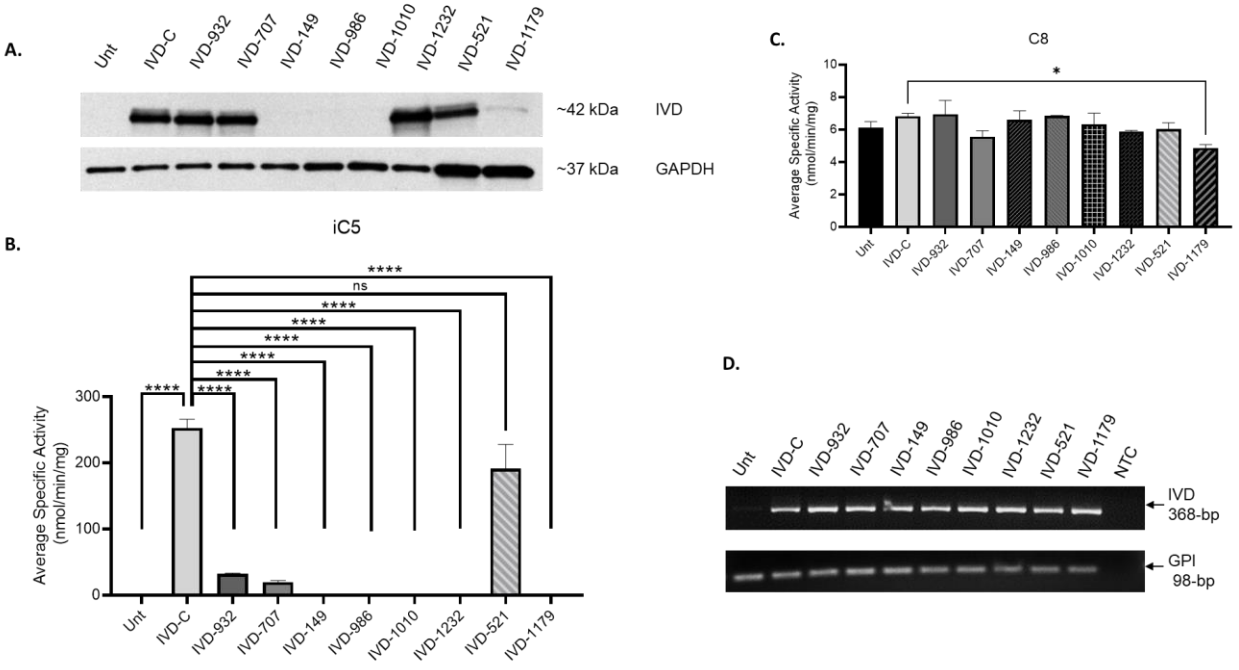

Figure 9. Expression and enzymatic activity of IVD VUSs in an IVD null HEK293T cell line.

(A) Detection of IVDH protein levels by western blot to evaluate protein stability of control and variants expressed from cDNA vectors with GAPDH an internal loading standard. (B) Activity of IVDH and (C) MCAD using the ETF fluorescence reduction assay. IVDH activity assays were done in triplicates and octanoyl-CoA assays were done in duplicates. Means and standard deviations were calculated. Data were analyzed using unpaired t test showing significant difference, ****$p<0.0001$, *$p<0.05$, ns = no statistical difference.

Table 1. Identified IVD mutations and their corresponding pcDNA3.1(+) plasmid designations and corresponding fibroblast line origin.

Cell Line Designation Origin	Mutation	Functional Protein Seq#/location	Plasmid ID	Key Interacting Residue(s)**/ Ligand	Experimental Finding	Current ClinVar Status	Proposed ClinVar Status***
FB826	Control	N/A	IVD-C	N/A	IVDH protein: normal Enzyme activity: normal	––	––
FB825	c.932C>T*, p.Ala311Val	Ala282Val α-helices G-H loop	IVD-932	Adenine of the C5-CoA	IVDH protein: normal Enzyme activity: reduced	Pathogenic	Pathogenic
FB825	c.707C>T, p.Thr236Ile	Thr207Ile β-strand 6	IVD-707	**Phe205**	IVDH protein: normal Enzyme activity: reduced	VUS	Pathogenic/Likely Pathogenic
FB118	c.149G>C*, p.Arg50Pro	**Arg21**Pro	IVD-149	Anchors Asp7 to **Tyr312**, Asn11, Leu81	IVDH protein: reduced Enzyme activity: reduced	Pathogenic/ Likely Pathogenic	Pathogenic/Likely Pathogenic
FB827	c.986T>C, p.Met329Thr	**Met300**Thr α-Helix H	IVD-986	Thr273, **Val342**, Cys349	IVDH protein: reduced Enzyme activity: reduced	VUS, Not in ClinVar	Pathogenic/Likely Pathogenic
FB827	c.1010G>A, p.Arg337Gln	**Arg308**Gln α-Helix H	IVD-1010	Asp7, **Gln267**, Leu304	IVDH protein: reduced Enzyme activity: reduced	VUS	Pathogenic/Likely Pathogenic
FB909	c.1232G>A*, p.Arg411Gln	**Arg382**Gln α-Helix K	IVD-1232	**Asp299''**, **Glu337, Glu379**	IVDH protein: normal Enzyme activity: reduced	VUS, Conflicting Interpretations	Pathogenic/Likely Pathogenic
FB925	c.521T>G, p.Val174Gly	**Val145**Gly	IVD-521	**Met248**, Ser190	IVDH protein: normal Enzyme activity: normal	VUS	Benign/Likely Benign
FB925	c.1179del> fs, p.Leu394Phe	Leu365Phe, 7 nonsense residues, and truncating α-Helix J and K	IVD-1179	--	IVDH protein: absent Enzyme activity: absent	Pathogenic/Likely pathogenic	Pathogenic

*See detailed molecular study [20]

**In bold, invariant residues.

***Pathogenicity increases under stress conditions.

2.4.5 Computational prediction of mutations' adverse structure/function effect

To assess the potential adverse structure/function caused by these mutations, two tools are utilized: *in silico* molecular modeling using the crystal structure of IVDH, a dimer of dimers, and a modeled IVDH:ETF mutant ternary complex and homology alignment of IVDH from various eukaryotic species (Fig. 10). Arg21 (mature numbering), an invariant across species, is located at the middle of α-helix A and is a structurally important residue as it functions synergistically with Arg308 (mature numbering), an invariant, to anchor the N-teminal α-helix A region to the rest of the monomer through α-helices G and C [15] (Fig. 10). Both arginines interact with Asp7, highly conserved, with the Arg21 also interacting with the invariant Tyr312 (mature numbering) and the Arg308 interacting with the invariant Gln267 (mature numbering). The kink introduced by the Arg21Pro mutation affects the secondary and supersecondary structure significantly of the monomer but also tetramer assembly as the N-teminal α-helix A region appears to be involved in the final the process of monomer folding as the 29-amino acid-precursor peptide is removed (Fig. 10). Moreover, proper positioning of residues in this region affects tetramer assembly as Ile10 residue, monomer A, would lose key hydrophobic interaction with the invariants Val314' and Ala317' (mature numbering) from the opposite fourth monomer D (Fig. 10). On the other hand, the Arg308Gln replacement is predicted as a milder change, albeit weakening the same region proper side chains alignments of key residues, but patients with this mutation may potentially respond to treatments that promote stability of the monomer, including substrate analogs (Fig. 10).

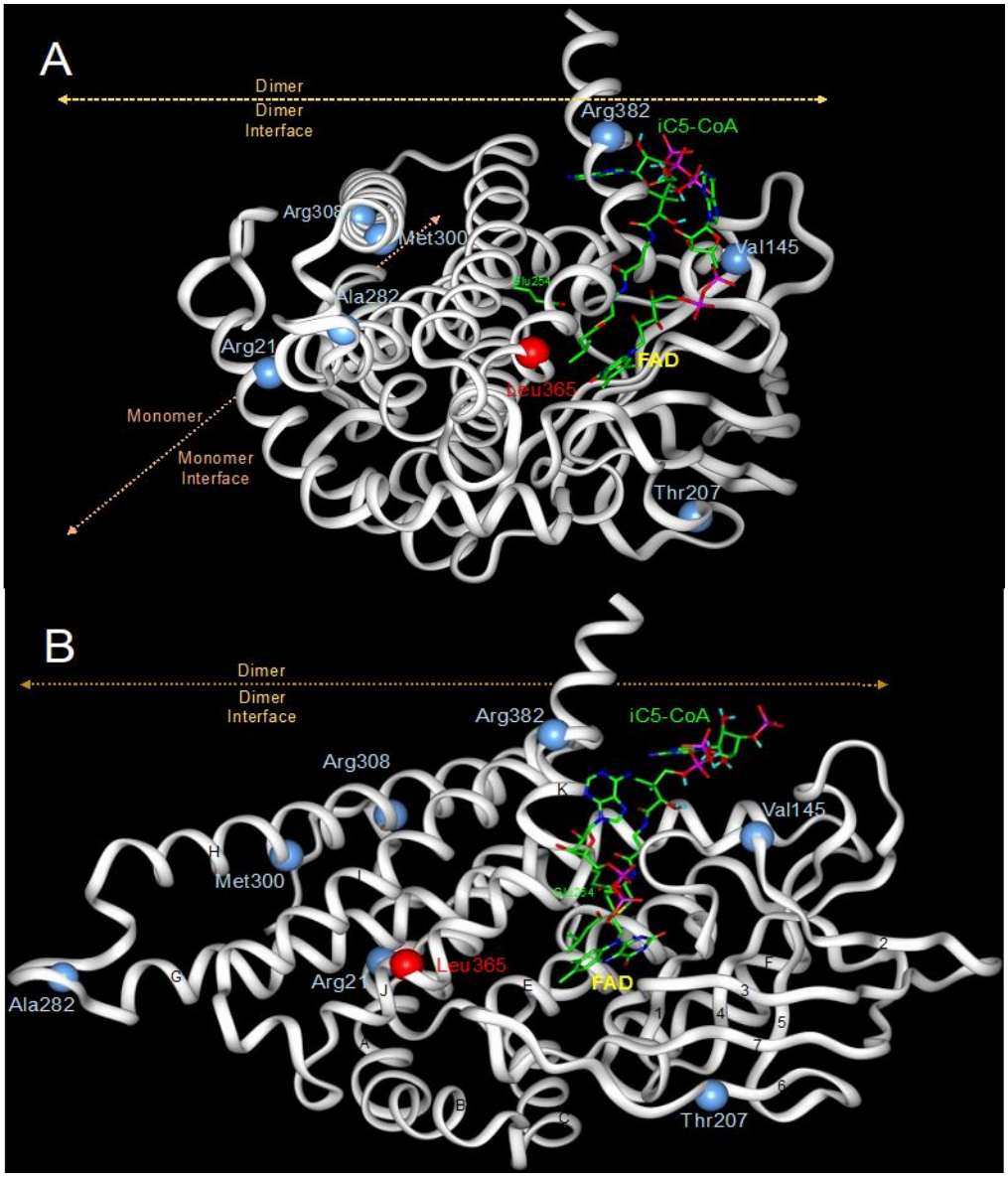

Figure 10. Ribbon representation of the three dimensional structure of an IVDH monomer using published atomic coordinates, PDB: 1IVH [96].

iC5-CoA is modeled in the active site in place of the CoA-persulfide in the published structure. The A and B views, at near right angle, depict the position of the backbone carbon atom, in blue, of amino acid residues replaced by missense mutations in the *IVD* gene in patients with IVA listed in Table 1. The c.1179del causes a frameshift and a Leu365Phe mutation, position marked in red, and premature termination and leading to the loss of most of the a-helix J and a-helix K and greatly reduced IVDH protein, see Fig. 9.

While Thr207 residue is located on β-strand 6, an important component of the β-sheet domain critical for FAD binding [15], the residue is structurally dispensable as it is conserved among higher eukaryotes but not so in lower eukaryotes (it is a valine in Drosophila, glutamine in *C. elegans*, and Arg in mosquito). Since the Thr207 methyl moiety is within interacting distance, 3.9 Å to, Phe205, which is an invariant, this implies that other than Thr has to fit in a specific conformation. While the side chain of a valine would fit spatially in the space occupied by a threonine side chain, but *in silico* replacement predicts a Gln is less accommodated. Interestingly, *in silico* replacement with an Arg at this position, and Pro at position 209, has significantly lower energy as the side chain as the guandinium moiety projects out towards the solvent. As discussed previously Ala282Val adversely affect binding of the substrate bound to the second subunit in the dimer set. However, the replacement also has some impact on protein stability [11, 20]. The IVDH Ala282Val instability is exhibited by the recombinant purified form lower melting temperature that does not improve in the presence of substrate analogues [11], providing evidence that fever is a risk factor for IVA patients with this mutation.

The c.986T>C nucleotide mutation cause an Met300Thr (mature numbering) change. Met300 residue located near the middle of α-helix H is an invariant residue located in a hydrophobic pocket formed by Val269, Thr273, Leu304, Val342 (invariant), and others (Fig. 10). The hydrophobic pocket stabilizes the supersecondary interactions of α-helices H and G. Although replacement of Met300 with a Thr should disrupt the supersecondary “glue” stabilizing function of the hydrophobic pocket, it could be tolerated to some extent provided folding is completed to the functionally active protein. Similar to the Arg308Gln mutation discussed above, this mutation may also respond to substrate analogue treatment.

The effect of c.1232G>A mutation leading to the Arg382Gln (mature numbering) change on protein stability has been examined previously [20], errored as an Arg382Leu change). The guanidinium group of Arg382 in monomer A plays a role in tetramer assembly and maintain the protein quartnary structure as both its η-N nitrogens are locked in their spatial position by the carboxylates of the invariants Glu337 and Glu379 from monomer A while its ε-N nitrogen interact with the carboxylate of the invariant Asp299" of monomer D [15]. The Arg382Gln should thus disrupt the efficiency of tetramer assembly and cause instability when formed. Because of the contribution the Gln291" residue (an invariant) of monomer D in stabilizing binding of the adenine of the FAD bound to monomer A, enzyme kinetic mechanism is also likely affected assuming cooperativity between the two subunits is a valid proposition [126, 127]. In addition, it is also reasonable to assume with multiple points of contact between the adenine of the FAD bound to monomer A and monomer D that the FAD adenine contributes to the quaternary stability of the tetramer, and therefore maximum amounts of free FAD in mitochondria may be helpful in stabilizing this IVDH Arg382Gln mutant and hence riboflavin (vitamin B2) treatment may be beneficial in treating patients with this mutation.

The c.521T>G nucleotide mutation cause a Val145Gly change. Val145 (mature numbering) is located at the end of the loop connecting β-strands 1 and 2 and juxtaposed to the ribose moiety of the CoA substrate and the loop connecting β-strands 4 and 5, which is involved in binding of the ribose moiety 2'-phosphate of the CoA substrate through the highly conserved Arg191 (mature numbering) (Fig. 10). While binding affinity and K_m of the substrate is expected to be affected, folding and/or stability is also expected to be affected, but to a lesser extent compared to the IVDH Ala311Val (Ala282Val) mutant.

2.5 DISCUSSION

Except in specific disorders, most patients with inborn errors of metabolism are identified with rare unique mutations in the disease gene, many of which are formally classified as VUSs. Indeed, new guidance by ClinVar following the American College of Medical Genetics and Genomics (ACMG) and Association for Molecular Pathology (AMP) standards and guidelines for variant calling, requires specific demonstration of impaired function of individual variant alleles to be classified as pathogenic [93, 102, 103]. To meet this goal, it will be necessary to develop high throughput methods to assess the functional effects of mutant alleles on enzyme activity for most of the inborn errors of metabolism identified by NBS. We have previously used both prokaryotic and eukaryotic expression systems (including in HEK293 deletion cell lines) to demonstrate the effect of variants in most of the acyl-CoA dehydrogenases including mutations in *ACADVL, ACADM, ACADS, IVD, SBCADH, ACAD8, and ACAD9* [19, 20, 58, 128-132]. However, our previous techniques were not particularly well suited to high throughput analysis. In this study, we describe the generation of a deletion in the *IVD* gene in HEK293T cells using CRISPR/Cas9 technology that can readily be applied to any gene of interest. HEK293T is a well-established cell line to study expression recombinant proteins [133] and though it is aneuploid at multiple loci [124, 125] we were able to obtain a high frequency of CRISPR/Cas9 genome-edited *IVD* null lines. By using a commercial gene synthesis service to rapidly generate *IVD* variants for expression in our *IVD* null HEK293T cells, we have been able to confirm pathogenicity of 5 previously uncharacterized variants, and confirmed the partial retention of activity of the common *IVD* variant identified through NBS. These studies were in keeping with confirmation of IVDH-deficiency in cell lines from four patients identified by NBS as likely having IVA. Of note, one IVA patient (FB909) was of Ashkenazi Jewish origin and had a homozygous c.1232G>A

(p.Arg411Gln) VUS with minimal enzymatic activity suggesting this mutation may be an *IVD* variant specific and of importance to this population. Molecular modeling results are consistent with our *in vitro* findings and provide additional insight into the molecular pathophysiology of the individual mutants. results are consistent with our in vitro findings and provide additional insight into the molecular pathophysiology of the individual mutants.

Based on the results above, we propose that the VUSs examined here be reclassified in ClinVar. Variants c.707T>C, (p.Thr236Ile), c.986T>C (p.Met329Thr), c.1010G>A (p.Arg337Gln), and c.1232G>A (p.Arg411Gln) should be reclassified from VUS to pathogenic/likely pathogenic; and c.521T>G (p.Val174Gly) from VUS to benign/likely benign. Variants c.932C>T (p.Ala311Val), c.149G>C (p.Arg50Pro), and c.1179del (p.Leu394 fs) should maintain their pathogenic/likely pathogenic status.

While this study used a traditional cuvette based fluorometric assay to measure IVDH activity, we have recently published a microplate version of this assay that is more amenable to high throughput analysis and can be applied to any of the acyl-CoA dehydrogenases [134]. For enzymes relevant to metabolic disease identified by NBS but without an assay amendable to high throughput analysis, an indirect assay can still lead to high throughput confirmation of pathogenicity. In the context of most disorders identified by tandem mass spectrometry, an adaptation of the standard whole cell acylcarnitine profiling should be possible with appropriate gene deleted HEK293T or other cell lines. Ultimately, development of a panel of such cell lines should allow relatively rapid confirmation of pathogenicity of variants identified in infants through NBS without the need for an invasive procedure such as a skin biopsy.

In summary, we have developed an *IVD* null HEK293T cell line with no IVDH protein or activity that allowed determination of pathogenicity of several previous VUSs found in patients

with suspected IVA identified by NBS. This model will allow for high throughput assessment of the function of VUSs in multiple genes for disorders identified by NBS and would be an ideal supplement to existing newborn screening programs to provide greater clarity of screening results.

2.6 ACKNOWLEDGEMENTS

JV was supported in part by NIH grant R01 DK109907. We thank the staff from the Core Flow Cytometry Laboratory from the University of Pittsburgh, Children's Hospital of UPMC for help with flow sorting of GFP positive cells. We thank Yuxun Zhang, PhD from Eric Goetzman, PhD Laboratory University of Pittsburgh, Children's Hospital of UPMC for ETF for the ETF fluorescence reduction assays.

2.7 AUTHOR CONTRIBUTIONS

OMD compiled data, completed all repeat experiments (clonal western blot screen, initial *IVD* variant plasmid transfection for four plasmids), performed ddPCR for the clonal screen. OMD performed western blotting and ETF fluorescence reduction assay for IVA patient fibroblasts and western blotting, ETF fluorescence reduction assay, and RT-PCR for *IVD* variant plasmid transfections in *IVD* null HEK293T cell lines to determine *IVD* variant pathogenicity. OMD reviewed literature, performed statistical analysis, drafted and revised manuscript. EAK developed CRISPR/Cas9 experimental design, sgRNA design, and ddPCR experimental design. EAK helped

with additional DNA sequencing analysis for IVA patient fibroblasts and HEK293T *IVD* null cell lines, and revision of manuscript. ANA developed experimental design, initial clonal screen, and *IVD* mammalian expression plasmid design. CK completed ETF fluorescence reduction assay for the HEK293T null *IVD* clonal screen. AK completed initial western blot for the HEK293T *IVD* null clonal screen. A-WM completed the *in silico IVD* variant modeling. JV developed experimental design and reviewed manuscript. All authors reviewed manuscript prior to publication.

3.0 DEVELOP AND CHARACTERIZE AN *ACADVL* NULL HEK293T MODEL TO ALLOW FOR RAPID ANALYSIS OF VARIANTS OF UNCERTAIN SIGNIFICANCE

This chapter has been published in the Journal of Inherited Metabolic Disease. The article is reproduced here under license from Wiley with only minor formatting and non-scientific changes. The original article and supporting information are available online at https://doi.org/10.1002/jimd.12492.

Olivia M. D'Annibale[1,2], Erik A. Koppes[1], Meena Sethuraman[3], Kaitlyn Bloom[1], Al-Walid Mohsen[1,2], Jerry Vockley[1,2]

[1]Division of Genetic and Genomic Medicine, Department of Pediatrics, University of Pittsburgh School of Medicine, and UPMC Children's Hospital of Pittsburgh, Pittsburgh, PA 15224;

[2]Department of Human Genetics, University of Pittsburgh Graduate School of Public Health, Pittsburgh, PA 15261;

[3]University of Pittsburgh School of Medicine, Pittsburgh, PA 15261.

3.1 ABSTRACT

Very long-chain acyl-CoA dehydrogenase deficiency (VLCADD) is an autosomal recessive disease caused by mutations in the *ACADVL* gene and is among the disorders tested for in newborn screening (NBS) panels. Confirmatory sequencing following suspected VLCADD

NBS results often identifies variants of uncertain significance (VUS) in the *ACADVL* gene, leading to uncertainty of diagnosis and providing effective treatment regimen. Currently, *ACADVL* has >350 VUSs in the ClinVar database that requiring characterization to determine potential pathogenicity. In this study, CRISPR/Cas9 genome editing was used to knock out *ACADVL* in HEK293T cells, and targeted deletion was confirmed by droplet digital PCR. No VLCAD protein was detected and an 84% decrease in enzyme activity using the ETF fluorescence reduction assay and C21-CoA as substrate was observed compared to control. Plasmids containing control or variant *ACADVL* coding sequence were transfected into the *ACADVL* null HEK293T. While transfection of control *ACADVL* restored VLCAD protein and enzyme activity, cells expressing the VLCAD Val283Ala (precursor numbering) mutant had 18% VLCAD enzyme activity and reduced protein compared to control. VLCAD Ile420Leu, Gly179Arg, and Gln406Pro produced protein comparable to control but 25%, 4%, and 5% VLCAD enzyme activity, respectively. Leu540Pro and Asp570_Ala572dup had reduced VLCAD protein and 10% and 3% VLCAD enzyme activity, respectively. VLCADD fibroblasts containing the same variations had decreased VLCAD protein and activity comparable to the transfection experiments. Generating *ACADVL* null HEK293T cell line allowed functional studies to determine pathogenicity of *ACADVL* exonic variants. This approach can be applied to multiple genes for other disorders identified through NBS.

3.2 INTRODUCTION

Very long-chain acyl-CoA dehydrogenase (VLCAD) deficiency (OMIM 201475) is an autosomal recessive disorder caused by biallelic mutations in the *ACADVL* gene, 17p13.1 [41].

VLCAD catalyzes the first intra-mitochondrial step of the mitochondrial β-oxidation of long-chain fatty acids with carbon length chain of 14 to 20 [41, 110]. The frequency of VLCADD is about 1:30,000 to 1:100,000 live births world [29, 33]. Symptoms of VLCADD include hypoglycemia, recurrent rhabdomyolysis, myopathy, hepatopathy, and cardiomyopathy and can present in infancy or later in childhood or adulthood [135]. Treatment for VLCADD patients involves a reduced-fat diet containing medium chain triglyceride (MCT) or triheptanoin supplementation and avoidance of high stress and exercise [44-47]. In the United States and many other developed countries, VLCAD deficient patients are identified through newborn screening of dried blood spots with an elevated C14:1 and/or C14:1/C12:1 ratio [33]. Ultimate outcome is improved by identification of the disorder through newborn screening [136-138]. However, many patients upon follow up sequencing of *ACADVL* are found to have at least one VUS. There are currently over 350 VUSs in the ClinVar database at the time of writing.

Measuring characteristic metabolites from dried blood spots by tandem mass spectrometry (MS/MS) is the clinical standard for newborn screening (NBS) for many inborn errors of metabolism, but requires genetic or functional follow up testing to confirm a diagnosis [32]. Increasingly, diagnosis by molecular analysis through targeted, exome or whole-genome DNA sequencing is becoming the *de facto* norm for many disorders. Given the only recent emergence of these technologies as employed to diagnose rare-diseases there are only a limited number of clinically described and annotated pathogenic alleles. Therefore, DNA sequencing-based diagnostic methods often result in identification of variants of uncertain significance (VUS) in at least one allele, leading to uncertainty of the diagnosis [92]. In this situation, a definitive diagnosis can only be made through functional testing (*e.g.* enzymatic activity assays from patient dermal

fibroblast), which is often either not available or cumbersome to obtain and can lead to a significant delay of treatment implementation [92, 94].

In this study, we describe a scalable approach to determine the functional significance of VUSs identified by NBS in a timely manner to facilitate better diagnostic and therapeutic outcomes. We have previously developed an *IVD* null HEK293T model to screen VUS mutations in *IVD* [139]. Here we present an expansion of this system by examining the functional effect of VUSs identified in newborns in an *ACADVL* null HEK293T cell line generated with CRISPR/Cas9 genome-editing. This model enables determination of pathogenicity of individual *ACADVL* VUSs, and is amendable for development as a high throughput platforms for screening VUSs in other inborn errors of metabolism.

3.3 MATERIALS AND METHODS

Experiments were performed in accordance with the approved guidelines and regulations. Experimental human protocols were approved by the Institutional Review Board at the University of Pittsburgh, protocol 19030195.

3.3.1 Subjects

Subjects were identified through abnormal NBS with elevation of C14:1-carnitine consistent with VLCAD deficiency (Supplementary Table S5). Sequencing of *ACADVL* was performed on a clinical basis in a CLIA certified laboratory on the proband and parents to determine *ACADVL* mutation and phase. Skin biopsies for fibroblast culture were performed on a

clinical basis from infants with consent of parents and/or legal guardians. Control fibroblast cells were obtained from the American Type Culture Collection (ATCC.org).

3.3.2 Cell lines & culture

HEK293T (obtained from the American Type Culture Collection) and fibroblast cell lines were grown in Dulbecco's Modified Eagle Medium (DMEM; Corning Life Sciences, Manassas, VA) containing 4.5 g/L glucose and supplemented with 10% fetal bovine serum, 4 mM glutamine and 100 IU penicillin and 100 µg/ml streptomycin (Corning Life Sciences, Manassas, VA) at 37 °C in a 5% CO_2 humidified atmosphere.

3.3.3 CRISPR/Cas9 genome-editing

Genome-editing of HEK293T cells using a plasmid vector based CRISPR/Cas9 strategy was accomplished as described before [139]. In brief, we utilized single-guide RNAs (sgRNAs) within *ACADVL* exon 12 and exon 16 cloned into pSpCas9(BB)-2A-GFP vector (PX458; Addgene #48138) [105] to generate deletions of the intervening *ACADVL* sequence encoding a crucial region of the catalytic domain. Following plasmid transfection and single-cell GFP(+) flow sorting clonal genome-edited lines were grown and screened by breakpoint deletion PCR and positive clones further analyzed by *ACADVL* copy number and VLCAD protein assays. Oligonucleotides used for sgRNA cloning adapters and breakpoint deletion PCR primers are listed in Supplementary Table S6.

3.3.4 Western blot

Fibroblasts and HEK293T cells were grown in T175 flasks to 90% confluence, harvested by trypsinization, pelleted, and stored at -80°C for western blot. Frozen pellets were treated with 50 µL of radioimmunoprecipitation assay (RIPA) buffer (Thermofisher Scientific) and 1X Protease Inhibitor Cocktail (PI) (Roche, St Louis, MO) for 30 minutes on ice and centrifuged at 14,000 x g for 15 minutes at 4°C. Supernatants were collected and 25 µg of protein was loaded onto a 4 to 15% gradient Criterion precast SDS-PAGE gel (Biorad, Hercules, CA). Following electrophoresis, the gel was blotted onto a nitrocellulose membrane and incubated with mouse anti-ACADVL antibody (1:2000; Invitrogen, Waltham, MA), then incubated with secondary goat anti-mouse-HRP antibody (1:3000, Biorad). Pierce ECL Western Blotting Substrate kit (Thermofisher Scientific) was used to visualize bands. Membranes were stripped and re-probed with mouse anti-glyceraldehyde 3-phosphate dehydrogenase (GAPDH; 1:25,000) monoclonal antibody (Abcam, Cambridge, MA) to verify equal loading.

3.3.5 ETF fluorescence reduction assay via cuvette

The electron transfer flavoprotein (ETF) fluorescence reduction assay was performed using a Jasco FP-6300 spectrofluorometer (Easton, MD) with cuvette holder heated with circulating water at 32°C, as previously described [19, 117]. ETF was diluted 1200-fold into a buffer containing 50 mM Tris, pH 8.0, 5 mM EDTA and 50% glycerol, and 10 µl were used for each assay. The ETF concentration in the reaction mixture was 2 µM. 30 µM of palmitoyl-CoA lithium salt hydrate (C16-CoA; Sigma-Aldrich Co., St. Louis, MO) or heneicosanoyl-CoA ammonium salt (C21-CoA; Avanti Polar Lipids, Alabaster, AL) were used to measure VLCAD activity. 30 µM of

octanoyl-CoA lithium salt hydrate (C8-CoA; Sigma Aldrich Co.) was used to measure medium chain acyl-CoA dehydrogenase (MCAD) activity. Spectra Manager 2 software (Jasco, Inc.) was used to collect data and calculate reaction rate and Microsoft Excel was used to calculate kinetic parameters.

3.3.6 ETF fluorescence reduction assay via microplate

Recombinant pig ETF was purified according to the method published earlier [134]. A microtiter plate adaptation of the ETF fluorescence reduction assay was performed using FLUOstar Omega (BMG Labtech, Cary, NC) microplate reader set to 32°C, with excitation/emission wavelengths of Ex_{340}/Em_{490} as previously described [19, 117, 134]. Briefly, the final reaction volume of 200 µl contain 30 µg of sample and the ETF concentration, glucose/oxidase concentrations and substrate concentration were the same as for the cuvette assay. Sample and all reagents except substrate were added in triplicate to a glass-bottomed, black walled plate. With background fluorescence zeroed, baseline ETF fluorescence was monitored for 60 s, substrate was added with a multi-channel pipettor, and the plate was immediately read for another 60 s. Slopes and Y-intercepts were automatically calculated by the instrument software and enzymatic activity was calculated in Microsoft Excel.

3.3.7 Digital droplet polymerase chain reaction (ddPCR)

Copy number assays using ddPCR probe-based assays were designed and completed as previously described [139]. Genomic DNA from parental HEK293T and *ACADVL* CRISPR-Cas9 targeted clonal lines, was restriction digested with *EcoRI*-HF (New England Biolabs, Ipswich,

MA) and diluted to a concentration of 20 ng/µl with 2 µl used as input per reaction. Multiplex ddPCR assays utilized PrimeTime 5′ nuclease probes (IDT, Coralville, IA) which were FAM labeled for *ACADVL* intron 11 and exons 10, 15, or 20 and HEX labeled for the autosomal *RPP30* reference locus (Oligonucleotide probe and primers given in **Supplemental Table 3**). The ddPCR reactions were run on an automated droplet generator and QX200 reader (Biorad). The genomic copy number of the target *ACADVL* region was calculated under the assumption that *RPP30* was diploid (i.e. the ratio of the concentration of target *ACADVL* amplicon to *RPP30* multiplied by 2) with a 95% confidence interval indicated by Poisson statistics [118].

3.3.8 *ACADVL* variant vector design and isolation

Control and variant *ACADVL* gene pcDNA3.1(+) mammalian expression vectors were constructed by BioMatik (Willmington, DE). To produce the expression plasmids in amounts for transfection experiments, *ACADVL* pcDNA3.1(+) vectors were transformed into XL-1-Blue supercompetent Escherichia coli (Agilent Technologies, Santa Clara, CA) and grown in Luria-Bertani (LB) broth and 100 µg/mL ampicillin. Plasmids DNA were isolated using a midi prep kit (Zymo Research, Irvine, CA).

3.3.9 Transfection of ACADVL mutant vectors

ACADVL null HEK293T cells were seeded into 6-well plates or 10 cm^2 dishes and co-transfected with 2.5 or 15 µg of plasmid DNA, respectively, at 60% confluency using *Trans*IT X2 (Mirus Bio LLC, Madison, WI). Cells were incubated for 48 hours and then harvested for western blotting and ETF reduction assay for VLCAD protein presence and enzyme activity.

3.3.10 ACADVL cDNA analysis

ACADVL variant plasmid transfected *ACADVL* null HEK293T mRNA was isolated using an RNeasy Mini kit with on column DNaseI digestion (Qiagen). First strand synthesis of complementary DNA (cDNA) from 500 ng of mRNA was performed using the Superscript Vilo IV Master Mix (Qiagen). Reverse transcription PCR (RT-PCR) of full-length and partial *ACADVL* cDNA regions was performed with Q5 DNA polymerase (New England Biolabs). Quantitative PCR was performed with equivalent amount of cDNA on a Bio-Rad CFX96 Real-Time PCR Instrument, with SYBR Green Master Mix (Thermo Fisher Scientific). *ACADVL*, and *GAPDH* were assayed (Supplementary Table S8). Expression levels were normalized to *GAPDH* and the data were analyzed by the $2^{-\Delta\Delta Ct}$ method [140].

3.3.11 *ACADVL* mutant modeling

VLCAD structure visualization and mutation modeling was performed using a Silicon Graphics Fuel workstation (Mountain View, CA) and the *Insight* II 2005 software package, using the atomic coordinates of recombinant human VLCAD (pdb code: 3B96) [16]. Residues at the mutation sites were replaced manually and best energy conforming conformation, with least energy fit, was adopted for further analysis of interactions with juxtaposed residues.

3.4 RESULTS

3.4.1 CRISPR/Cas9 ACADVL gene editing

To generate a cell culture model in which to study *ACADVL* mutations with unknown functional significance, we employed CRISPR-Cas9 genome-editing to introduce null mutations into the HEK293T cell line. A dual sgRNA strategy was used to induce double-stranded DNA breaks at *ACADVL* exons 12 to 16 and delete the intervening region (Fig. 11A), including exon 15 encoding key residues of the VLCAD catalytic core [16]. From 24 clonally isolated HEK293T CRISPR-Cas9 transfected cells mutations were detected by deletion breakpoint-PCR in 14 clonal lines (Supplemental Fig. 1A-C). Further characterization of candidate genome-edited clonal lines by genomic copy number ddPCR identified 4 clonal lines (A1-02, A1-07, A1-11 and A1-15) without an intact copy of *ACADVL* exon 15 **(**Fig. 11B, Supplemental Fig. 1D). Not unexpectantly, given the heterogenous chromosomal ploidy in HEK293T [124, 125], and our previous genome editing study deriving *IVD* null HEK293T lines [139], normalization of *ACADVL* ddPCR amplicons to *RPP30* yielded evidence for an *ACADVL* haploid line with a deletion (A1-02), one diploid line with homozygous *ACADVL* deletion (A1-11), and two *ACADVL* diploid lines in with both copies harbored a deletion but which were triploid for RPP30 (A1-07 and A1-15) (Fig. 11B).

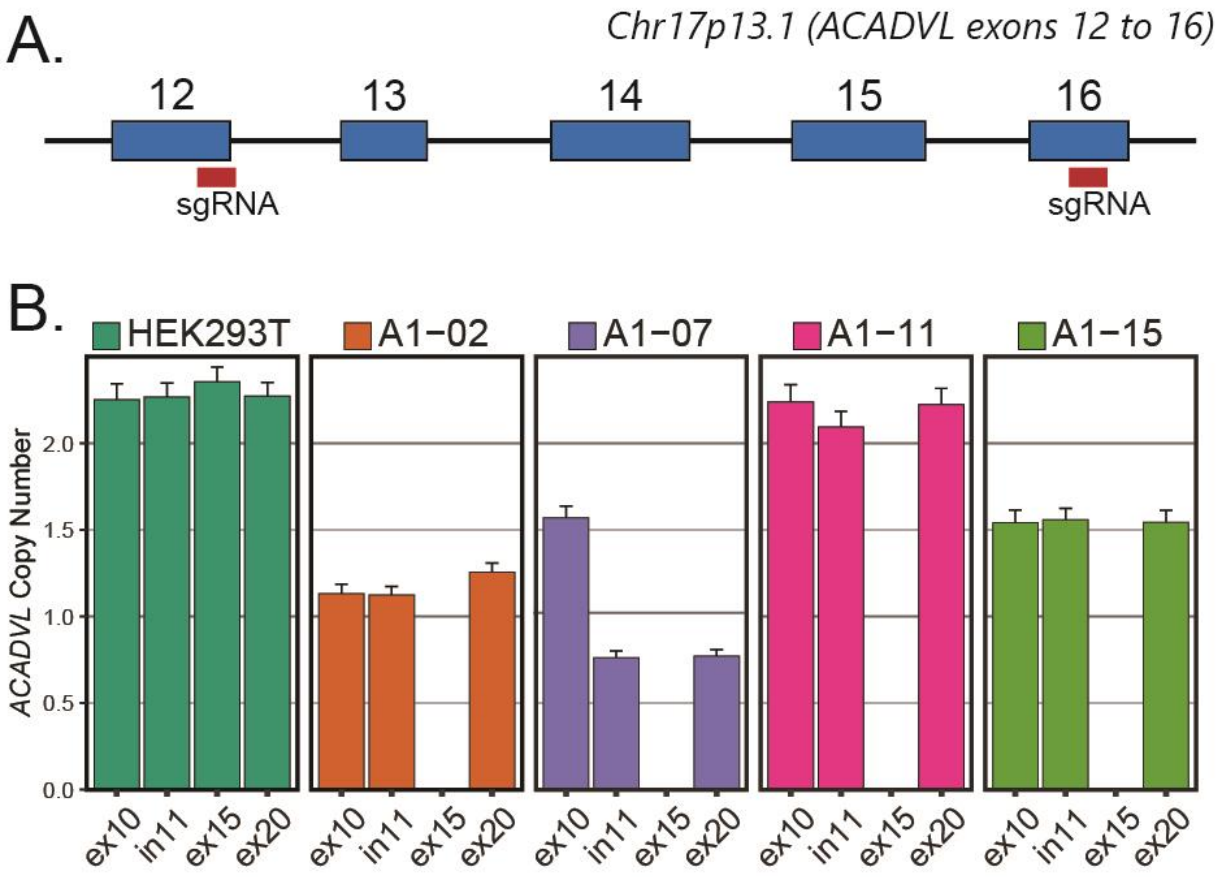

Figure 11. Targeted deletion of ACADVL exons 12-16 using CRISPR-Cas9 genome-editing.

(A) Diagram of dual sgRNA CRISPR-Cas9 strategy targeting *ACADVL*. Key: Blue box, *ACADVL* exons with intervening introns; red rectangles, sgRNA sites. (B) Genomic copy number (CN) of ACADVL exon 10, intron 11, exon 15 and exon 20 as quantified by ddPCR with normalization to the *RPP30* locus. Notably the HEK293T is near diploid (CN=2) for ACADVL across the gene whereas each clonal line exhibited complete loss of the targeted exon 15. A1-02 showed deletion of exon 15 with a haploid number (CN=1) across the untargeted region; A1-07 and A1-15 display deletion of exon15 with an inferred 3N copies of RPP30 leading to CN=1.5 for untargeted regions, with A1-07 likely having one deletion allele extending both into intron 11 proximally and through exon 20 distally; and A1-15 with an expected diploid *ACADVL* deletion pattern with observed CN of 2N at the untargeted regions and 0N at exon 15.

3.4.2 Functional characterization of ACADVL null HEK293T cells

Each of the four genome-edited clonal lines with deleted *ACADVL* exon 15 (A1-02, A1-07, A1-11 and A1-15; Fig. 11) were shown to lack detectable expression of the VLCAD protein by western blotting, thereby confirming the null mutations (Fig. 12A). VLCAD and MCAD activity were assessed using the ETF fluorescence reduction assay (Fig. 12B,C). All *ACADVL* null HEK293T clones had reduced enzyme activity measured with C16-CoA as substrate (Fig. 12B: 36 to 41% of control HEK293T). As expected, there was no statistical difference in MCAD activity between the control and clones (Fig. 12C).

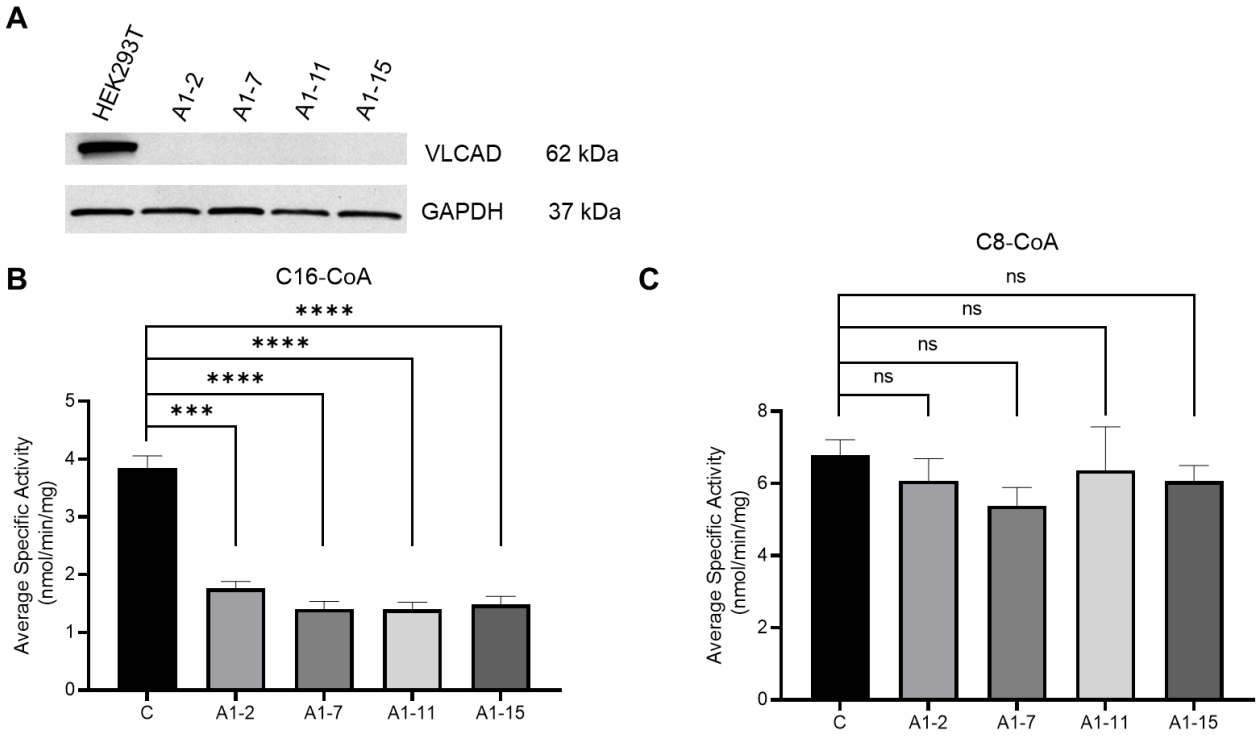

Figure 12. VLCADD protein and enzyme activity in cellular extracts from control and ACADVL null HEK293T lines.

(A) Western blot for VLCAD confirms its absence in clonal lines A1-2, A1-7, A1-11, and A1-15. Molecular mass markers are from Precision Plus Protein Dual Color Standards (BioRad)mix. (B, C) Enzymatic activity of HEK293 *ACADVL* KO extracts measure with palmitoyl-CoA (B) and octanoyl-CoA as substrate (C). All assays were performed in triplicates. Means and standard deviations calculated with an unpaired t-test are shown. ****$p<0.0001$, ***$p<0.001$, ns = no statistical difference.

The remaining activity detected by palmitoyl-CoA is related to long-chain acyl-CoA dehydrogenase (LCAD) and acyl-CoA dehydrogenase family member 9 (ACAD9) activity. To determine the level of LCAD activity, we used 2,6-dimethylheptanoyl-CoA, a specific substrate of LCAD [141]. To diminish the contribution of other ACADs having long chain activity on measuring VLCAD activity using the ETF fluorescence reduction assay, we next measured the ACAD activity using heneicosanoyl-CoA (C21-CoA), which is best utilized by VLCAD compared to LCAD and ACAD9 [142]. Clone A1-7 had reduced activity using both 16-CoA and C21-CoA compared to control, but the apparent reduction was greater with the more specific substrate, 42% and 16%, respectively, (Fig. 13A,B). While MCAD was reduced in clone A1-7 compared to control, it is still within a range seen in other experiments (Fig. 13C). LCAD activity was not statistically different in control and A1-7 clone (Fig. 13D).

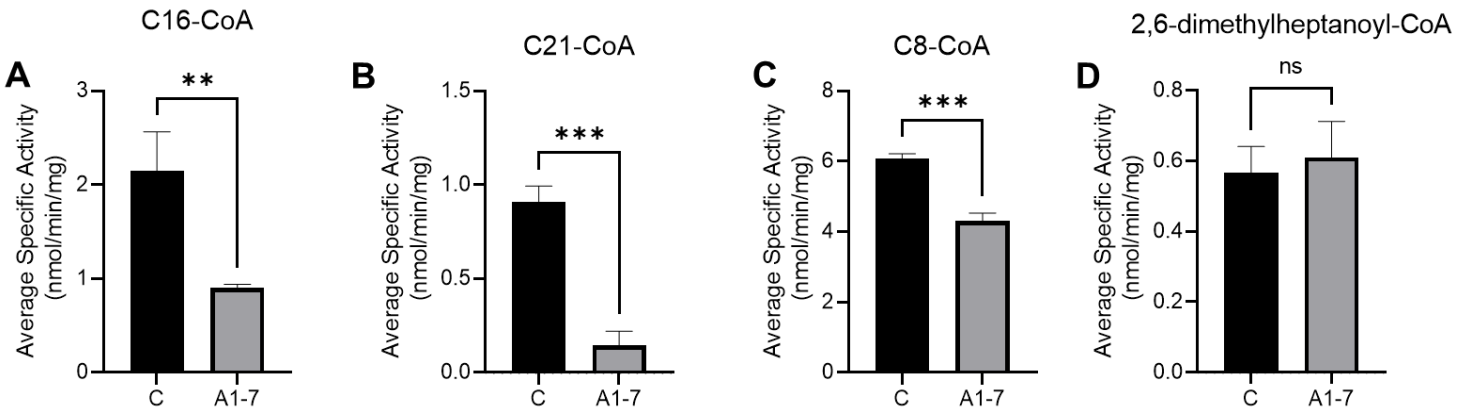

Figure 13. ACAD enzymatic activity of control and ACADVL HEK293T ACADVL null clone A1-7.

Activity of control and clone A1-7 were measured with palmitoyl-CoA (A), VLCAD (heneicosanoyl-CoA (C21)) (B), octanoyl-CoA (C), and 2,6-dimethylheptanoyl-CoA (D) as substrates. Assays were performed in triplicates. Means and standard deviations were calculated using an unpaired t-test. ***$p<0.001$, **$p<0.01$, ns = no statistical difference.

Based on the absence of VLCAD protein and activity, we selected clone A1-7 as our *ACADVL* null HEK293T cell line and used this cell line for all additional experiments, and performed subsequent long chain assays with C21-CoA.

3.4.3 Genetic and functional validation of variants of uncertain significance in VLCAD deficient fibroblasts

Fibroblasts from five VLCADD patients based on metabolite parameters and clinically determined variants, including at least one VUS, were analyzed for VLCAD activity using the cuvette based ETF fluorescence reduction assay (Supplementary Table S5). All five cell lines had reduced VLCAD protein presence in cell lysates as determined by western blotting (Fig. 14A) and reduced VLCAD enzyme activity compared to control (Fig. 14B), consistent with clinically

defined diagnosis. LCAD activity was not measured as fibroblasts have previously been shown to contain no LCAD enzyme [143]. All five VLCADD cell lines had variable changes in MCAD activity compared to a concurrent control, but within the normal variation seen in fibroblasts (Fig. 14C).

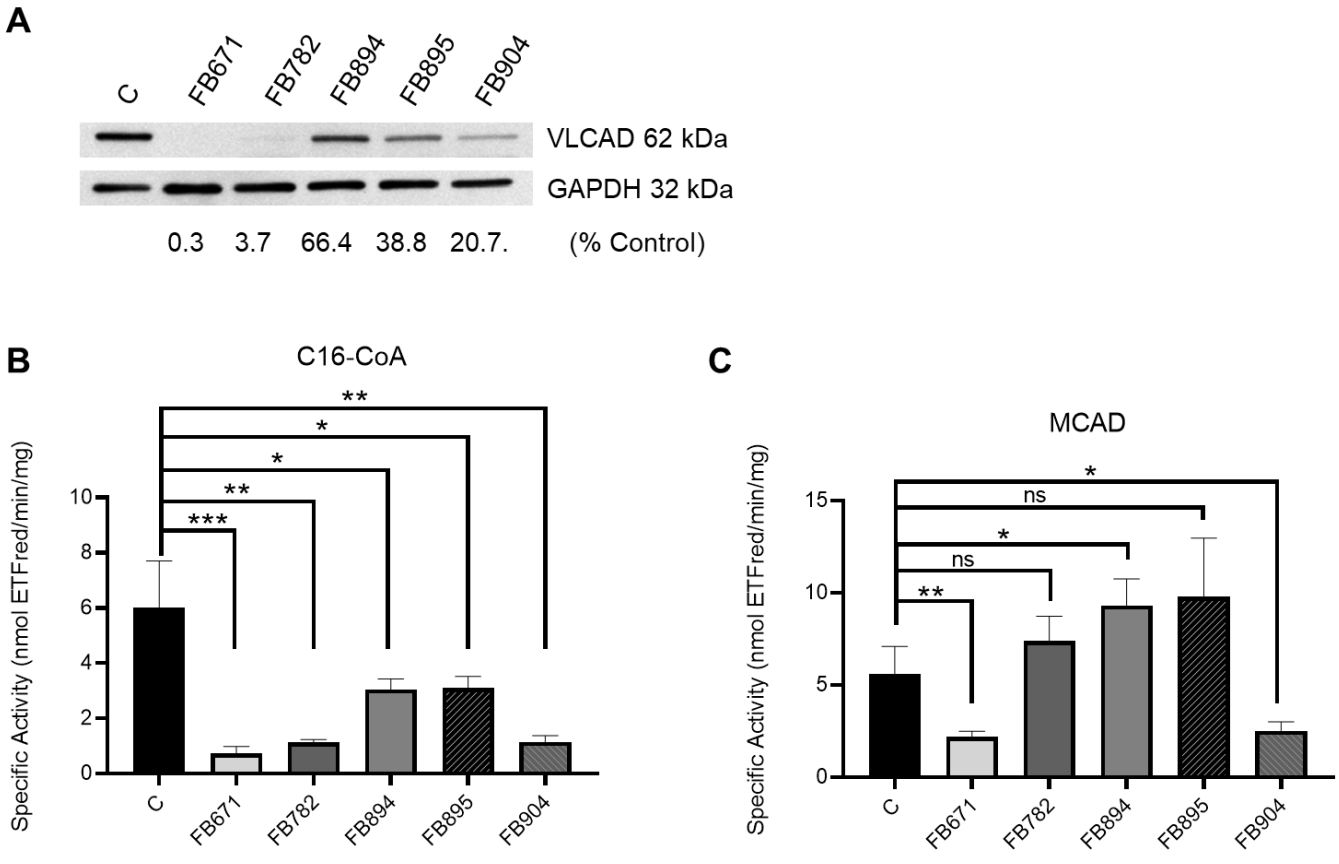

Figure 14. Western blotting and enzymatic activity of VLCAD deficient patient-derived fibroblasts.

Western blot of VLCAD deficient patient and control fibroblasts for detection of VLCAD and GAPDH (A). Enzymatic assay using palmitoyl-CoA or (B), octanoyl-CoA as substrate (C). Activity assays were performed in triplicate. Means and standard deviations were calculated using an unpaired t-test. ***p<0.001, **p<0.01, *p<0.05, ns = no statistical difference.

3.4.4 Functional analysis of individual VUS alleles in HEK293T *ACADVL* null lines

To evaluate the effect of *ACADVL* VUS alleles, we evaluated VLCAD protein and enzymatic activity in *ACADVL* null HEK293T cells that were transfected with vectors driving expression of normal consensus *ACADVL* cDNA or *ACADVL* cDNA containing individual mutations from variants identified in the VCLAD deficient patients (Table 1, Fig. 15). RT-PCR and qPCR analysis confirmed there was no *ACADVL* expression in the HEK293T knock out cells, and that all transfected cells had abundant levels of *ACADVL* mRNA, confirming that the expression plasmid was expressing the *ACADVL* gene properly (Fig. 15A). Abundant VLCAD protein levels were observed with transfection of control, c.848T>C (p.Val283Ala), c.1248A>C (p.Ile420Leu), c.535G>A (p.Gly179Arg), and c.1217A>C (p.Gln406Pro) inserts (Fig. 15B). In contrast, VLCAD protein was barely observed following expression with c.1619T>C p.(Leu540Pro) and c.1707_1715dup (p.Asp570_Ala572dup) inserts (Fig. 15B). Expression of the control cDNA in *ACADVL* null HEK293T cells led to dramatic increase in VLCAD activity (Fig. 15C and D). All tested variants showed little or no enzyme activity using either C16- or C21-CoA as substrate (Fig. 15C and D). Extracts from cells expressing the common variant, c.848T>C (p.Val283Ala) had 18% of the control plasmid activity as measured with C21-CoA, consistent with previous reports of 22% VLCAD activity compared to control in fibroblasts [42, 58]. MCAD activity varied in cells expressing the variant *ACADVL* cDNAs, though still well above the VLCAD levels (Fig. 15E).

Table 2. Identified *ACADVL* mutations and their corresponding pcDNA3.1(+) plasmid designations and corresponding fibroblast line origin.

Cell Line Origin	Mutation	Plasmid ID	Experimental Findings	Current ClinVar Status	Proposed ClinVar Status
FB826	Control	ACADVL-C	VLCAD protein: normal Enzyme activity: normal	--	--
FB671	c.1619T>C, p.Leu540Pro	ACADVL-1619	VLCAD protein: reduced Enzyme activity: reduced	VUS (not reported)	Pathogenic
FB671	c.1707_1715dup, p.Asp570_Ala572dup	ACADVL-1707	VLCAD protein: reduced Enzyme activity: reduced	VUS	Pathogenic
FB782	c.848T>C, p.Val283Ala	ACADVL-848	VLCAD protein: reduced Enzyme activity: reduced	Pathogenic	Pathogenic
FB782	c.1248A>C, p.Ile420Leu	ACADVL-1248	VLCAD protein: reduced Enzyme activity: reduced	VUS (not reported)	Pathogenic
FB894, FB895	c.535G>A, p.Gly179Arg	ACADVL-535	VLCAD protein: normal Enzyme activity: reduced	VUS	Pathogenic
FB904	c.1217A>C, p.Gln406Pro	ACADVL-1217	VLCAD protein: normal Enzyme activity: reduced	VUS	Pathogenic

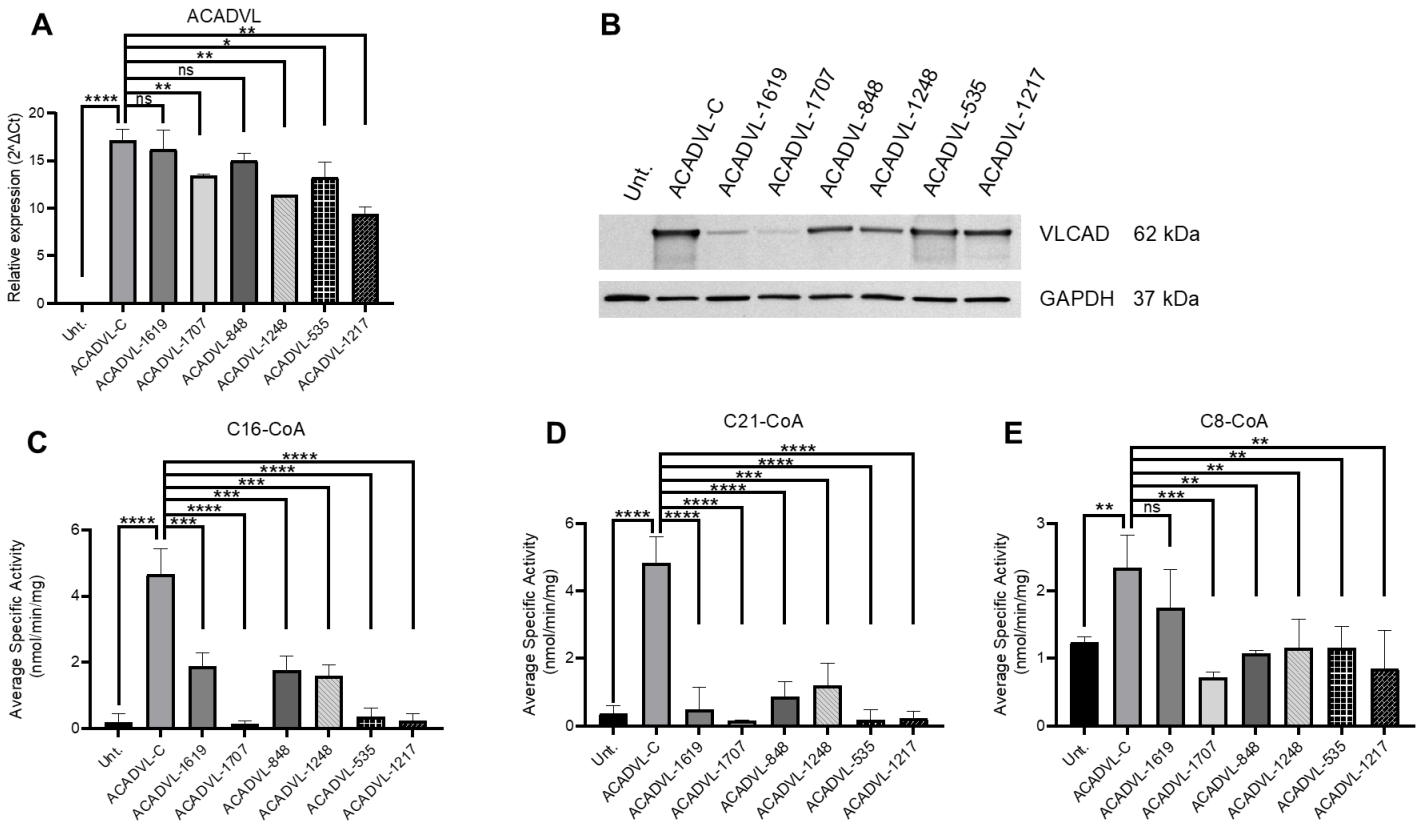

Figure 15. Expression of ACADVL VUS inserts in a ACADVL null HEK293T cell line.

Quantitative PCR of ACADVL mRNA from HEK293T untransfected, or transfected with wild type or variant VLCAD plasmids (A). Stable VLCAD protein was detected by western blot with GAPDH used as an internal loading standard. Molecular mass standards were Precision Plus Protein Dual Color Standards (BioRad) (B). Activity assay of cellular extracts following transfection with palmitoyl-CoA (C), heneicosanoyl-CoA (C21) (D), and octanoyl-CoA (E) as substrate. Assays were performed in triplicates. Means and standard deviations were using an unpaired t-test showing significant difference, ****p< 0.0001, ***p<0.001, **p<0.01, ns = no statistical difference.

3.4.5 Computational prediction of mutation's adverse structure/function effect

The effect of the mutations reported in this study can be further evaluated using *in silico* molecular modeling that can bring structure function relationship insights. Val283Ala and Ile420Leu are predicted to be the most stable among the mutations. The latter is the most intriguing of the two since despite being a conservative replacement there is an obvious detectable adverse effect on enzyme activity and stability. Ile420 is located at the interface between the ACAD-like catalytic domain and the C-terminus region that replaces the third, or fourth, monomer region in the tetrameric version (Fig. 16). The C-terminus domain is believed to function to anchor the protein to the long chain fatty acid β-oxidation complex, membrane, or other macromolecule. The Ile420 residue is part of a hydrophobic pocket that provide stability to the ACAD-like domain C-terminus domain interface (Fig. 16). It is located near the middle of α-Helix I and is at interacting distance on one side with Leu468 and Val472, further distance from Ala416 and Ile417, and across from Ile573 of the C-terminus α-helix M (Fig. 16). Key to Ile420 residue's importance seems to be its apparent dual role as part of this hydrophobic pocket. It has a particularly important anchoring interaction to the C-terminus with Ile573, but it also enhances the tightness of the salt bridge formed between Arg469 and Glu424. The salt bridge between these two residues is conserved in ACAD9, a homologous dimeric ACAD. The ε-N of the Arg469 guanidinium group is in close interacting proximity with the carboxylate of Asp570 of the C-terminus α-helix M. Replacement of Ile420 with a Leu, albeit slightly tolerated, partially disrupts the intricate proximity to the salt bridge (Fig. 16). While in ACAD9 the equivalent residue to Ile420 is a Val, the orientation of the Val side chain can likely interact better with the equivalent salt bridge.

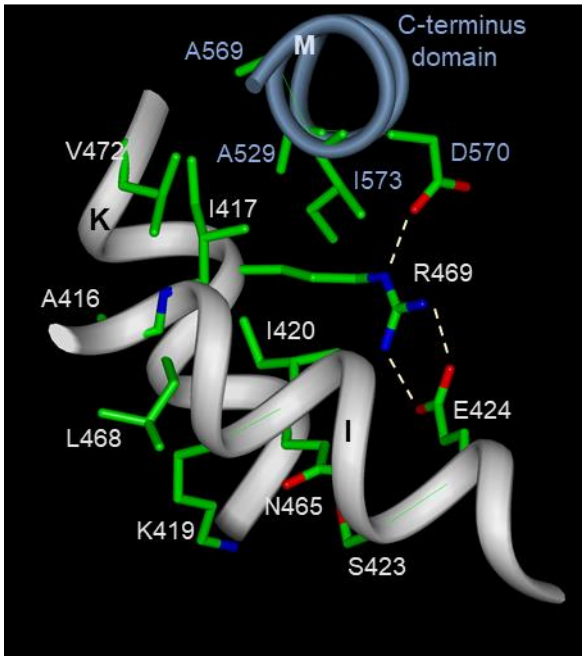

Figure 16. Ribbon representation of relevant area of VLCAD depicting the location of Ile420, interacting residues, and juxtaposed residues that could be affected indirectly by its replacement.

An Ile420 (380 mature numbering) to Leu would affect alignment of Arg469 guanidinium nitrogen to interact with E424 and D570. The published atomic coordinates for VLCAD, 3B96.pdb, were used for the modeling [16].

Gln406 is located at the N-terminus of the loop connecting α-helices H and I. A change to proline at any position is usually assumed to be devastating for protein structure unless, it is in a loop and the trajectory or the secondary and tertiary fold of the structurally important peptide to the C-terminus side is not affected. In this case, VLCAD Gln406Pro was detectable in appreciable amounts in the HEK293T cells expressing the mutant. This implies that despite this being a folding mutation, some protein might yet be present in cells and that will be amenable to chaperone therapy.

The mutations Asp570_Ala572dup and Leu540Pro are in the middle of α-helices M and N, respectively, of the C-terminus and are expected to be detrimental to structural stability. Gly179 is located at the active site as part of α-helix E. While its replacement with an Arg would affect

folding, it seems to be energetically well tolerated as the side chain sits in the active site. However, the positioning would prevent substrate binding.

3.5 DISCUSSION

We have previously confirmed the pathogenicity of *ACADVL* mutations directly in patient fibroblasts using a prokaryotic system and a relatively large volume cuvette assay as well as a high throughput microtiter plate assay [55, 58]. However, establishing a fibroblast culture requires an invasive procedure in a newborn as well as significant time to grow to sufficient quantity to be assayed. In addition, most VLCAD deficient patients have unique combinations of variants and the relative effect of each cannot be addressed with fibroblast assays. We have recently developed *IVD* and *ACAD9* null HEK293T lines to assess *IVD* and *ACAD9* variant pathogenicity, respectively [128, 139]. In this study, we describe the generation of a deletion in the *ACADVL* gene in HEK293T cells using CRISPR/Cas9 technology that can similarly be used to study expression of variant recombinant proteins [133]. To better address the need for rapid turnaround time, we utilized a commercial gene synthesis service to rapidly generate *ACADVL* variants for expression in our *ACADVL* null HEK293T cells, and then confirmed that our microtiter plate assay gave a robust differentiation between control and inactivating variant containing inserts. Because this assay requires less sample, the time from transfection to assay was also minimized compared to fibroblast cultures. Plasmid design and ordering requires 1 day and are typically delivered in 2-4 weeks. Transformation of E. coli with *ACADVL* plasmid colony selection, and midi prep of culture is 4 days. Seeding of ACADVL null HEK293T cells requires 1 day, transfection of ACADVL plasmid 2 day incubation, and harvest of plates requires 1 day. Traditional western

blotting requires 2 days for results and the ETF fluorescent reduction microplate assay requires 3 hours to measure all 7 plasmids described in this manuscript in triplicates of 3 Co-A substrates compared to 2-3 days to measure the same amount of samples in the traditional cuvette assay. Thus, from the time of receiving the variant plasmid until final result was 11 days.

To test this system, we examined the pathogenicity of 5 variants previously designated VUSs in the ClinVar database, as well as the effect on activity of the common *ACADVL* variant identified through NBS. The inactivating nature of each of the variants agreed with the more laborious and time consuming fibroblast assays from the patients in which each variant was detected. In this regard, our approach can be used to address the pathogenicity of VUSs in any gene in which a clear biochemical marker can be measured following transfection of an expression plasmid into easily made HEK293T (or other) cells. Thus, our plate ACAD assay can easily measure the activity of any of the other ACAD deficiencies identified by newborn screening (IVD, IBD, SBCAD, and MCAD). Similarly, any defects identified by tandem mass spectrometry could easily measure accumulation of the diagnostic metabolite in the cellular medium as an indicator of pathogenicity. Of note, only one VUS in *ACADVL* was identified by clinical sequencing in three patients in this study even though they clearly had VLCAD deficiency based on clinical presentation and fibroblast testing. While we were able to confirm the pathogenicity of the VUS identified in each patient, determining the second mutation was not a focus of this study.

Based on this study, we propose that the VUSs examined be reclassified in ClinVar. Variants c.1619T>C, (p.Leu540Pro), c.1707_1715dup, (p.Asp570_Ala572dup), c.1248A>C, (p.Ile420Leu), c.535G>A (p.Gly179Arg), and c.1217A>C, (p.Gln406Pro) be reclassified from VUS to pathogenic/likely pathogenic; and c.848T>C, (p.Val283Ala) should maintain its pathogenic status.

In this study we were able to apply the high throughput ETF fluorescence reduction microplate assay over the traditional cuvette assay. The application of the microplate version of the assay allowed us to decrease reagent amount and time required for the assay [134]. This allowed us to screen more variants, in a shorter time frame. This microplate assay can be applied to any of the acyl-CoA dehydrogenases. Alternatively, acylcarnitine profiling through tandem mass spectrometry in media collected from cultured cells will allow for the confirmation of pathogenicity in disorders without an enzyme activity assay. The addition of the ETF fluorescence reduction microplate assay will allow for rapid confirmation of *ACADVL* variant pathogenicity in infants identified through NBS without the need for an invasive procedure such as a skin biopsy.

Examining possible adverse effects on structure and function of amino acid residue replacements *in silico* complements these functional studies and leads to important insight into the scope and severity of each defect at the molecular level, potentially suggesting alternative treatment options. For example, concurrent experimental and *in silico* indications of a mild structural effect would suggest modification of dietary plans, including dietary recommendations for fat intake. This study also demonstrates that the severity of the effect of mutations in the C-terminus region on protein instability is hard to assess solely from assay of patient cells. For *in silico* modeling provided the impetus to evaluate the effects Ile420Leu in our expression system because of predicted structural plasticity, and the possibility that the mutation could still support production of functional protein. Indeed, while assay of patient cells with this mutation failed to detect VLCAD protein, our expression system instead demonstrated that mutant protein could be stable and thus a candidate for therapy with a molecular chaperonin.

In summary, we have developed an *ACADVL* null HEK293T cell line with no VLCAD protein or activity that allowed determination of pathogenicity of several previous VUSs found in

patients with suspected VLCAD deficiency identified through NBS. This model will allow for high throughput assessment of the function of VUSs in multiple genes for disorders identified through NBS. In addition, our functional expression system in combination with molecular modeling serves as the beginning of a personalized medicine approach that will ultimately allow better targeted therapies for patients.

3.6 ACKNOWLEDGEMENTS

JV was supported in part by NIH grant R01 DK109907. We thank the staff from the Core Flow Cytometry Laboratory from the University of Pittsburgh, Children's Hospital of UPMC for help with flow sorting of GFP positive cells. We thank Yuxun Zhang, PhD from Eric Goetzman, PhD Laboratory University of Pittsburgh, Children's Hospital of UPMC for providing ETF for the ETF fluorescence reduction assays.

3.7 AUTHOR CONTRIBUTIONS

OMD reviewed literature, developed experimental design, performed CRISPR/Cas transfection and clonal screening and expansion to generate *ACADVL* null HEK293T cell lines. OMD completed most experiments including *ACADVL* null western blot and ETF fluorescence reduction assay for the clonal screen to select *ACADVL* null cell line. OMD performed western blotting and most ETF fluorescence reduction assays for VLCADD patient fibroblasts. OMD optimized and performed ETF fluorescence reduction microplate assay for HEK293T *ACADVL*

variant transfections. OMD performed statistical analysis, compiled data, drafted and reviewed the manuscript. EAK developed CRISPR/Cas and ddPCR experimental design, manuscript preparation, and reviewed manuscript. MS compiled patient data and performed ddPCR and western blotting for ACADVL variant transfections. KB performed three ETF fluorescence reduction assay for VLCADD patient fibroblasts. A-WM conducted *ACADVL* variant enzyme modeling, manuscript preparation, and reviewed manuscript. JV developed the experimental design and reviewed manuscript. All authors discussed the results and contributed to the final manuscript.

4.0 TREATMENT OF VLCAD DEFICIENT PATIENT FIBROBLASTS WITH PEROXISOME PROLIFERATOR ACTIVATED RECEPTOR δ AGONIST IMRPOVES CELLULAR BIOENERGETICS

A manuscript based on this chapter has been submitted to Scientific Reports for peer review.

Olivia M. D'Annibale[1,2], Yu Leng Phua[1], Clinton Van't Land[1], Anuradha Karunanidhi[1], Alejandro Dorenbaum[3], Al-Walid Mohsen[1,2], Jerry Vockley[1,2]

[1] Division of Genetic and Genomic Medicine, Department of Pediatrics, University of Pittsburgh School of Medicine, and UPMC Children's Hospital of Pittsburgh, Pittsburgh, PA 15224;

[2] Department of Human Genetics, University of Pittsburgh Graduate School of Public Health, Pittsburgh, PA 15261;

[3] Reneo Pharmaceuticals, Inc., 18575 Jamboree Road Suite 275-S, Irvine, CA, USA.

4.1 ABSTRACT

Background: Very long chain acyl-CoA dehydrogenase (VLCAD) deficiency is an autosomal recessive disease that prevents the body from utilizing long chain fatty acids for energy, most needed during stress and fasting. Symptoms can appear from infancy through childhood and adolescence or early adulthood, and include hypoglycemia, recurrent rhabdomyolysis, myopathy, hepatopathy, and cardiomyopathy. REN001 is a peroxisome proliferator activated receptor delta (PPARδ) agonist that modulates expression of the genes coding for fatty acid β-oxidation enzymes and proteins involved in oxidative phosphorylation. Here we assessed the effect of REN001 on VLCAD deficient patient fibroblasts.

Methods: VLCAD deficient patient and control fibroblasts were treated with REN001. Cells were harvested for gene expression analysis, protein content, VLCAD enzyme activity, cellular bioenergetics and ATP production.

Results: VLCAD deficient cell lines responded differently to REN001 based on genotype. All cells had statistically significant increases in *ACADVL* gene expression. Small increases in VLCAD protein and enzyme activity were observed and were cell line and dose dependent. Even with these small increases, cellular bioenergetics improved in all cell lines in the presence of REN001 as demonstrated by oxygen consumption rate and ATP production. VLCAD deficient cell lines containing missense mutations responded better to REN001 treatment than one containing a duplication mutation in *ACADVL*.

Discussion: Treating VLCAD deficient fibroblasts with the REN001 PPARδ agonist results in an increase in VLCAD protein, enzyme activity, and a decrease in cellular stress. These results establish REN001 as a potential therapy for VLCAD as enhanced expression may provide

therapeutic increase in total VLCAD activity but suggest the need to mutation specific treatment augmented by other treatment measures.

4.2 INTRODUCTION

Long chain fatty acids enter cells *via* protein fatty acid transporters on the cell surface concurrent with or followed by conjugation to a CoA group by a fatty acyl-CoA synthase (FACS) [5, 6]. Long chain fats are activated in the cytoplasm and require a series of three enzymatic steps that constitute what is known as the carnitine cycle [5, 6]. Carnitine palmitoyl transferase 1 (CPT1) replaces the CoA moiety of the long-chain acyl-CoA with carnitine (acylcarnitine), which is transported by carnitine-acylcarnitine translocase (CAT) across the inner mitochondrial membrane in exchange for a free carnitine molecule from the mitochondrial matrix [5, 6]. The carnitine of the acylcarnitine is replaced with a CoA and is released as an acyl-CoA ester by carnitine palmitoyl transferase 2 (CPT2), where it can then enter the fatty acid β-oxidation pathway, a series of four enzymatic steps that results in the production of a two carbon acetyl-CoA, one NADH, and one $FADH_2$, regenerating an acyl-CoA that is now two carbons shorter [5-7]. Very long-chain acyl-CoA dehydrogenase (VLCAD) catalyzes the α,β-dehydrogenation of long chain acyl-CoA substrates with various carbon chain length and maximal activity to C14-CoA, to its enoyl-CoA product utilizing the electron transfer flavoprotein (ETF), a mitochondrial matrix electron shuttle protein, as an electron acceptor [5, 6, 8]. Reduced ETF transfers its' reducing equivalents to its redox partner, the ETF dehydrogenase (ETFDH), which in turn delivers the reducing equivalents to the ubiquinone pool and complex III of the electrons transport chain (ETC) [5, 6, 8].

VLCAD deficiency (VLCADD) is an autosomal recessive disorder caused by biallelic mutations in *ACADVL* gene [41]. The frequency of VLCADD in various populations is about 1:30,000 to 1:100,000 live births [29, 33]. Symptoms of VLCADD include hypoglycemia, recurrent rhabdomyolysis, myopathy, hepatopathy, and cardiomyopathy. Symptoms can present in infancy, later in childhood, or in adolescence or early adulthood [135]. Treatment for VLCADD patients involves a low-fat diet consisting mainly of medium chain triglyceride (MCT) or triheptanoin supplementation with smaller more frequent meals [44-47]. However, many patients still have episodes of rhabdomyolysis and cardiomyopathy that can lead to hospitalization suggesting the need for additional treatment options. Episodes of metabolic decompensation are typically triggered by physiologic stress such as illness or excess exercise, but the cause often remains unidentified [144]. Ultimate outcome is improved by identification of the disorder through newborn screening [57].

Peroxisome proliferator-activated receptors (PPAR) are nuclear receptors that play key roles in the regulation of fatty acid β-oxidation, lipid metabolism, inflammation, and cellular growth and differentiation [62-66]. They are divided into several categories based on the specific promotors that they stimulate. PPARδ is a major activator of oxidative metabolism and is ubiquitously expressed [62, 69, 70]. It is activated by polyunsaturated fatty acids such as arachidonic acid, oleic acid, dexamethasone, and eicosanoids such as prostaglandin 1 (PGA_1), carbaprostacyclin (cPGI), and 15-deoxy-$\Delta^{12,14}$-prostaglandin J_2 (15d-J_2) [71, 72]. *In vivo* experiments with PPARδ agonists have examined their effects in a variety of diseases and cellular processes including diabetes, obesity, and lipid metabolism. In a two week clinical study, treatment of moderately obese men with dyslipidemia with GW501516, a PPARδ agonist, resulted in a decrease in fasting and postprandial plasma triglycerides, low-density lipoprotein (LDL)

cholesterol, apoB compared to placebo, as well as reduction in liver fat content and urinary isoprostanes (a marker of whole-body oxidative stress) [74]. Four weeks of treatment of insulin-resistant middle-aged obese rhesus monkeys with GW501516 induced a dose-dependent rise in serum high density lipoprotein cholesterol while lowering the levels of small-dense LDL, fasting triglycerides, and fasting insulin [75]. Genetically obese *ob/ob* mice had reduced plasma glucose and blood insulin levels after treatment GW501516 [69]. Genetically predisposed obese $Lepr^{db/db}$mice treated with GW501516 demonstrated a decrease in lipid accumulation, while PPARδ-deficient mice were prone to obesity on a high-fat diet [66]. Recent studies with herbal supplements such as bavachinin (a pan-PPAR agonist) from the glucose-lowering malaytea scurfpea herb and ginger (a PPARδ agonist) reduced obesity in obese *db/db* mice, and diet induced obesity in C57BL6J mice, respectively [76, 77].

REN001 (formerly known as HPP593), a PPARδ agonist (Reneo Pharmaceuticals), has been shown to reduce oxidative stress and inflammation in renovascular hypertensive Goldbatt's 2 kidney 1 clip (2KIC) rats [145]. 2KIC mice treated with this REN001 for 30 days had no necrosis in kidneys, reduced oxidative stress-responsive proteins, and decreased pro-death protein BNIP3 in kidney tubules [145]. REN001's proposed mechanism is the inhibition of BNIP3 activation resulting in preserved mitochondrial function and oxidative stress control.

Bezafibrate is a pan-PPAR agonist used to treat hyperlipidemia as it increases high density (HDL) cholesterol levels, decreasing total and LDL cholesterol levels [78]. Since PPARs can increase fatty acid β-oxidation there has been interest in repurposing bezafibrate as a treatment for fatty acid oxidation disorders. In an *in vitro* study, VLCADD patient derived fibroblast cell lines treated with two versions of bezafibrate demonstrated a 3-fold increase in palmitate oxidation with an increase in VLCAD mRNA, protein, and enzyme activity. RT-PCR showed an increase in other

genes encoding proteins in the β-oxidation pathway [79]. Similarly, treatment of CPT2 deficient human myoblast cells with bezafibrate, and the PPARα agonist GWδ 0742 led to an increase in *CPT1-B* and *CPT2* mRNA levels with increased CPT2 activity, while GWα 7647, another PPARα agonist, had minimal effect [80]. Treatment with bezafibrate of fibroblasts from 26 patients with mitochondrial fatty acid oxidation trifunctional protein (MTP) deficiency with various mutations led to improved cellular palmitate oxidation in 6 of 26 cell lines [81]. In an open label trial treating patients with CPT2 deficiency, patients showed an increased or no change in incidence of rhabdomyolysis episodes, but an improvement in quality of life scores [146, 147]. However, in a randomized double blind placebo control clinical trial in patients with VLCAD or CPT2 deficiency, bezafibrate failed to improve cardiac function or whole-body fatty acid oxidation [82]. One possibility for this dichotomy is the limited PPARδ effect of bezafibrate. Thus, a clinical need for additional therapies for this group of disorders remains.

In this study, we examined the effects of REN001 in VLCADD patient derived fibroblast cell lines in advance of clinical trials with this agent.

4.3 MATERIALS AND METHODS

Experiments were performed in accordance with the approved guidelines and regulations. Experimental human protocols were approved by the Institutional Review Board at the University of Pittsburgh, protocol 19030195.

4.3.1 Subjects

Skin biopsies for fibroblast culture were performed on a clinical basis from patients with various mutations in *ACADVL* with written informed consent from patients and/or parents (Table 1). Control fibroblast cells were obtained from American Type Culture Collection (ATCC.org).

Table 3. List of VLCAD deficient cell lines used in this project with their corresponding mutations in *ACADVL* and phenotypic severity.

Cell Line	Laboratory Designation	Age	Sex	Mutations	Phenotypic Severity
Control-1	FB826	40 yrs	F	N/A	Control
Control-2	FB549	3 yrs	M	N/A	Control
Control-3	FB902	22 yrs	M	N/A	Control
VLCAD-1	FB833	3 yrs	M	c.520G>A (p.Val174Met)/c.1825G>A (p.Glu609Lys)	Mild
VLCAD-2	FB671	6 months	F	c.1619T>C (p.Leu540Pro)/c.1707-1715dup (p.Asp570_Ala572dup)	Severe
VLCAD-3	FB863	2 yrs	F	c.896_898del (p.Lys299del)/c.1147C>G (p.Leu383Val)	Mild
VLCAD-4	FB782	6 months	M	c.848T>C (p.Val283Ala)/c.1258A>C (p.Ile420Leu)	Mild

*All fibroblasts were used between passage 4 and 8.

4.3.2 Cell culture and treatments

Cell lines were grown in Dulbecco's Modified Eagle Medium (DMEM, Corning Life Sciences, Manassas, VA), containing high glucose levels (4.5 g/L) or in DMEM devoid of glucose for 48 hr. Both media were supplemented with 10% fetal bovine serum (FBS), 4 mM L-glutamine,

and 100 IU penicillin and 100 µg/ml streptomycin (Corning Life Sciences). REN001 was obtained from Reneo Pharmaceuticals, San Diego, CA, and resuspended from a powder in DMSO.

Cells were treated with REN001 at 85% confluency at the following concentrations: 0, 15, 30, 60 and 120 nM. Additional cultures were treated with 600 µM bezafibrate (Sigma Aldrich, St. Louis, MO). The 0 nM treatment was given DMSO as a control for both REN001 and bezafibrate. Cultures were incubated for 48 hr at 37°C, 5% CO_2 and were harvested for analysis.

4.3.3 Real-time quantitative polymerase chain reaction (qPCR)

Total RNA was isolated using the RNeasy Mini Kit (Qiagen, Valencia, CA) from REN001 treated VLCAD and control fibroblast with on column DNaseI digestion (Qiagen). First strand synthesis of complementary DNA (cDNA) was reverse-transcribed from 2,500 ng of total RNA using the Super Vilo IV Master Mix (Qiagen). Quantitative PCR was performed with equivalent amount of cDNA on a Bio-Rad CFX96 Real-Time PCR Instrument, with SYBR Green Master Mix (Thermo Fisher Scientific, Waltham, MA). *ACADVL*, *HADHA*, *HADHB*, *ETFDH*, *UQCRC2* and *NDUFS2* were assayed using primers were obtained from PrimerBank [148-150] (Supplementary Table S9). Expression levels were normalized to *TOMM20* and the data were analyzed by the $2^{-\Delta\Delta Ct}$ method [140].

4.3.4 PPARδ binding site analysis

ChIP-seq analysis for PPARδ binding sites was performed using the publicly available dataset on Gene Expression Omnibus (GSE 50144) (PMID: 24721177), and binding sites were identified with the use of MACS2 (PMID: 24743991). ChIP-seq peaks were visualized using the

IGV viewer (PMID: 21221095), and gene ontology enrichment for PPARδ target genes and pathways were analyzed using the Cistrome-GO and GREAT GO tools (PMID: 20436461) (PMID: 31053864).

4.3.5 Whole cell lysate, protein concentration, SDS-PAGE gel, and western blot

Cell were treated with REN001 in complete DMEM with glucose for 48 hr, harvested via trypsinization, pelleted, and stored at -80 °C for western blot analysis. Pellets were lysed with 50 µl of radioimmunoprecipitation assay (RIPA) buffer (Thermo Fisher Scientific) with 1X Protease Inhibitor Cocktail (PI) (Roche, St. Louis, MO) for 30 min on ice and centrifuged at 14,000 x g for 15 min at 4 °C. Supernatants were collected and 25 µg of protein was loaded onto a 4-15% gradient Criterion precast SDS-PAGE gel (Bio-Rad, Hercules, CA). Following electrophoresis, the gel was blotted onto a nitrocellulose membrane and incubated with anti-VLCAD (VLCAD 1:1000, rabbit, Vockley lab), then incubated with secondary goat anti-rabbit-HRP antibody (1:3000, BioRad). Pierce ECL Western Blotting Substrate kit (Thermo Fisher Scientific) was used to visualize bands. Membranes were stripped and re-probed with TFP cocktail antibody (1:1000, rabbit, Vockley lab, [55]) containing antibodies for both the alpha and beta subunits, and with mouse-anti-glyceraldehyde 3-phosphate dehydrogenase (GAPDH; 1:25000) monoclonal antibody (ABCAM, Cambridge, MA) to verify equal loading. ImageLab software was used to quantify band intensity and bands were normalized to GAPDH intensity.

4.3.6 Immunofluorescence microscopy

Treated cultured fibroblasts were seeded at a concentration of $5x10^4$ cells/mL on Poly-L-Lysine coated glass cover slips in a 12-well plate and allowed to grow overnight in growth media at 37°C in a 5% CO_2 incubator. Cells were then fixed in 4% paraformaldehyde for 10 min and permeabilized with 0.1% Triton X100 and blocked after brief washings in 5% donkey serum at room temperature for 1 hr. Cells were briefly washed and treated with primary antibodies VLCAD (1:1000, Vockley Lab) and HADHA (1:100, Santa Cruz Biotechnology, Dallas, TX) overnight in 4°C. After brief washing with 1 X TBST, cells were incubated with the secondary antibodies donkey anti-rabbit Alexa Fluor 488 and donkey anti-mouse Alexa Fluor 594 (1:1000, Invitrogen, Waltham, MA) for 1 hr at RT. Nuclei were immunostained with NucBlue Fixed Cell ReadyProbes Reagent (DAPI; Invitrogen). The cover slips were then mounted using mounting media before imaging. All images were taken on a Zeiss LSM Confocal microscope using 63X magnification. Images were analyzed using ImageJ [151].

4.3.7 Electron transfer flavoprotein (ETF) fluorometric reduction assay

The ETF reduction assay was performed using a Jasco FP-6300 spectrofluorometer (Easton, MD) with a cuvette holder heated with circulating water at 32 °C as previously described [117]. Briefly, treated cell pellets were lysed using 50 mM Tris, pH 8.0 buffer and 0.1 X protease inhibitor EDTA-free and sonicated twice in an ice-cold water bath sonicator at amplitude 45 for 1.5 min with 15 sec intervals. The assay was otherwise performed as described, at the indicated substrate concentrations [117]. The enzyme was diluted 1200-fold into buffer containing 50 mM Tris, pH 8.0, 5 mM EDTA and 50% glycerol, and 10 µl was used for each assay. The ETF

concentration was 2 µM. Spectra Manager 2 software (Jasco, Inc.) was used to collect data and calculate reaction rate and Microsoft Excel was used to calculate the kinetic parameters.

4.3.8 Fatty acid oxidation (FAO) flux analysis

Tritium-release assay was performed as previously described with the noted changes [152]. Cells were grown in T175 flasks and seeded at 350,000 cells per well in 6-well plates in triplicates and in duplicate wells for protein concentration for normalization, and grown for 24 hr in complete DMEM. Wells were treated with REN001 in complete DMEM for 48 hr in 37 °C/5% CO_2 incubator. Cells were washed once with PBS and incubated with 0.34 µCi [9,10-^{3}H] oleate (45.5Ci/mmol; Perkin Elmer, Waltham, MA) in 50 nmol of oleate prepared in 0.5 ml glucose-free DMEM with 1 µg/ml L-carnitine and 2 mg/ml alpha-cyclodextrin for 2 hr at 37 °C. Fatty acids were solubilized with alpha-cyclodextrin as described [153]. After incubation, ^3H_2O released was separated from the oleate on a column containing 750 µl of anion exchange resin (AG 1 x 8, acetate, 100-200 Mesh, BioRad) prepared in water. After the incubation medium was passed through the column, the plate was washed with 1 ml of water, which was also transferred to the column, and resin was washed with 1 ml of water. All eluates were collected in a scintillation vial and mixed with 10 ml of scintillation fluid (Eco-lite, MP), followed by counting in a Beckman scintillation counter in the tritium window. Standards contained a 10 µl aliquot of the incubation mix with 3 ml of deionized water and 10 ml of scintillation fluid.

4.3.9 Measurement of mitochondrial respiration

Oxygen consumption rate (OCR) was measured with a Seahorse XF^{e}96 Extracellular Flux Analyzer Cell Mito Stress Test Kit (Agilent Technologies, Santa Clara, CA). Fibroblasts were treated with REN001 in DMEM without glucose for 48 hr in 37°C/5% CO_2 incubator. Fibroblasts were harvested and seeded at a density of 60,000 cells per well in a 96-well seahorse plate coated in poly-D-lysine the day of assay. Plate was centrifuged at 300 rpm for 1 min, rotated, and centrifuged again at the same settings. Cells were incubated in for 1 hr without CO_2 in buffered Seahorse XF Assay Media (Agilent Technologies) and supplemented with 1 mM sodium pyruvate and 2 mM L-glutamine. Manufacturer's directions were otherwise followed for the XF Mito Stress Test kit (Agilent Technologies).

4.3.10 Measurement of ATP production

Glycolytic and mitochondrial ATP production was measured with a Seahorse XF^{e}96 Extracellular Flux Analyzer with a XF Real-Time ATP Rate Assay kit (Agilent Technologies). Fibroblasts were seeded at 40,000 cells per well in complete DMEM and grown overnight at 37 °C/5% CO_2 incubator. Growth media was removed and fibroblasts were treated with REN001 in complete DMEM for 48 hrs. Cells were washed twice with water and incubated in for 1 hr without CO_2 in buffered Seahorse XF Assay Media (Agilent Technologies) supplemented with 1 mM sodium pyruvate, 2 mM L-glutamine, and 10 mM L-glucose. Manufacturer's directions were otherwise followed for the Real-Time ATP Rate assay kit (Agilent Technologies).

4.3.11 Acylcarnitine profile analysis

Acylcarnitine profiles were determined as previously described [154-156]. Cells were seeded at 350,000 cells per well in 6-well plates in triplicates in complete DMEM. Growth media was changed to Ham's F12 media (Gibco, Waltham, MA) supplemented with 10% FBS, 4 mM L-glutamine, and 100 IU penicillin and 100 µg/ml streptomycin (Corning Life Sciences) for 24 hr. Wells were incubated with REN001 200 µM palmitic acid, 400 µM L-carnitine, and 0.4% fatty acid free BSA in Essential Medium (MEM; Gibco) with no supplementation. Plates were incubated in a 37°C/5% CO_2 incubator for 72 hr. Media was collected, cells were lysed with 250 µL of RIPA buffer for 30 min at room temperature, and protein concentration was determined.

Aliquots (75 µL) of medium were mixed with methanol (20 µL) containing isotope-labeled carnitine standards and the protein precipitated by addition of absolute ethanol (905 µL) and centrifugation (13,000 rpm, 10 min). A portion of the supernatant (50 µL) was dried under a stream of nitrogen gas and the acylcarnitine butyl esters generated by reaction (60 °C for 15 min) in 100 µL of 3N HCl in butanol. Dried residues were reconstituted in acetonitrile-water (80:20) for flow injection ESI-MS-MS analysis. Analysis was performed on a triple quadrupole API4000 mass spectrometer (AB Sciex™, Framingham, MA) equipped with a ExionLC™ 100 HPLC system (Shimadzu Scientific Instruments™, Columbia, MD). Analyst™ (V1.6.3, AB Sciex ©2015) was utilized for data acquisition and ChemoView™ software (V2.0.3, AB Sciex ©2014) for quantitation using isotope-labeled carnitine standards. Acylcarnitine standards were purchased from Amsterdam UMC – VUmc (Amsterdam, NL) and Cambridge Isotope Laboratories, Inc. (Andover, MA). Acylcarnitines were measured using multiple reaction monitoring (MRM) for free carnitine (C0, m/z 218 > m/z 103) and acetylcarnitine (C2, m/z 260 > m/z 85) and Precursor Scan

for precursor ions (Q1) of acylcarnitines (C3 to C18, scan range m/z 270 to 502) that generated a product ion (Q3) at *m/z* 85.

4.3.12 Statistical analysis

Calculations were performed in Microsoft Excel. Student's *t* test was used to determine statistical significance in Prism GraphPad (Version 7, graphpad.com).

4.4 RESULTS

4.4.1 PPARδ agonists upregulates genes associated with fatty acid oxidation and mitochondrial ETC complexes

PPARδ agonists are known to upregulate transcription of FAO and ETC genes [62-66, 69, 70]. Despite the well-established association between PPARδ and improved FAO *in vitro*, the direct target genes of PPARδ remain unclear [157]. To deduce the binding profile and target gene repertoire of PPARδ in an unbiased and genome-wide manner, we re-assessed a prior PPARδ ChIP-seq data that was generated using HUVEC cells (GSE 50144) (PMID: 24721177) (Supplementary Fig. S9). MACS2 analysis of the ChIP-seq data identified a high enrichment of binding events (83%) that were localized to the intergenic region, with a consensus binding motif of GGTCAAAGGTCA that corresponds to PPARδ under the family and class of thyroid hormone receptor-related factors (NR1): Nuclear receptors with C4 zinc fingers (JASPAR) (Supplementary Fig. S9A). Given the enrichment of PPARδ binding sites being primarily localized within 5 kb

downstream of transcription start sites, such observation supports PPARδ primary role as a transcriptional enhancer (Supplementary Fig. S9B). Of note, functional interpretation of *cis*-regulatory regions of PPARδ binding peaks using GREAT and Cistrome GO analysis tools consistently revealed a high degree of confidence in the fatty acid metabolism pathway that is predicted to be enriched by PPARδ target genes (Supplementary Fig. S9C). Notably, PPARδ target genes were also found to be implicated in multiple human phenotypes that are highly reminiscent of FAO disorders, including, but not limited to, hypoglycemia, hepatic steatosis and rhabdomyolysis (Supplementary Fig. S9D)

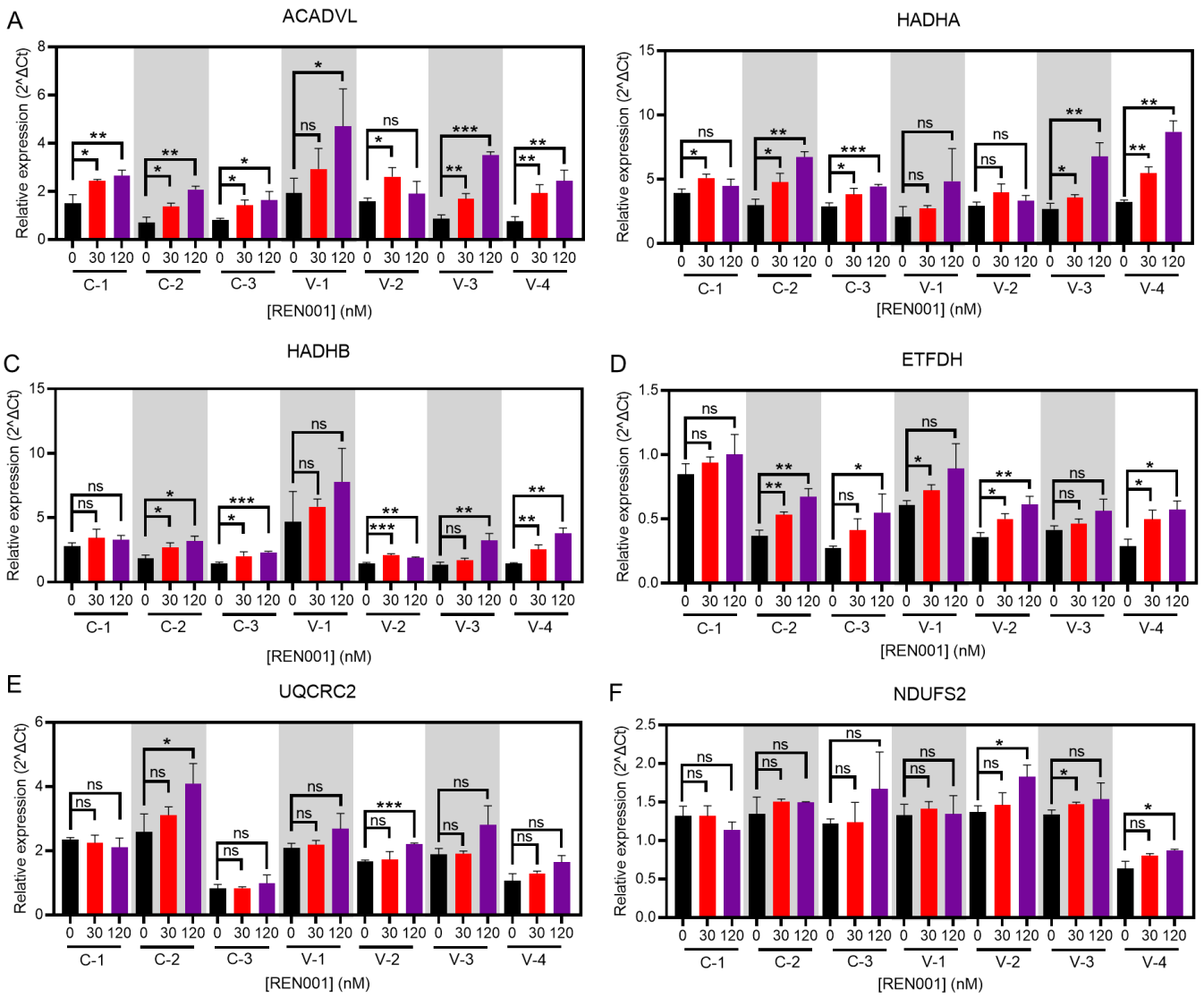

Figure 17. qPCR in control and VLCAD deficient fibroblasts treated with REN001 for 48 hr.

Bars represent mean and standard deviations in duplicate assays. *$p < 0.05$, **$p < 0.01$, ***$p < 0.001$, ns = not significant, compared to each cell lines own 0 nM treatment (t test for unpaired samples).

To determine if REN001 increases transcripts associated with FAO, we quantified mRNA levels via real-time qPCR. In this manner, all control and VLCAD cell lines demonstrated statistical improvement in both FAO and ETC complexes at the transcript level (Fig. 17A-F). Specifically, all treated VLCAD cell lines demonstrated a statistically significant upregulation of *ACADVL* in response to either 30 or 120 nM REN001, with the VLCAD-1 cell line demonstrating at least 2-fold increase in *ACADVL* when treated with 120 nM REN001 (Fig. 17A). Similarly, *HADHA* and *HADHB*, the genes encoding for TFP subunits, also trended upwards with a small but statistically significant increase of transcripts (Fig. 17B, C). Consistent with the positive effects of REN001 on FAO-associated genes, we also observed upregulation of *ETFDH*. To deduce the overall specificity of REN001 and demonstrate that the gene expression changes are not attributable to an off-target effect, we analyzed *UQCRC2* (Complex III) and *NDUFS2* (Complex I), genes that are not known to be targeted by PPARδ agonists based on the ChIP-seq analysis (PMID: 24721177) (Supplementary Fig. S9E). Indeed, qPCR analysis showed minimal changes in both *UQCRC2* and *NDUFS2*, validating the veracity of drug target specificity for REN001 in our assay (Fig. 17E, F, Supplementary Fig. S9E). We decided to use Control-1 cell line for all subsequent experiments as all three control cell lines had a similar increase in mRNA, with Control-1 having the largest increase in *ACADVL* (Fig. 17A).

4.4.2 Induction of fatty acid oxidation proteins

VLCAD deficient patient derived fibroblast cell lines showed decreased VLCAD protein and/or enzyme activity that varied with the *ACADVL* mutation (Supplementary Fig. S10A; Supplementary Fig. S11A). Treatment with REN001 for 48 hr increased VLCAD protein only in cell line 3, with 2.1-fold increase when treated with 30 nM as demonstrated via western blotting

(Fig. 18A). Neither of the other patient cell lines nor control cells showed significant changes in VLCAD protein signal, confirming the instability of mutant protein translated from the upregulated mRNA. Since PPARδ upregulates all the fatty acid β-oxidation genes, the level of TFPα and β subunits, the products of the *HADHA* and *HADAB* genes, respectively, was analyzed in patient cells. TFP is a component of the FAO/ETC macromolecular complex and interacts closely with VLCAD [8]. All cell lines had an increase in TFPα as demonstrated by western blotting (Fig. 18B). Control cells, along with patient cell lines 1 and 2 had increased TFPβ subunit across various concentrations (Figs. 18B, 18C). VLCAD-1 had a 1.7-fold change in TFPβ subunit at various concentrations of REN001, while patient cell lines 2 and 4 did not (Fig. 18C). Immunofluorescence (IF) staining of control fibroblast, FB826, was performed for VLCAD and HADHA antigens (Supplementary Fig. S11A). A 1.3-fold change in VLCAD was found with 30 nM REN001 via immunostaining (Supplementary Fig. S11B). Minimal change occurred in HADHA immunostaining both consistent with western blotting.

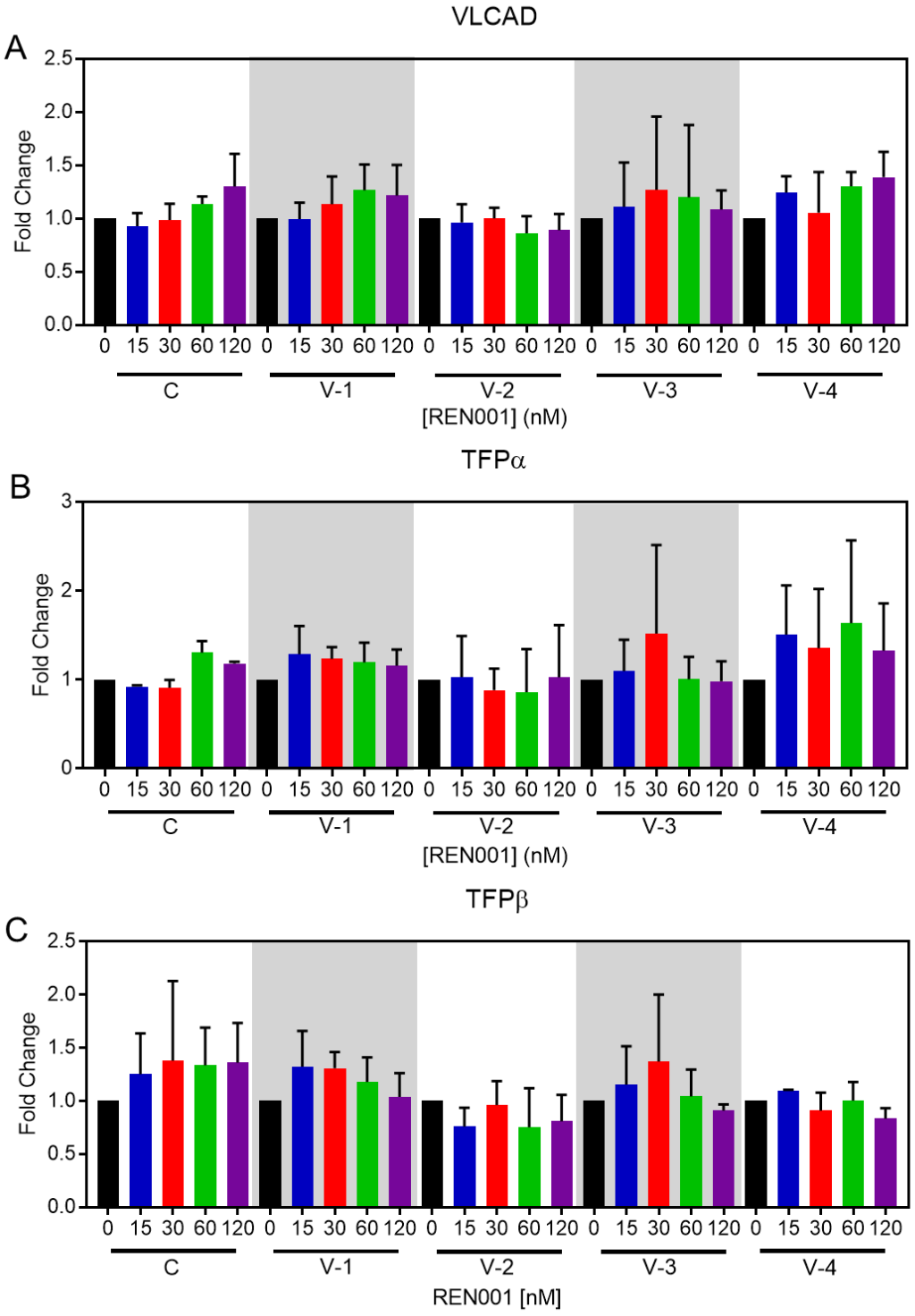

Figure 18. Western blot band quantification of REN001 treated VLCADD and control cells.

VLCAD (A), TFPα (B), and TFPβ (C) protein content were quantified from western blots of whole cell lysates prepared from REN001 treated fibroblasts. Data are fold changes compared to each cell lines own 0 nM treatment.

4.4.3 VLCAD enzyme activity

VLCAD enzyme activity was measured in patient and control cells treated with REN001. Not surprisingly, untreated VLCAD deficient patient derived fibroblasts had significant reductions in VLCAD activity while maintaining normal levels of medium chain acyl-CoA dehydrogenase (MCAD) activity measured as a control (Supplementary Fig. S12A). VLCAD deficient cell lines had a variable response to REN001. VLCAD-1 and -3 had statistically significant increases in VLCAD activity at 60 and 120 nM concentrations, respectively. Neither VLCAD-2 nor VLCAD-4 showed increased activity. The control cell line showed a trend of increasing VLCAD enzyme activity with increasing REN001 concentration that was not statistically significant. MCAD activity for all cell lines at most drug concentrations was unchanged, though VLCAD-3 treated with 60 nM REN001 was slightly decreased (Supplementary Fig. S12B). MCAD activity was not measured for VLCAD-4 due to a limited sample amount.

4.4.4 FAO Flux Assay

A whole cell [^{3}H]-oleate oxidation assay was used to measure overall flux through the fatty acid oxidation pathway and is a measure of VLCADD severity [158]. VLCAD-2, -3, and the control cell line no significant changes in oleate oxidation following drug treatment (Fig. 19). There was a trend towards an increase in flux in VLCAD-1 and VLCAD-4 suggesting minor improvement, but the change reached statistical significance only in VLCAD-4 treated with the highest concentration of REN001 (120 nM, Fig. 19). A minimal or no change in activity was not surprising as the mRNA and protein had small changes.

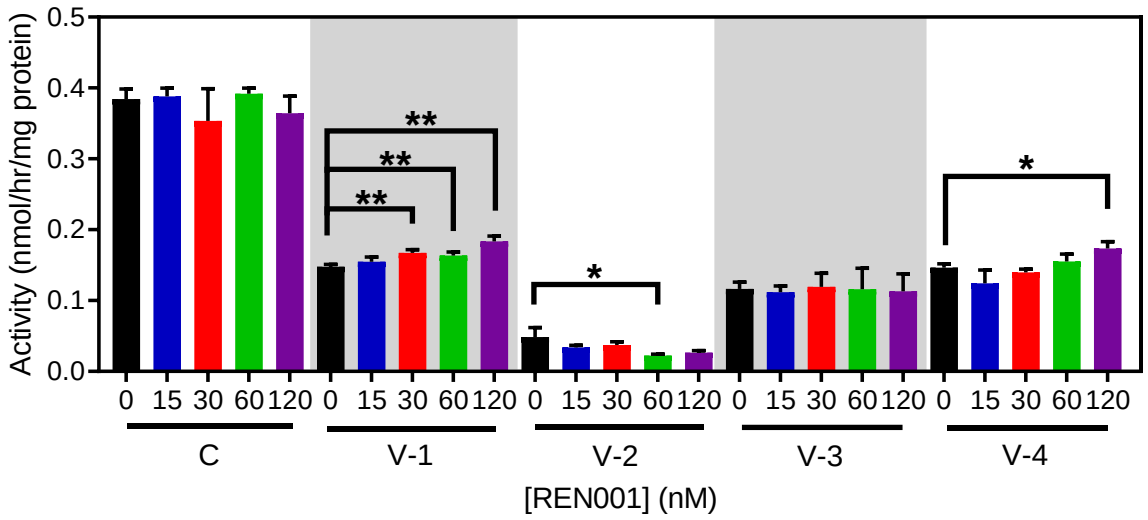

Figure 19. Fatty acid oxidation (FAO) flux in control and VLCAD deficient fibroblasts treated with REN001 for 48 hr.

Bars represent mean and standard deviations in duplicate assays. *p < 0.05, **p < 0.01, compared to each cell lines own 0 nM treatment (*t* test for unpaired samples).

4.4.5 Whole Cell Oximetry

We have previously shown that VLCADD cells show impaired oxidative phosphorylation as measured by whole cell oximetry [56], including VLCAD-1 and -2 used in this study. Oxygen consumption rate (OCR) was measured via a Seahorse XFe96 Extracellular Analyzer. The basal respiration was increased compared to control in all VLCAD deficient cell lines with an increase in maximum respiration and no change in spare capacity or ATP production, a pattern consistent with impaired oxidative phosphorylation and mitochondrial stress (Fig. 20, Supplementary Fig. S13). Control cells showed decreases in all respiratory parameters with REN001 treatment while they increased in VLCAD deficient cell lines. VLCAD-1 and VLCAD-3 had the highest increase in basal respiration at 30 nM while VLCAD-2 had the highest increase at 60 nM (Fig. 20A,

Supplementary Fig. S13D). The control cell line decreased in basal respiration with an increase in REN001 (Fig. 20A). Similarly, maximal respiration and spare respiratory capacity significantly increased across all VLCAD cell lines and significantly decreased in the control cell line (Figs. 20B, 20C). Calculated ATP production also significantly increased in the VLCADD cell lines with the highest increases at 30 nM or 60 nM (Fig. 20D, Supplementary Fig. S13D).

Previous cellular studies have reported variable results using bezafibrate to improve cellular bioenergetics [56, 59, 79, 159]. As a PPAR-δ agonist, REN001 should theoretically have more directed action on the targets of interest in VLCADS than bezafibrate. To test this hypothesis, we treated control and VLCADD fibroblasts with 600 μM bezafibrate and measured oxygen consumption rate (Supplementary Fig. 14). Control cells had decreased basal respiration, maximal respiration and ATP-linked respiration with bezafibrate treatment while there was no statistically significant change in spare respiratory capacity (Fig. 20E-H). VLCAD-1 and -3 had significantly reduced basal respiration, maximal respiration, and ATP-linked respiration with 600 μM Bezafibrate (Fig. 20 E, F, H). VLCAD-4 had no statistically significant differences in basal respiration, maximal respiration, spare respiratory capacity, or ATP-linked respiration (Fig. 20E-H). VLCAD-3 had no statistically significant differences in spare respiratory capacity. VLCAD-2 was an outlier in these experiments, with an improvement in all parameters with bezafibrate treatment (Fig. 20E-H).

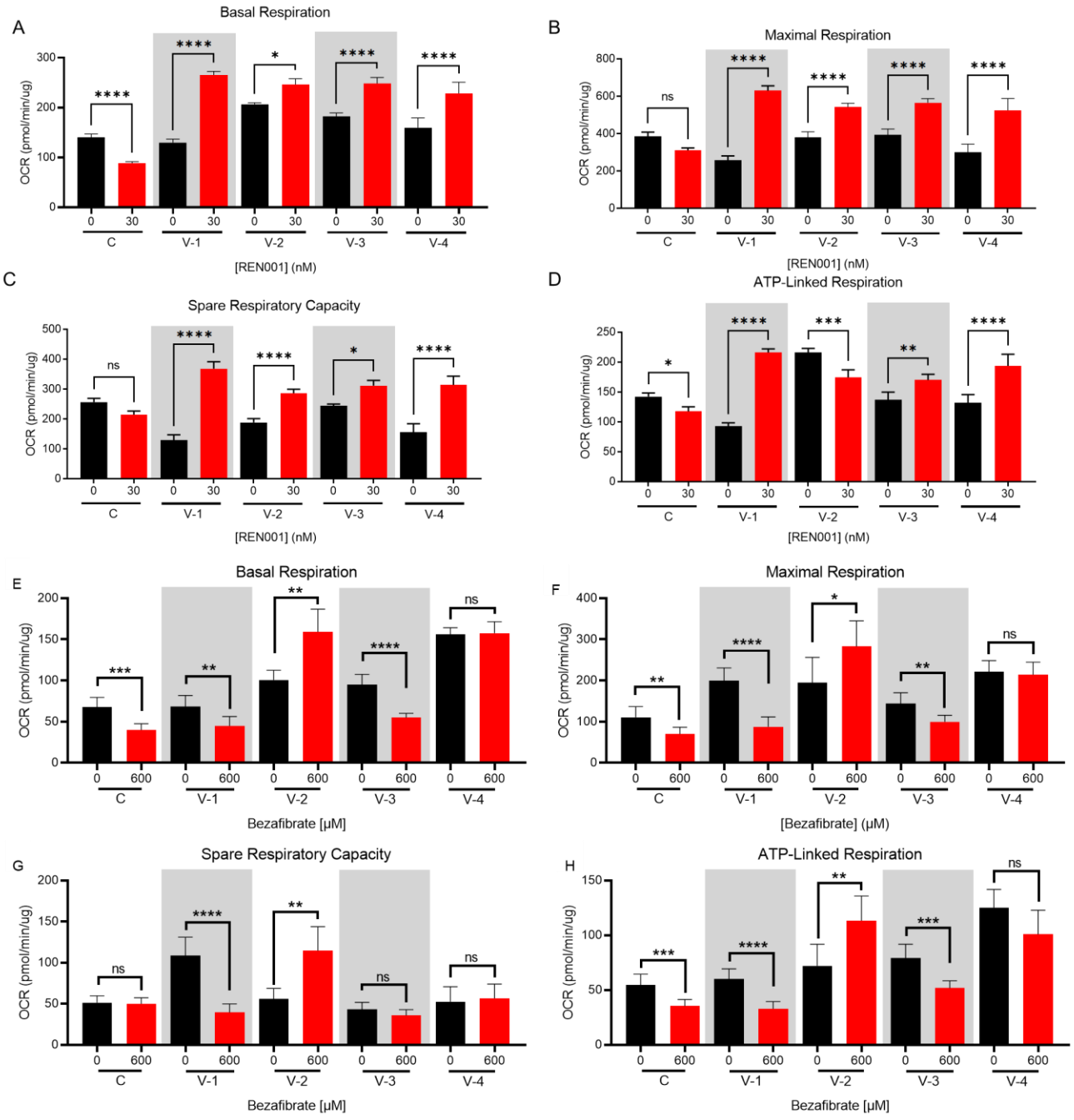

Figure 20. Oxygen consumption rate of control and VLCAD deficient cell lines treated with REN001 or bezafibrate for 48 hr.

Basal respiration (A, E), maximal respiration (B, F), spare respiratory capacity (C, G), and ATP production (D, Hn). Bars represent mean and standard deviations in duplicate assays. *p < 0.05, **p < 0.01, ***p <0.001, ****p < 0.0001, ns = no significant, compared to each cell lines own 0 nM treatment (t test for unpaired samples).

4.4.6 ATP Production

An increase in ATP production can be indicative of less cellular stress and increased FAO protein due to REN001 treatment. We therefore directly measured ATP production with a real-time rate ATP assay via a Seahorse XFe96 Extracellular Analyzer. All cell lines significantly increased their total ATP production (Fig. 21C). Glycolytic and mitochondrial ATP production were significantly increased across all VLCADD cell lines (Fig. 21A, 21B).

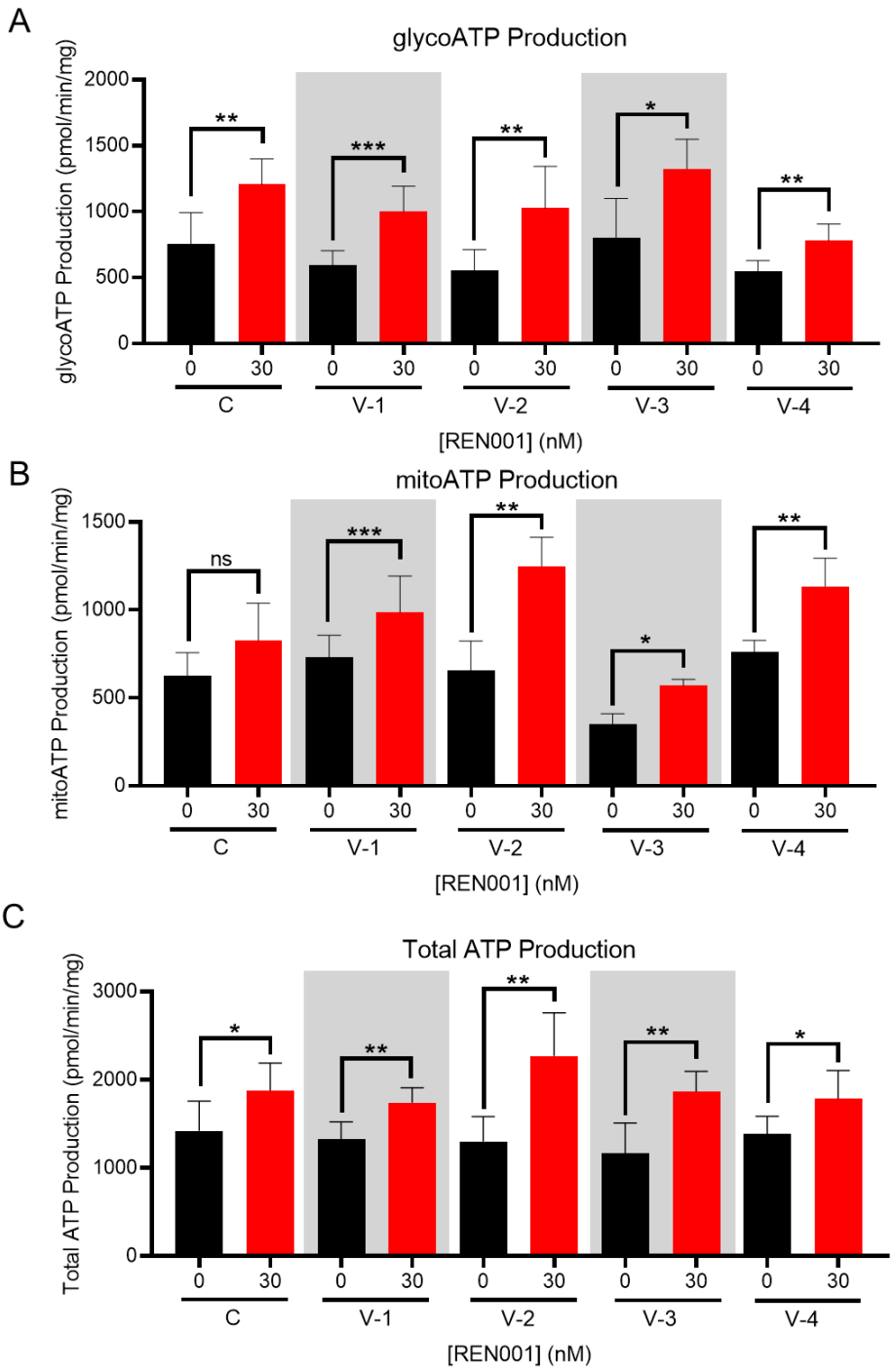

Figure 21. Real-time ATP production measured in control and VLCAD deficient fibroblasts treated with REN001 for 48 hr.

Bars represent mean and standard deviations in duplicate assays. *p < 0.05, **p < 0.01, p<0.001, ns = not significant, compared to each cell lines own 0 nM treatment (*t* test for unpaired samples).

4.4.7 Acylcarnitine profile analysis

Acylcarnitines in media accumulate from cellular metabolism and a characteristic pattern including increases in long chain saturated and unsaturated species can be detected in media from VLCAD deficient cells, consistent with the profile seen in blood samples from patients. Reduction of these species following REN001 treatment would suggest improved VLCAD function. As expected, palmitoylcarnitine (C16) was elevated in growth medium from all of the VLCADD patient fibroblasts, except VLCAD-1, compared to control (Supplementary Fig. S15C). REN001 treatment did not decrease palmitoylcarntine in any VLCADD cell lines treated at the various concentrations (Supplementary Fig. S15C). Palmitoylcarnitine significantly increased at 120 nM treatment in VLCAD-1, -3, and -4 suggesting that the higher dose of drug is toxic (Supplementary Fig. S15C). No change was seen in the media of VLCAD-2 cells at any drug level. Acetylcarnitine (C2) reflects levels of the acetyl-CoA end product of FAO and is typically lower in VLCAD deficient patients and patient cells. Increased flux through FAO in patient cells could increase acetylcarnitine, though alternative metabolic pathways would utilize increased acetyl-CoA before it can accumulate. An increase in acetylcarnitine was not detected in media of the patient cell lines with REN001 treatments, with VLCAD-1 and -2 having statistically significant decreased at 30 and 120 nM treatment (Supplementary Fig. S15A). Control cells did not significantly change in acetylcarnitine with REN001 treatment (Supplementary Fig. S15A). Both control and VLCADD cell lines did not statistically increase in C14:1 carnitine media levels, except VLCAD-4 (Supplementary Fig. S15B).

4.5 DISCUSSION

There is no effective treatment for VLCAD deficiency. Rather, current treatment protocols rely on dietary restrictions and replenishment of the deficiency in energy using a supplemental dietary energy source such as medium chain triglyceride oil or the newly FDA approved heptanoic acid in the triglyceride form, triheptanoin [46, 47, 160, 161]. However, the treatment is inadequate as episodes of rhabdomyolysis and cardiomyopathy persist. Gene therapy has been reported in mice, but has not been developed further for humans [162].

In this study, we focused on enhancing the expression of genes involved in mitochondrial bioenergetics, including FAO, using the PPARδ agonist REN001. We hypothesized that such a treatment could either directly or indirectly improve energy metabolism in cells from patients with VLCAD deficiency partly by raising the amount of partially active mutant VLCAD protein. Our results demonstrated a statistically significant increase in *ACADVL*, *HADHA* and *HADHB* via mRNA analysis following treatment of patient cells with REN001. Indeed, there was a small increase in protein levels of both VLCAD and TFP protein as well as cellular FAO flux in a dose dependent fashion. More importantly, we demonstrated an improvement in the cellular overall bioenergetic state with REN001 treatment as measured by oxygen consumption and ATP production. These findings, in combination, indicate an improvement in the overall bioenergetic health of patient fibroblasts, and identify REN001's potential as a therapeutic agent for VLCAD deficiency.

Not surprisingly, response of VLCAD deficient cell lines to REN001 was variable given that each had a unique mutant genotype VLCAD protein with variable instability. Similar results have been reported when treating VLCAD deficient fibroblasts with bezafibrate, a pan-PPAR activist with considerably less delta activity that REN001 [79]. In that study, fibroblasts with the

most protein damaging mutation had minimal effect with bezafibrate treatment, including no rescue of VLCAD protein. An additional study of VLCADD fibroblast from 33 different patients with 45 different *ACADVL* mutations similarly confirmed that bezafibrate treatment in cells with less damaging point mutations responded better than those with insertions, deletions, or frameshift mutations [59]. A similar finding was evident in our study. Fibroblasts VLCAD-2 (with the most severe predicted mutant genotype/least protein stability) exhibited only a small increase in enzyme activity and protein content with treatment, but no increase in fatty acid oxidation flux, and only minimal improvement in oxygen consumption rate. Of note, VLCADD fibroblasts containing the c.848T>C (p.Val283Ala) (VLCAD-4) and c.520G>A (p.Val174Met) (VLCAD-1) variants behaved similarly with REN001 treatment compared to cell lines containing the same mutations and treated with bezafibrate [59, 159]. Bezafibrate treatment restored FAO flux to 65 to 75% of control, 1.3 to 2.3 fold increase in VLCAD mRNA, and 2.2 to 4.8 fold increase in VLCAD activity in cell lines containing c.848T>C (p.Val283Ala). Bezafibrate treatment also increased FAO flux to 65% of control and 1.3 to 2.3 fold increase in VLCAD mRNA expression in a homozygous c.520G>A (p.Val174Met). In VLCAD-1, 120 nM REN001 treatment did not restore FAO flux, and elicited a minimal increase in VLCAD activity with a 2-fold increase VLCAD mRNA expression. Similarly, REN001 treatment minimally increased FAO flux and VLCAD expression, while VLCAD mRNA expression increased 3.1- fold in VLCAD-4 similar to bezafibrate treatment.

Our results confirm the need for an individual, mutation specific approach for selecting approach drug therapies for VLCADD patients. In considering the use of a PPARδ agonist for treatment of patients, it is likely that dosing differences related to the relative delta effects of the drugs are likely to be critical. Thus while, bezafibrate had some activity at high concentrations

(400-600 μM) in some previous *in vitro* studies, it was ineffective in others [56], and has not shown efficacy in clinical trials in patients [82]. For the most part, we found worsening or no change in oxygen consumption with bezafibrate treatment, even at 20,000-fold higher concentration bezafibrate (concentration based on previous published studies) compared to REN001. However, one cell line responded to bezafibrate treatment even though the cell line had minimal response with REN001, demonstrating a possible genotype specific effect. Importantly, the minimal effective dose for REN001 in our study was 30 nM, more amendable to dose escalation as needed in patients. A clinical trial for resveratrol, proposed to have both PPARα -γ agonist effects [163], showed no improvement on fatty acid oxidation or exercise capacity in VLCADD or CPT2 deficient patients [164].

One limitation of this study is that the treatments were performed in patient derived fibroblasts. VLCAD patients suffer from both cardiomyopathy and rhabdomyolysis due to dysfunction of heart and skeletal muscle, respectively [41, 43, 110, 165, 166]. Since fibroblasts contain fewer mitochondria compared to both, translation of fibroblast results to patients remains uncertain. Additional experiments in other long chain fatty acid oxidation disorders including TFP, LCHAD, and CPT2 deficiencies are necessary to expand our results to them. An *ACADVL* null mouse model with no residual protein [167, 168] is not ideal for testing REN001 given the lack of VLCAD protein. Rather, a point mutation in *ACADVL* generated via CRISPR/Cas technology would provide additional insight into the drug's effect in a whole organism [105, 106, 123].

In summary, our results identify PPARδ agonists, such as REN001, as a potential treatment for VLCAD deficiency, exhibiting a positive effect on enzyme activity and cellular bioenergetics. Since results are mutation specific, a personalized medicine approach will be necessary to assess the likelihood of utility based on their mutation status.

4.6 ACKNOWLEDGEMENTS

JV was supported in part by NIH grant R01 DK109907 and from a research grant from Reneo Pharmaceuticals. We thank Yuxun Zhang, PhD from Eric Goetzman, PhD Laboratory, University of Pittsburgh, Children's Hospital of UPMC for ETF supply for the ETF fluorescence reduction assays.

4.7 AUTHOR CONTRIBUTIONS

OMD reviewed literature, developed experimental design, and completed most functional studies including cell culture, compound treatments, western blotting, qPCR, ETF fluorescence reduction assay, oleate tritium release assay, Seahorse Mito Stress test, Seahorse ATP Rate Assay, and immunofluorescence (IF) staining and imaging. OMD compiled data, performed statistical analysis, and drafted manuscript. YLP completed the ChIP seq analysis for PPARδ and experimental design for qPCR. CVL performed media acylcarnitine profiling. AK developed experimental design and helped with western blotting, Seahorse experiments, and IF staining and imaging. AD reviewed the final manuscript. A-WM developed experimental design and reviewed manuscript. JV developed experimental design and reviewed manuscript. All authors discussed and approved the manuscript before submission.

5.0 CONCLUSIONS

5.1 SUMMARY OF FINDINGS

In Aims 1 and 2, I successfully generated two distinct null HEK293T models for *IVD* and *ACADVL* utilizing CRISPR/Cas technology. The *IVD* null HEK293T cell line contained no IVDH protein or enzyme activity, and thus was suitable for expression experiments with control and variant *IVD* variant plasmids. The variant expression studies correlated well to the level of IVDH activity and protein in patient, validating the utility of the system (Table 4). The *ACADVL* null HEK293T cells similarly contained no VLCAD protein or enzyme activity, and expression studies of variant plasmids confirmed pathogenicity. In addition, for the VLCAD studies, I adopted a high-throughput ETF fluorescence reduction microplate assay that allowed me to test 8 samples simultaneously, thus reducing overall assay time. Once again, results with the expression system compared favorably to patient fibroblast activity (Table 5).

Table 4. Comparison of IVA patient fibroblast and HEK293T expression system functional studies.

Cell Line Designation Origin	Mutation	Fibroblast Functional Studies		HEK293T Functional Studies	
		Western blot	IVD activity	Western blot	IVD activity
FB826	--	100%	100%	Normal	100%
FB825	c.932C>T, p.Ala311Val c.707C>T, p.Thr236Ile	50.7%	11.8%	Normal Normal	13% 8%
FB118	c.149G>C, p.Arg50Pro	ND	ND	Barely detected	0%
FB827	c.986T>C, p.Met329Thr c.1010G>A, p.Arg337Gln	0.1%	7.3%	Barely detected Barely detected	0% 0%
FB909	c.1232G>A, p.Arg411Gln	11.3%	27.9%	Normal	1%
FB925	c.521T>G, p.Val174Gly c.1179del>fs, p.Leu394Phe	6.0%	15.8%	Normal Barely detected	76% 0%

ND = Not determined

Table 5. Comparison of VLCADD patient fibroblast and HEK293T expression system functional studies.

Cell Line Designation Origin	Mutation	Fibroblast Functional Studies		HEK293T Functional Studies	
		Western blot	VLCAD Activity	Western blot	VLCAD Activity*
FB826	--	100%	100%	Normal	100%
FB671	c.1619T>C, p.Leu540Pro c.1707_1715dup, c.Asp570_Ala572dup	0.3%	12.2%	Barely detected Barely detected	10% 3%
FB782	c.848T>C, p.Val283Ala c.1248A>C, p.Ile420Leu	3.7%	18.7%	Reduced Reduced	18% 25%
FB894	c.535G>A, p.Gly179Arg	66.4%	50.6%	Normal	4%
FB895		38.8%	51.5%	Normal	
FB904	c.1217A>C, p.Gln406Pro	20.7%	19.0%	Normal	5%

*Activity measured with C21-CoA as substrate.

In Aim 3, I demonstrated that VLCADD patient derived fibroblasts had a variable effect in response to treatment with a PPARδ agonist, REN001. Not surprisingly, VLCADD cell lines containing point mutations had a more robust response to REN001 treatment with improved bioenergetics than those cell lines containing null mutations. These results demonstrate the need for individualized treatment plans for VLCADD patients based on their genotype.

5.2 STRENGTHS AND LIMITATIONS

Development of a high throughput expression and assay system based on null HEK293T cells offer the opportunity to assess the impact of any variant on enzyme function so long as a suitable readout of enzyme function is available. Of course, the starting point is to first introduce a null mutation into HEK293T cells, but thus far, this has not been difficult, and in addition to VLCAD and IVD deficiencies, we already have null cells for propionic acidemia, methylmalonic acidemia, PKU, SBCAD, and IBD deficiency. The nature of the functional assay must also be adaptable to high throughput methods. Here, the microtiter plate ETF reduction assay is suitable

for use in testing deficiency of any of the ACADs, all of which are identified through newborn screening. In other of the newborn screening diseases, accumulation of a characteristic metabolite identifiable by tandem MS offers the opportunity to show effect of loss of enzyme activity with another technique that is versatile and high throughput. Overall, this technique should be applicable to essentially all of the metabolic disorders identified by tandem MS NBS. Construction of variant expression plasmids is also straightforward as they can be ordered directly from a commercial service that provides quality testing and fast delivery that is amenable to clinical lab application. Since time is of the essence in a newborn screening situation, establishment of all the necessary cell lines and a reliable plasmid synthesizing facility will minimize the time from identification of VUS to establishment of pathogenicity, with results in as little as a week. Since all the currently screened metabolic disorders are autosomal recessive, it may ultimately be of interest to assess interacting effects of different mutations, for example testing for positive negative effects. This system is amenable to such studies, though they are likely to be of more academic than clinical interest.

Of note, this expression system is dependent on an activity assay that is specific for the targeted enzyme. In this regard, VLCAD activity presents difficulty due to the overlapping substrate specificity of LCAD and ACAD9 for long chain substrates. In practice, we overcame this problem through the use of C21-CoA as substrate, which is more efficiently utlilized by VLCAD as compared to the other two long chain enzymes. Another approach would be to generate HEK293T cells deleted of all of the long chain ACAD loci. Such an approach has been used by our collaborator Dr. Sandor Houten who has introduced as many as three mutations into a single cell line to isolate a single branched-chain ACAD activity.

Experiments with REN001 were exciting, but leave additional questions unanswered. First, other PPARδ agonists are available but their efficacy at the cellular level has not been compared to REN001. While this is technically possible, the practical reality is that none of the others are currently in clinical trials to treat VLCADD. Thus, it makes the most sense to continue to study REN001 for now. While in my studies, I did not see much effect of the drug on FAO flux in patient cells, this is almost certainly mutation dependent, and will vary depending on the level of residual activity seen with specific mutations. Regardless, even without increased FAO flux, treated cells showed an improvement in cellular bioenergetics including oxygen consumption and ATP production due to upregulation of the other PPARδ responsive pathways, factors that are likely to lead to improvement in patient outcomes. This result is not surprising as PPARδ agonists are known to upregulate additional pathways including the respiratory chain, TCA cycle and antioxidant pathways, which can improve energy metabolism directly or indirectly [66, 69, 70, 80].

The major limitation of my study is the lack of an appropriate animal model to test the effects in a whole organism. A VLCAD deficient mouse models exists, however, it is a knock out model. Thus, REN001 treatment will not directly affect FAO function as no stable VLCAD protein can be expressed. However, as with patients with functionally null *ACADVL* mutations, the effect of drug on the other pathways would still be addressed. In this regard, it would serve as a useful model of human disease. Another valuable option would be to generate a mouse model containing an *ACADVL* point mutation using Crispr/Cas9 technology, especially one with known partial activity such as the p.1258A>C (p.Ile420Leu) variant.

5.3 COMPARISON OF PRIMARY FIBROBLASTS AND HEK293T EXPRESSION SYSTEMS

Primary human fibroblast cells lines historically have been utilized to perform functional studies for FAO and BCAA VUS determination and treatment studies of potential drugs. Benefits of using the patient fibroblast cells are allele interactions can be determined, measuring the effect of both variants on total enzyme activity, plus any additional variation in the patient's genome that could affect the overall health. Drawbacks of fibroblasts cell lines include not being able to study one variant at a time and isolate the effect on enzyme activity and stability. Additionally, patients and/or parents/guardians need to consent for a skin biopsy in order to isolate and culture fibroblasts. A skin biopsy while easy to perform, is invasive and families may not always be willing to consider the procedure, especially if their child is currently healthy. Fibroblast cultures require 4 weeks to 4 months of culturing in order to isolate fibroblasts from other skin cells and expand the cultures enough to perform the functional studies. Additionally, FAO and BCAA patient fibroblasts can grow slower than control fibroblasts which can lengthen the time to culture enough cells for functional studies.

A recombinant protein expression system is when an expression plasmid containing the gene of interest are transfected into a prokaryote or eukaryotic cell. These cells express the plasmid utilizing their endogenous cellular machinery and transcribe and translate the protein from the DNA template in the expression plasmid. Benefits of expression systems include generating a large amount of the desired protein for functional studies, generation of protein quickly, and the possibility to perform other experiments including purification for protein crystal structure. Limitations of expression systems include incorrect protein folding, inclusion bodies, and non-physiologic protein:protein interactions.

Prokaryotic expression systems have several advantages over eukaryotic systems. *E. coli* is most commonly used in prokaryotic expression systems due to their short doubling time (about 20 minutes), easy and quick transfection, and ability to generate a large volume of protein in several hours [169, 170]. Limitations of *E. coli* expression include that the recombinant peptide expressed in the *E.coli* requires different pH, cofactors, and folding mechanisms that may not be available in the *E. coli* environment [169, 170]. Protein modifications such as glycosylation and acylation also do not occur. This environment and the large volume of peptide can result in protein instability and aggregation, leading to inclusion bodies. [169, 170]. The inactive protein in inclusion bodies cannot be utilized for most other functional *in vitro* studies.

Eukaryotic expression systems overcome some of these limitations. Mammalian expression systems specifically have several advantages over other eukaryotic expression systems such as yeast or insect systems. The major advantage of utilization of a mammalian expression system is the ability of the mammalian cells to perform post-translational modifications to the expressed proteins [171]. These post-translational modifications include modifications to amino acids such as removal of the first methionine residue, removal of targeting peptides, glycosylation, acylation, phosphorylation and disulfide bridge formation or reduction [171, 172]. Not all of these modifications occur in *E. coli* or yeast and thus such proteins may not be an accurate representation of the mature native enzyme [169, 171]. A common cell line used for mammalian expression systems is the human embryonic kidney (HEK) 293T cells [173]. HEK293 cells were derived in 1973 from the kidney of an aborted human embryo of unknown parenthood by transformation with sheared Adenovirus 5 DNA [125, 174]. In 1985. They were further derived by transfecting the plasmid pRSV-1609 which contained neomycin/G418 resistance and expression of the tsA1609 allele of the Simian Vacuolating Virus 40 TAg (SV40) large T antigen [175, 176]. The modified

HEK293 cell line, HEK293T, containing the SV40 T antigen enables the amplification of vectors containing the SV40 origin of replication that can replicate in the HEK293T cells [125, 133, 175, 176]. This maintains a high copy number of plasmid and thus considerably increases the expression levels obtained with transient transfection [175, 176].

Utilization of both the *IVD* and *ACADVL* null HEK293T expression systems has reduced the overall time to perform functional studies and report results to clinicians to modify treatment plans if necessary. We have modified the mammalian expression plasmid, plasmid cloning vector (pcDNA3.1(+)), which contains the SV40 T antigen origin of replication, to include either the *IVD* or *ACADVL* control or variant gene. Traditional fibroblast functional studies from time of skin biopsy to final results is about 6 to 12 months while utilization of the expression system from time of confirmatory DNA sequencing results to final results is 1 month. However, if the plasmid design, order, and preparation (plasmid transformation into *E. coli* and midi prep) are excluded, the total time from transfection to functional study results is 3-5 days (Fig. 22).

The utilization of a microplate assay instead of a cuvette assay for the ETF fluorescence reduction assay for ACAD activity has greatly reduced the time required for the assay and reagent amounts needed. This is important as ETF is not commercially available and must be generated in house for experiments. While ETF has been traditionally harvested from pig liver [177], we utilized a recombinant ETF in an *E. coli* expression system to generate the amount of ETF needed for these experiments [134]. This allowed for less labor intensive purification and a higher yield of ETF. The microplate assay also allowed for 8 samples to be performed in the same amount of time as one cuvette assay. This greatly reduced the time needed to perform replicates and allowed for more CoA substrates to be assayed in the same day. A 96-well microplate assay can analyze the same amount of assay reactions that the cuvette assay would take 3 days to perform.

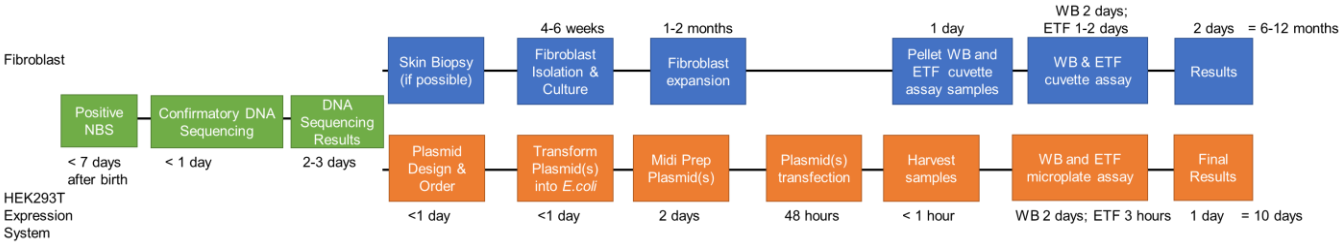

Figure 22. Timeline comparison of fibroblast analysis vs HEK293T expression system.

ACAD deficient fibroblast collection and functional analysis requires 6-12 months total time in addition to the patient/parent or guardian consenting to the intial fibroblast collection. The HEK293T expression system requires 10 days total, most of this time is plasmid design and expansion. The functional studies for the HEK293T expression system, inlcuding the ETF microplate assay, requires only 3 days.

5.4 TRANSLATING CELLULAR DATA TO CLINICAL TRIALS

Preliminary data is needed to move a new treatment to clinical trial and ultimately obtain FDA approval. In Aim 3, I demonstrated that REN001 treatment improved cellular bioenergetics in four different cell lines with various *ACADVL* mutations with a variable response. While these changes are small and are not statistically significant in terms of VLCAD protein, enzyme activity, FAO flux, and acylcarnitine profiling, upregulation of other energy pathways appeared to improve cellular bioenergetics in the patient cells tested. While I did not explore the change in the full transcriptome induced by out PPARδ agonists, those that were examined behaved as expected with upregulation. These genes include the FAO, ETC, TCA cycle, and mitochondrial antioxidant pathway genes. These additional upregulations likely explain the improvement in cellular bioenergetics observed as demonstrated by the increase in whole cell oximetry and ATP production in patient fibroblasts. Cells did not show any toxicity with REN001 treatment.

Notably, the control cell line used in the Seahorse assays had reduced basal respiration compared to some of the VLCADD cell lines (Fig. 20A). We hypothesize that this is an artifact due to the difference in the control fibroblast donor compared to patients. The control cell line is from a 40 year old woman while the VLCADD cell lines are from patients 6 months to 2 years old (Table 3). However, the cells still showed otherwise normal bioenergetics compared to patient cells. Testing of additional cell lines from various aged donors would allow this issue to be directly addressed

5.5 PUBLIC HEALTH SIGNIFICANCE

IEMs are individually rare, but collectively common. ACAD deficiencies, such as IVA and VLCADD, are identified through newborn screening, the largest public health genetics program in the United States. Follow up confirmatory DNA sequencing after a positive newborn screen often result in VUSs in *IVD* and *ACADVL*. This leads to uncertainty in treatment plans and is a large cost burden on the health care system. The faster the appropriate diagnosis and treatment plan can be established, the less likely a patient is to be hospitalized with metabolic decompensation which is a costly emergency room and admittance. By eliminating the need for an invasive skin biopsy and utilizing a mammalian expression system to perform functional studies, I have been able to decrease the time to determine a VUS pathogenicity in accordance with ACMG guidelines. This will allow for faster IVA or VLCADD confirmatory diagnosis which will lead to the most appropriate treatment plan for patients.

While some treatments such as low-fat diet, triphetanonin or MCT oil supplementation and/or L-carnitine supplementation are available for VLCADD, in severe cases episodes of rhabdomyolysis, hypoglycemia, and metabolic decompensation still occur. When VLCADD patients experience metabolic decompensation, they are admitted into the hospital to receive IV glucose transfusions to stabilize [178]. Patients can be in the hospital for days at significant financial and emotional cost to patients, families and the health care system. While triheptanoin reduces the number of major clinical episodes (MCEs; rhabdomyolysis, hypoglycemia, and cardiomyopathy) and length of hospitalization, MCEs still occur, especially rhabdomyolysis [46, 47, 51, 53, 54, 144]. REN001 treatment in VLCADD could further reduce or prevent these metabolic decompensation episodes and improve quality of life. Other FAO deficiencies such as

TFP, LCHAD, and CPT2, have similar rates of MCEs and hospitalization even with trihepantoin treatment, thus REN001 treatment could be generalizable to these deficiencies.

5.6 FUTURE DIRECTIONS

IVD and *ACADVL* combined have over 400 reported VUSs in the ClinVar database. Use of my high throughput model should allow assessment of all of these variants, assuming a suitable funding source, thus improving the knowledge base of mutations for these disorders and improving outcomes in NBS programs. Application of the ETF fluorescence reduction microplate assay to the *IVD* VUS screen will increase efficiency and allow for more VUS to be screened in a shorter period of time. Submitting functional studies on VUSs to the ClinVar database will greatly improve its utility to those in the field.

Additional null models for genetic disorders for BCAA and FAO disorders can be generated, and used in expression studies to determine pathogenicity of VUS as described in Aims 1 and 2. The list of current MS identified disorders in the RUSP are listed in Table 4, along with the number of VUSs listed in ClinVar. Clearly there is much to do beyond the scope of my original targets.

From a therapeutic standpoint, the PPARδ agonist REN001 can be explored as treatment for most of the other know FAO deficiencies as fibroblast cell lines are available for all of them in the Vockley. Of note, even though *CPT2* gene expression is not thought to be controlled by PPARδ, patients may still benefit from the other positive bioenergetic effects of the drug. Other potential FAO targets include TFP, isolated LCHAD, and MCAD deficiencies, none of which currently have approved therapies.

Table 6. Compilation of BCAA and FAO disorders and number of variants of uncertain signficance associatd with genes causing disorders.

Disorder	Associated Gene(s)	ClinVar VUS
Propionic acidemia (PPA)	*PCCA*	108
	PCCB	111
Methylmalonic acidemia (MMA)	*MMUT*	131
	MMAA	144
	MMAB	130
	MMADHC	37
	MCEE	19
Maple syrup urine disease (MSUD)	*BCKDHA*	77
	BCKDHB	110
	DBT	168
Carnitine palmitoyltransferase II (CPT2) deficiency	*CPT2*	181
Medium chain acyl-CoA dehydrogenase (MCAD) deficiency	*ACADM*	128
Mitochondrial trifunctional protein (TFP) deficiency	*HADHA*	107
	HADHB	69
Long-chain 3-hydroxyl-CoA dehydrogenase (LCHAD)	*HADHA*	107

Appendix A Supplemental Material for Chapter 2

Supplementary Table S1. Clinical information of IVA patients and corresponding fibroblast number designation.

Cell Line	Age	Sex	Mutation	C5-carnitine	Symptoms	Treatment
FB825	6 months	M	c.707C>T, p.Thr236Ile/ c.932C>T, p.Ala311Val	Day 1 of life 0.88mmol/L (NI <0.62) Day 9 of life 1.46 Day 12 of life 1.39	Asymptomatic, normal development	Leu restricted formula levocarnitine 100 mg/mL oral solution: 340 mg, 3.4 mL PO, everyday divided tid or quid
FB827	4.6 months	M	c.986T>C, p.Met329Thr/ c.1010G>A, p.Arg337Gln	Elevated C5-carnitine	Presented with moderate acidosis, no hyperammonemia Asymptomatic with treatment, normal development	Moderate Leu restricted diet, supplement with glycine 90 mg/kg/day and carnitine 80 mg/kg/day
FB909	3 months	F	c.1232G>A, p.Arg411Gln/ c.1232G>A, p.Arg411Gln	Day 2 of life 6.60 Day 3 of life 13.22 (NI <0.35 isovaleryl glycine) Day 9 of life Urine organic acids >1,000 mmol/mol	Asymptomatic with treatment, normal development	Leu restricted diet and breastfeed Glycine 2.2 cc, PO, TID levOCARNitine 100 mg/mL oral solution 1 cc, PO, TID
FB925	3.5 months	F	c.1179del, p.Leu394 fs/c.521T>G, p.Val174Gly	Day 2 of life 0.92 mcmol/L Day 9 of life 0.69	Asymptomatic	No dietary restriction or L-carnitine supplementation

Summary of clinical information of IVA patients. Age represents age of patient at time of skin biopsy.

Supplementary Table S2. Oligonucleotide sequences for sgRNA cloning and genomic PCR screening for generation of CRISPR/Cas9 genome-edited IVD null lines.

Oligo Name	Sequence (5′ to 3′)
IVD_F1_Intron1	CACCgCTTCAGCCTAGACAGCTTGA
IVD_R1_Intron1	AAACTCAAGCTGTCTAGGCTGAAGc
IVD_F2_Intron1 (*)	CACCgAGCATCAGACTGAAACTGAG
IVD_R2_Intron1 (*)	AAACCTCAGTTTCAGTCTCATGCTc
IVD_F1_Intron3	CACCgTGTTTAATAGGCTGTCCGGA
IVD_R1_Intron3	AAACTCCGGACAGCCTATTAAACAc
IVD_F2_Intron3 (*)	CACCgTATAAGCTTTGTCCTACCAG
IVD_R2_Intron3 (*)	AAACCTGGTAGGACAAAGCTTATAc
IVD_F1	CTAGTAGGCCTGGGTGAGAAGC
IVD_F2	CTCATTGTTCCAGCCACATGTG
IVD_R1	TTCAGAGAGAGGGGCTGCATTC
IVD_R2	ATCATCCAAACCAGAGCCTGCT

(Top 8) Sense and anti-sense BbsI cloning adapters of alternative pairs of intron 1 and intron 3 sgRNAs. Note that sgRNAs derived from adapters marked with (*) were ultimately used in the dual sgRNA targeting screen. (Bottom 4) Forward and reverse primers used for genomic deletion-breakpoint, inversion-breakpoint and sgRNA site PCRs as depicted in Figures 1A and S1A.

Supplementary Table S3. Oligonucleotide sequence of primer and Taqman probes used in IVD ddPCR genomic copy number assays.

Oligo Name	Sequence (5′ to 3′)
IVD_ex1_fwd	GATTGGTGGAGCTAAGAGCTG
IVD_ex1_rev	TGGGAAACGAAGCCGGCAAG
IVD_ex1_FAM	/56-FAM/TCTTCGTGC/ZEN/ATGGCAGAGATGGC/3IABkFQ/
IVD_ex2_fwd	ATGGCTAAGTTCCTTCAGGAG
IVD_ex2_rev	GCAGGTTCTTGAACTCATTGC
IVD_ex2_FAM	/56-FAM/AAGGCCCAG/ZEN/GAGATCGATCGCA/3IABkFQ/
IVD_ex3_rev	GGCTGTGATGCCCAATACGC
IVD_ex3_FAM	/56-FAM/TCTGCTCCA/ZEN/TTCTGTTGGCAGGAA/3IABkFQ/
IVD_in3_fwd	CACCACTCACAGTTCAGTATGG
IVD_ex4_rev	TGGAGTGGGCACCGTAACTG
IVD_ex4_FAM	/56-FAM/ATCTCCTCC/ZEN/ATCACCAGCACATGC/3IABkFQ/
IVD_ex4_HEX	/5HEX/ATCTCCTCC/ZEN/ATCACCAGCACATGC/3IABkFQ/
IVD_ex9_fwd	CCACACCATTCCCTACCTGC
IVD_in9_rev	TGCCCACCTCACTTCCTCTC
IVD_ex9_FAM	/56-FAM/CGTGAGGGA/ZEN/AGCCTTTGGCCAG/3IABkFQ/
IVD_ex12_fwd	CGAGATGCCAAGCTGTATGAG
IVD_ex12_rev	TCAGGACTAGTGAAAGTCTGC
IVD_ex12_FAM	/56-FAM/CGAGGTGAG/ZEN/GCGGCTGGTCATC/3IABkFQ/
Hs_RPP30_in1_fwd	TTCCTAGCGCGGGAAACTCG
Hs_RPP30_in1_rev	TGCAAATCCCTCGCCCTCGT
Hs_RPP30_in1_HEX	/5HEX/TCCTGCAAT/ZEN/GAGGGAACTGAGGC/3IABkFQ/
XIST_ex4_fwd	ACTACCACTGGGCAACAACC
XIST_in4_rev	TTACGCACCTTGACGTGTGG
XIST_ex4_HEX	/5HEX/TCAAGATAC/ZEN/TTTCCTGGTCCCAG/3IABkFQ/

Primer and Taqman probe sets designed using a combination of Primer-BLAST (https://www.ncbi.nlm.nih.gov/tools/primer-blast/) and the IDT PrimerQuest Tool

(https://www.idtdna.com/Primerquest/Home/Index). Note that IVD_ex3_rev was used in conjunction with CRISPE genotyping primer IVD_F2 (Table S2).

Supplementary Table S4. Oligonucleotide sequence of primers used in IVD cDNA or genomic amplification.

Oligo Name	Sequence (5′ to 3′)
IVD_ex1_fwd_2	CGTGGACGATGCAATCAATGG
IVD_ex3_fwd	GCGTATTGGGCATCACAGCC
IVD_ex4_rev	TGGAGTGGGCACCGTAACTG
IVD_ex7_fwd	AGCACCTCTAAGAAGCTGGAC
IVD_ex8_rev	GTAGACACCCTTATTCTCATGG
IVD_ex11_rev	CAGTCCTTAGCAGTGCAATGG
IVD_ex12_fwd2	GGCAATGGCTACATCAATGAC
IVD__ex12_rev_2_UTR	GAGCAAGGGCACAGAGTCAC
IVD_alt3UTR_rev	TTCAGGCAGGAGGATCTTGCA
GPI_fwd	CACCAAGGCACCAAGATGATAC
GPI_rev	AGGAGGATCTTGTGATGCAGAC

Primers listed were used in combination with those listed in Table S3 to validate patient-specific mutations at the mRNA and/or genomic levels.

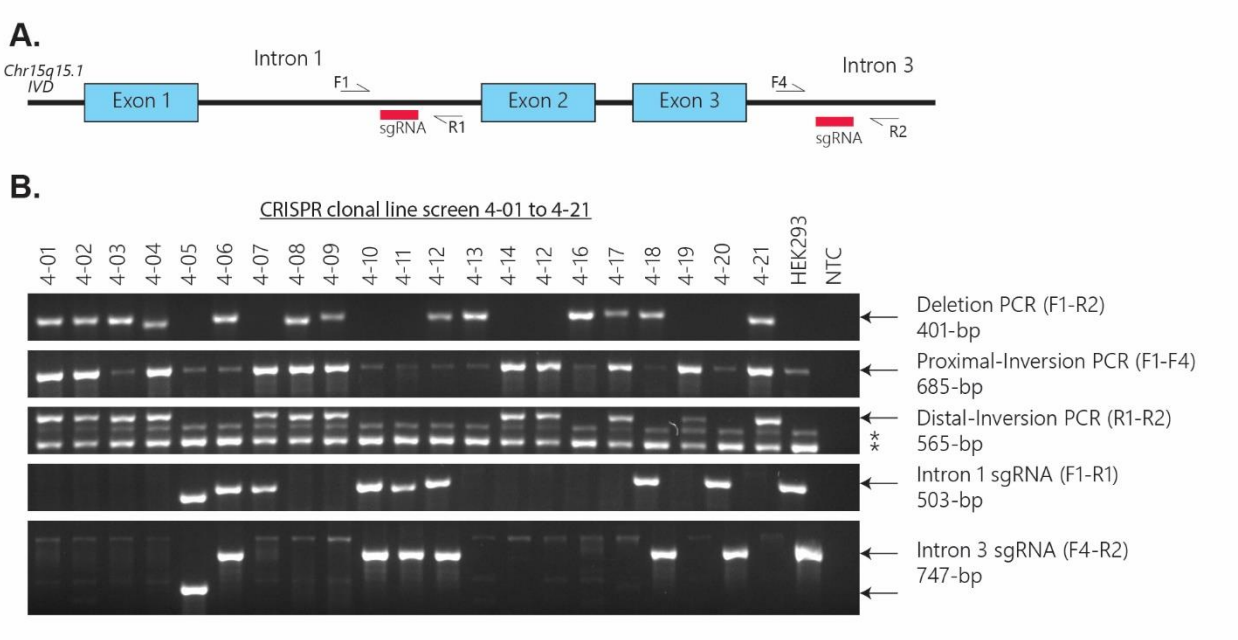

Supplementary Figure S1. A CRISPR/Cas9 screen in HEK293T cells to identify genome-edited clonal lines with *IVD* exons 2-3 either deleted or inverted.

(A) Diagram of CRISPR/Cas9 dual sgRNA targeting of *IVD* exons 2-3. Key: Blue box, *IVD* exons with intervening introns; pink rectangles, sgRNA intron 1 and 3 sites; directional arrows, genotyping primers. (B) Genotyping PCR assays identifying *IVD* null clonal HEK293T lines through presence of deletion (top) and/or inversion (second from top) breakpoint-PCR bands and lack of intact sgRNA sites (bottom). * indicates non-specific band.

Supplementary Figure S2. Direct Sanger sequencing of genomic PCRs to determine molecular composition of CRISPR/Cas9 genome-edited IVD alleles.

Direct Sanger sequencing of (A) deletion-breakpoint PCRs (B) Distal-inversion PCR products (C) intron 1 sgRNA PCR products and (D) intron 3 sgRNA products from clonal null lines and controls. Key for A-D highlight of

sequence: Yellow, intron 1; green, intron 3; grey, sgRNA PAM sequence; magenta, sgRNA intron 1 site; blue, sgRNA intron 3 site; orange, underlying dual waveform chromatograph; and pink, point mutation.

A.

```
A16_2      AAGAGGGGTGAAGATCATCTCTGAGGAGGCATAAACTACTGAGGCCTCTCT-CAGTGGCCTCTCGGCAGGAACACTCTGGGCAGGTGTGTCCCTGCAGGGA100
A16_7      AAGAGGGGTGAAGATCATCTCTGAGGAGGCATAAACTACTGAGGCCTCTCT-CAGTGGCCTCTCGGCAGGAACACTCTGGGCAGGTGTGTCCCTGCAGGGA100
A16_1      AAGAGGGGTGAAGATCATCTCTGAGGAGGCATAAACTACTGAGGCCTCTCT-CAGTGGCCTCTCGGCAGGAACACTCTGGGCAGGTGTGTCCCTGCAGGGA100
A16_6      AAGAGGGGTGAAGATCATCTCTGAGGAGGCATAAACTACTGAGGCCTCTCACCAGTGGCCTCTCGGCAGGAACACTCTGGGCAGGTGTGTCCCTGCAGGG-100
A16_4      AAGAGGGGTGAAGATCATCTCTGAGGAGGCATAAACTACTGAGGCCTCTCACCAGTGGCCTCTCGGCAGGAACACTCTGGGCAGGTGTGTCCCTGCAGGG-100
           ************************************************  ************************************************
```

B.

```
D11_1      AAGAGGGGTGAAGATCATCTCTGAGGAGGCATAAACTACTGAG---GCCTCTCTGTTTGGGGAAGTTACTTGTGGCCTTTTCTCTTGAATGTGTCTGGGTAGT100
D11_2      AAGAGGGGTGAAGATCATCTCTGAGGAGGCATAAACTACTGAG---GCCTCTCTGTTTGGGGAAGTTACTTGTGGCCTTTTCTCTTGAATGTGTCTGGGTAGT100
D11_3      AAGAGGGGTGAAGATCATCTCTGAGGAGGCATAAACTACTGAG---GCCTCTCTGTTTGGGGAAGTTACTTGTGGCCTTTTCTCTTGAATGTGTCTGGGTAGT100
D11_4      AAGAGGGGTGAAGATCATCTCTGAGGAGGCATAAACTACTGAG---GCCTCTCTGTTTGGGGAAGTTACTTGTGGCCTTTTCTCTTGAATGTGTCTGGGTAGT100
D11_5      AAGAGGGGTGAAGATCATCTCTGAGGAGGCATAAACTAGTTTCAGTCTGATGCTGTTTGGGGAAGTTACTTGTGGCCTTTTCTCTTGAATGTGTCTGGGT---100
           ************************************ *            ************************************************
```

C.

```
E11_1  GTCCCTGCAGGGACACACCTGCCCAGAGTGTTCCTGCCGAGAGGCCACTGGTA-------------GGGATTAGGGGAGGCAGTAAGACTGAGGTACTATGAAGACAACCACT     100
E11_2  GTCCCTGCAGGGACACACCTGCCCAGAGTGTTCCTGCCGAGAGGCCACTGGTA-------------GGGATTAGGGGAGGCAGTAAGACTGAGGTACTATGAAGACAACCACT     100
E11_6  GTCCCTGCAGGGACACACCTGCCCAGAGTGTTCCTGCCGAGAGGCCACTGGTA-------------GGGATTAGGGGAGGCAGTAAGACTGAGGTACTATGAAGACAACCACT     100
E11_7  GTCCCTGCAGGGACACACCTGCCCAGAGTGTTCCTGCCGAGAGGCCACTGGTA-------------GGGATTAGGGGAGGCAGTAAGACTGAGGTACTATGAAGACAACCACT     100
E11_11 GTCCCTGCAGGGACACACCTGCCCAGAGTGTTCCTGCCGAGAGGCCACTGGTA-------------GGGATTAGGGGAGGCAGTAAGACTGAGGTACTATGAAGACAACCACT     100
E11_8  GTCCCTGCAGGGACACACCTGCCCAGAGTGTTCCTGCCGAGAGGCCACTGGTA-------------GGGATTAGGGGAGGCAGTAAGACTGAGGTACTATGAAGACAACCACT     100
E11_9  GTCCCTGCAGGGACACACCTGCCCAGAGTGTTCCTGCCGAGAGGCCACTGGTA-------------GGGATTAGGGGAGGCAGTAAGACTGAGGTACTATGAAGACAACCACT     100
E11_10 GTCCCTGCAGGGACACACCTGCCCAGAGTGTTCCTGCCGAGAGGCCACTGGTA-------------GGGATTAGGGGAGGCAGTAAGACTGAGGTACTATGAAGACAACCACT     100
E11_13 GTCCCTGCAGGGACACACCTGCCCAGAGTGTTCCTGCCGAGAGGCCACTGTAGGACAAAGCTTATAGGGATTAGGGGAGGCAGTAAGACTGAGGTACTAT-------------     100
E12_12 GTCCCTGCAGGGACACACCTGCCCAGAGTGTTCCTGCCGAGAGGCCACTGTAGGACAAAGCTTATAGGGATTAGGGGAGGCAGTAAGACTGAGGTACTAT-------------     100
           ************************************************              *********************************
```

Supplementary Figure S3. Sanger sequencing of pJet2.1 cloned genomic PCRs to determine allelic phasing CRISPR/Cas9 genome-edited *IVD* alleles.

Where dual waveforms were observed in chromatographs indicating heterozygosity of genome-edited alleles PCR products were cloned into pJet2.1 and multiple alleles sequenced and aligned. (A) Two distinct near canonical CRISPR/Cas9 deletion breakpoints were identified in clonal line 4-16. (B and C) intron 1 and intron 3 sgRNA sites in HEK293T control line 4-11 sgRNA reveal heterozygosity indicating sgRNA "scarred" alleles with unique indel

mutations without recombination between the two sites. Sequence alignments were carried out using Clustal Omega multiple sequence aligner (https://www.ebi.ac.uk/Tools/msa/clustalo/).

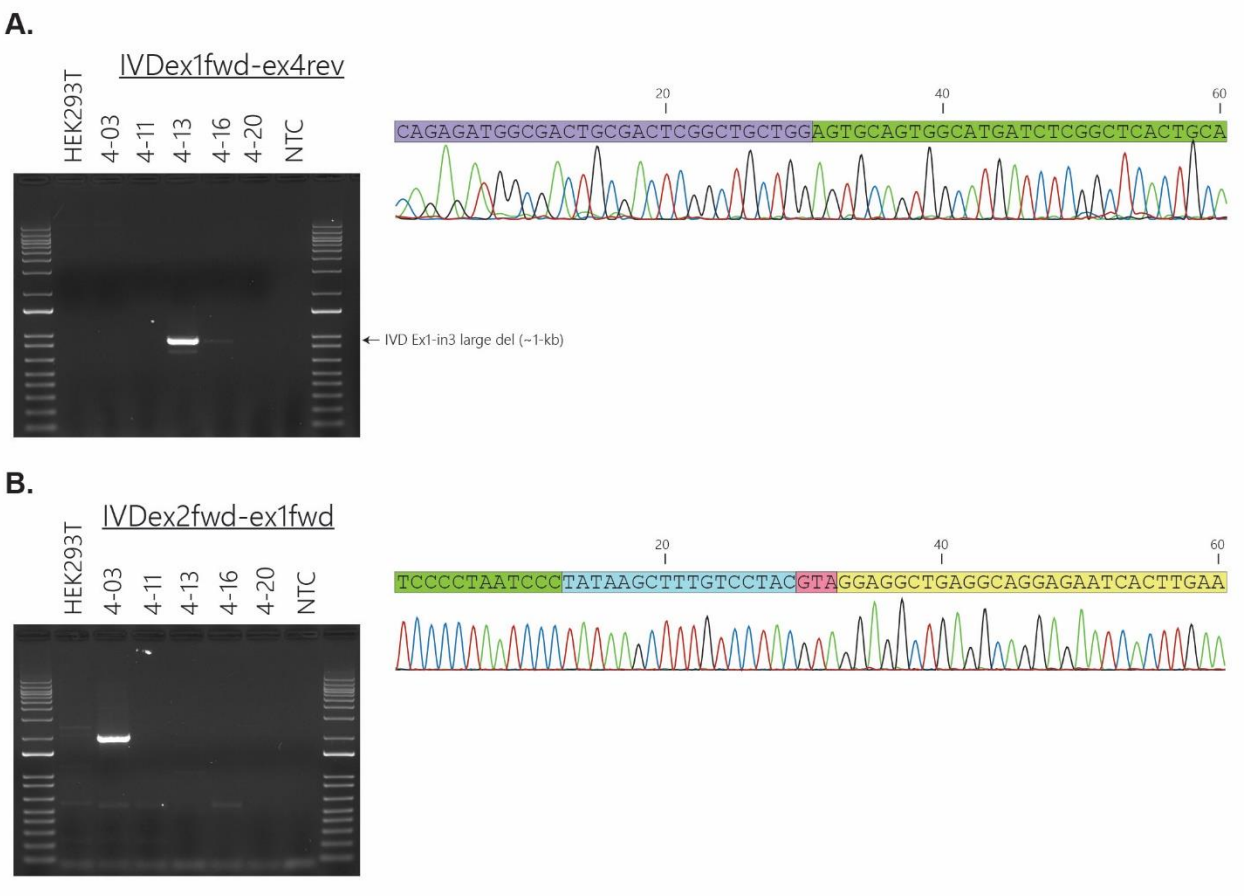

Supplementary Figure S4. Molecular characterization of larger than expected inversion and deletion genome-edited alleles in clonal lines 4-3 and 4-13.

(A) Amplification and DNA sequence of an exon1-exon4 PCR product in 4-13 indicating a 4032-bp deletion including partial deletion of exon 1. (B) Amplification and DNA sequence the proximal-inversion breakpoint in 4-3 indicating a segmental deletion of 531-bp of intron1 upstream of the intron 1 sgRNA PAM site concomitant with the inversion event. Key for A and B highlight of sequence: Purple, exon 1; green, intron 3; yellow, intron 1; blue, sgRNA intron 3 site; and pink, 3-nt insertion.

A.

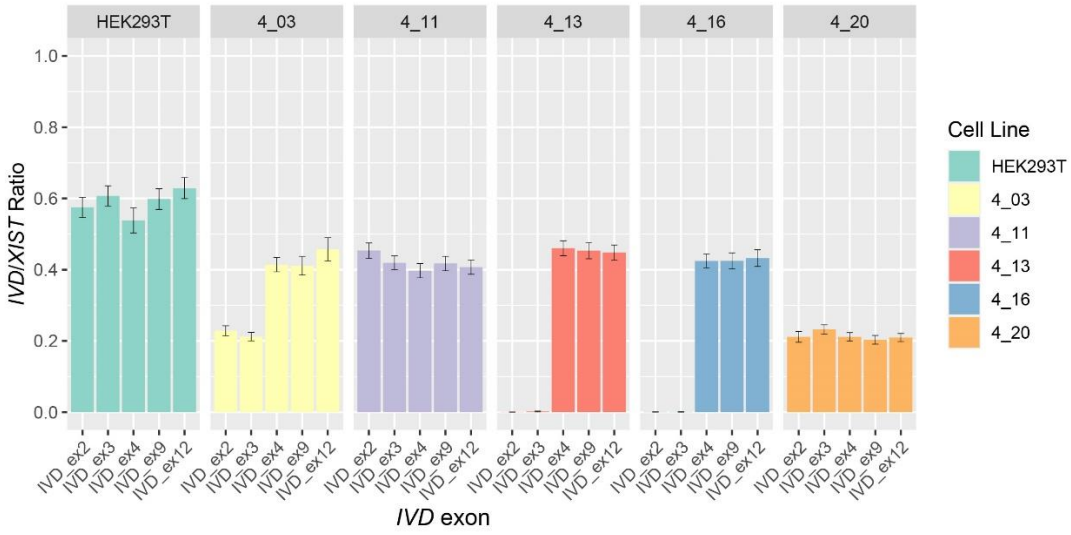

B.

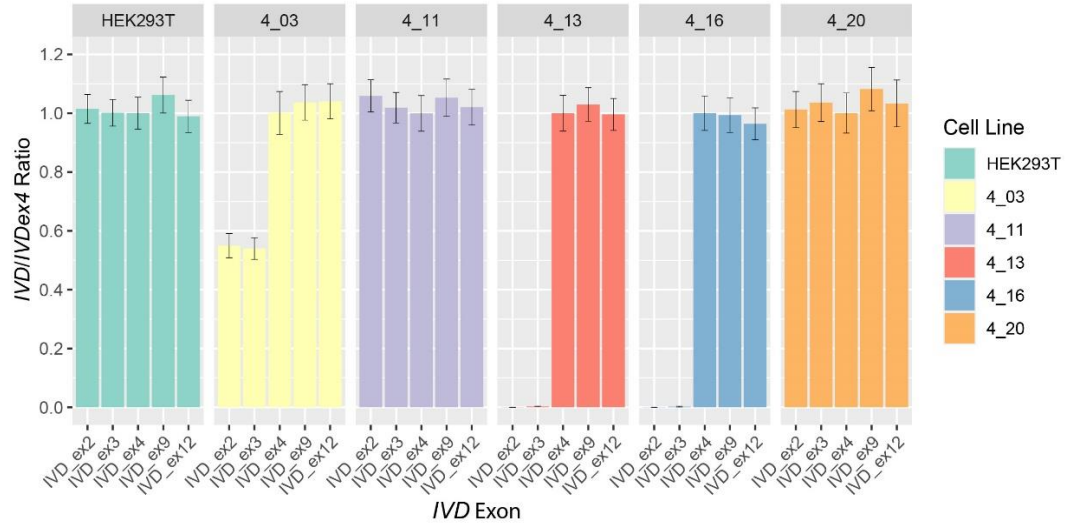

Supplementary Figure S5. Genomic copy number ddPCR assays across the IVD locus using alternative reference loci confirming CRISPR/Cas9 mediated genome-editing.

(A)Genomic copy number as assayed as relative unlinked reference gene XIST. (B) Genomic copy number relative to internal *IVD* exon 4 reference. *IVD* exon 1 has been excluded due to technical error.

A.

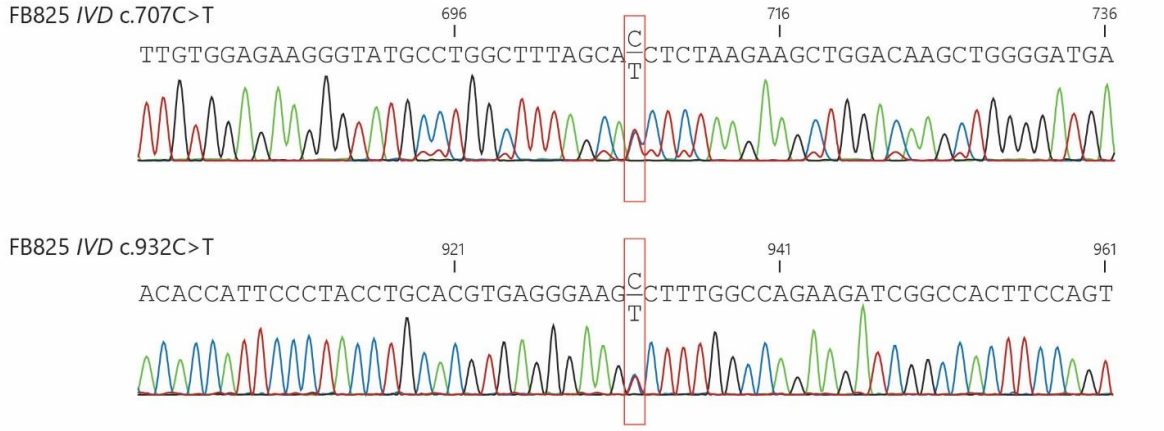
FB825 *IVD* c.707C>T
696
716
736
TTGTGGAGAAGGGTATGCCTGGCTTTAGCA C/T CTCTAAGAAGCTGGACAAGCTGGGGATGA
FB825 *IVD* c.932C>T
921
941
961
ACACCATTCCCTACCTGCACGTGAGGGAAG C/T CTTTGGCCAGAAGATCGGCCACTTCCAGT

B.

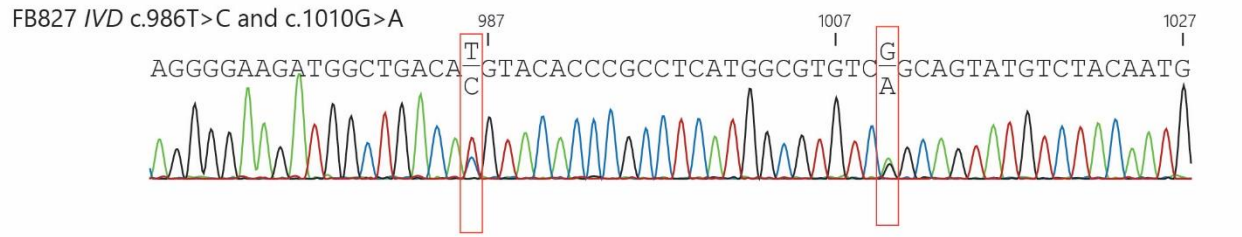
FB827 *IVD* c.986T>C and c.1010G>A
987
1007
1027
AGGGGAAGATGGCTGACA T/C GTACACCCGCCTCATGGCGTGTC G/A GCAGTATGTCTACAATG

C.

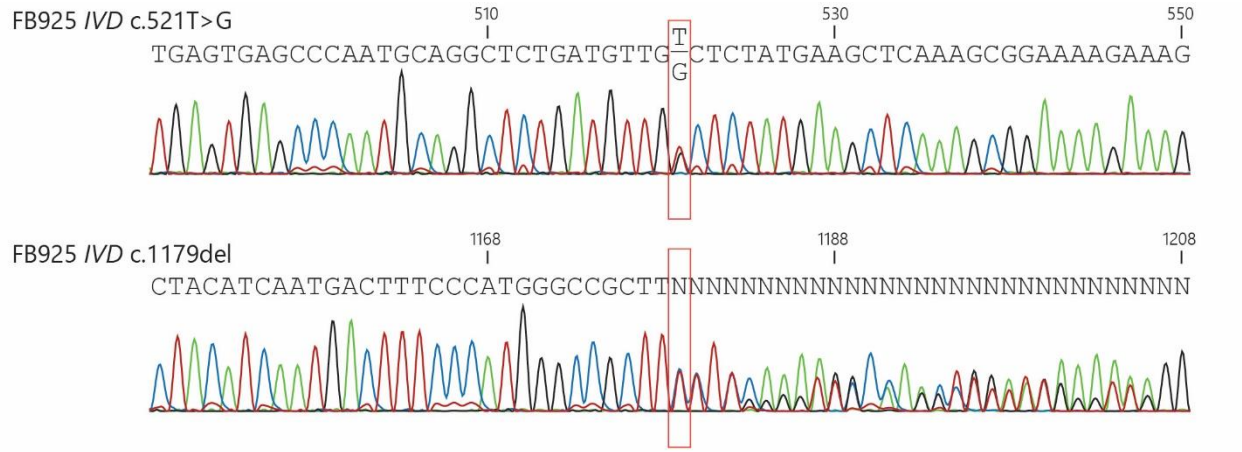
FB925 *IVD* c.521T>G
510
530
550
TGAGTGAGCCCAATGCAGGCTCTGATGTTG T/G CTCTATGAAGCTCAAAGCGGAAAAGAAAG
FB925 *IVD* c.1179del
1168
1188
1208
CTACATCAATGACTTTCCCATGGGCCGCTTNNNNNNNNNNNNNNNNNNNNNNNNNNNNNNN

D.

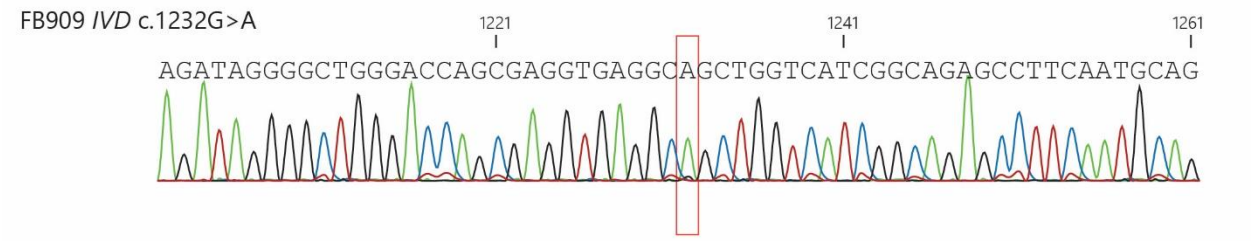

E.

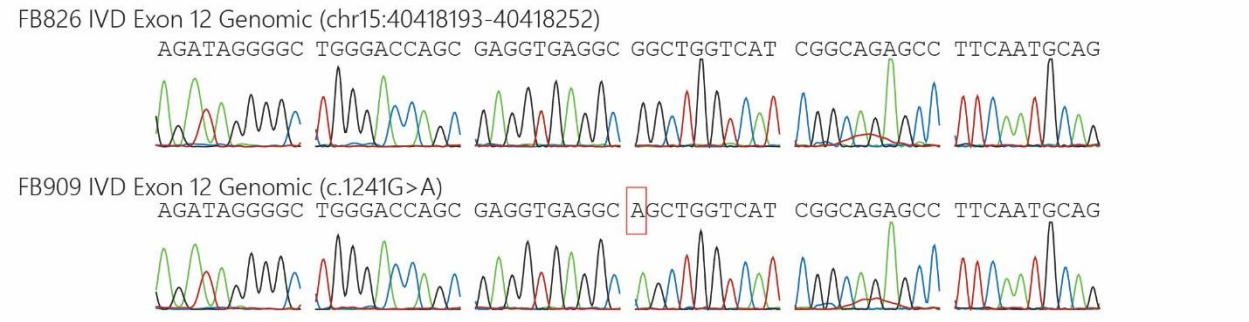

Supplementary Figure S6. Sanger sequencing confirming IVA patient mutations.

(A) Heterozygousity of mRNA expression from patient fibroblasts (A) FB825 exon 7 c.707C>T VUS and exon 9 c.932C>T common mutation (B) FB827 adjacent VUS mutations within exon 10 c.986T>C and c.1010G>A, and (C) FB925 mutations in exon 5 c.521T>G and exon 12 c.1179del. (D) A single homozygous expressed mutation in exon 12 was observed in FB909 and confirmed in (E) at the genomic level.

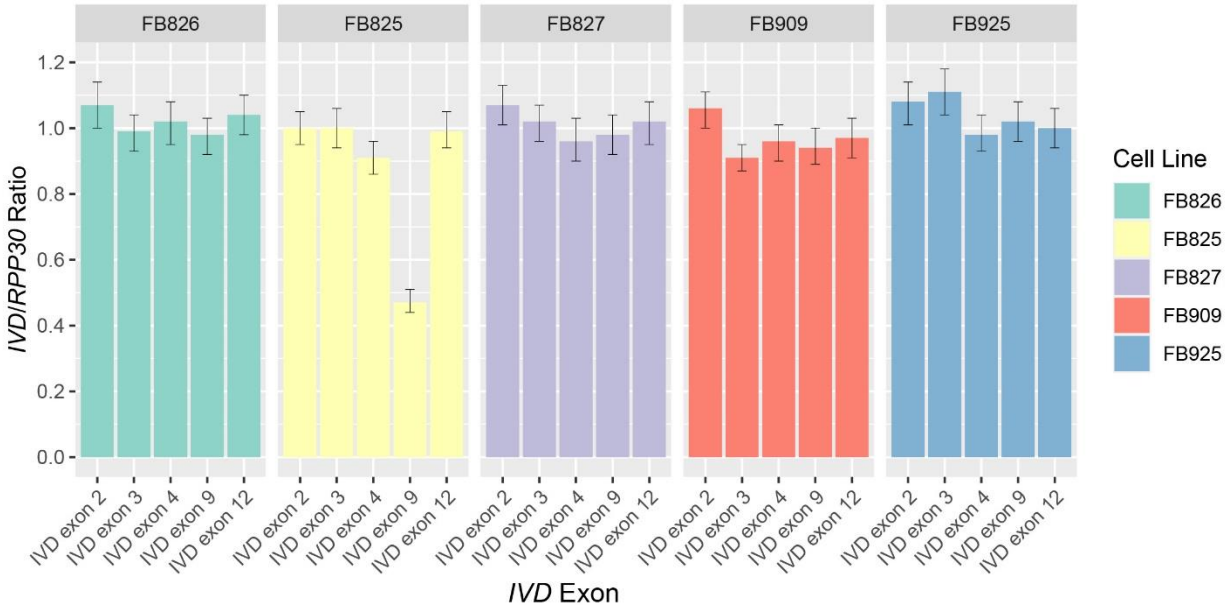

Supplementary Figure S7. Genomic copy number assay across *IVD* in fibroblasts derived from IVA patients. The ratio of IVD to unlinked RPP30 as a measure of genomic copy number. Nearly all samples across each exon have a ratio approaching 1.0 indicating a full diploid complement with the exception of FB825 in which the c.932C>T the heterozygous presence of the common variant allele is discriminated by the overlapping Taqman probe.

Appendix B Supplemental Information Chapter 3

Supplementary Table S5. Clinical information of VLCADD patients and corresponding fibroblast cell line designation.

Cell Line	Age	Sex	00Mutation	Acylcarnitine Profile	Symptoms	Treatment
FB671	Newborn	F	c.1619T>C, p.Leu540Pro / c.1707_1715dup, p.Asp570_Ala572dup	Multiple abnormal ACNs over many years diagnostic of VLCAD deficiency. Most recent 0.16 (nl)/2.93 (very high)/0.55 (high)	Recurrent rhabdomyolysis episodes every 4 weeks; chronic inflammatory state; headaches; chronic fatigue	IV fluids for rhabdomyolysis; 55 mL Dojolvi mixed with milk throughout the day; research trial with C7: 45 cc/d; Remicade injections since 3/2016; G-tube
FB782	10 months	M	c.848T>C, p.Val283Ala / c.1258A>C, p.Ile420Leu	Abnormal NBS C14 1.76 (0.97) C14:1 2.59 (1.5)	Four hospital admissions with fever and weakness (clinician notes they do not believe this is due to VLCADD)	IV fluid of D10 normal saline for hospital admissions; Pantothenic acid and 2tsp per day of canola oil; diet is Monogen 40 oz per day
FB894*	Newborn	M	c.535G>A, p.Gly179Arg	Abnormal NBS & ACP.	Clinically well as of 6/4/2019	None
FB895*	Newborn	M	c.535G>A, p.Gly179Arg	Abnormal NBS & ACP.	Clinically well as of 6/4/2019	None
FB904*	Newborn	M	c.1217A>C, p.Gln406Pro	Abnormal NBS &ACP. C14:1 1(0.7), C12:1 0.68(0.5), C14 0.87(0.7), C14:1/C16 0.23(0.2)	Clinically well as of 4/1/2021	None

Summary of clinical information of VLCADD patients. Age is time of fibroblast collection. *only one variant detected in patient.

Supplementary Table S6. Oligonucleotide sgRNA cloning adapter and breakpoint-PCR primer sequences for generation and initial screening of CRISPR-Cas9 genome-edited ACADVL null lines.

Oligo Name	Sequence (5′ to 3′)
sgRNA_12-1_sense	CACCGCAAAATCTTTGGCTCGGTG
sgRNA_12-1_antisense	AAACCACCGAGCCAAAGATTTTGC
sgRNA_16-1_sense	CACCgCACTCCGACTCAACTCCGGG
sgRNA_16-1_antisense	AAACCCCGGAGTTGAGTCGGAGTGc
ACADVL_ex12_fwd	ACATGGTGAGTGCTAACATGG
ACADVL_ex18_rev	CGAGAGAACCACCACCATGG

Complementary oligonucleotides phosphorylated and annealed for use as BbsI cloning adapters to ligate into pX458 targeting either ACADVL exon 12 or exon 16. Exon12 forward and exon18 reverse PCR primers used to detect the expected 421-bp deletion-breakpoint PCR band in Supplemental Figure S1C.

Supplementary Table S7. PrimeTime 5'-nuclease probe based ACADVL ddPCR genomic copy number assays.

Oligo Name	Sequence (5′ to 3′)
ACADVL_ex10_fwd	GTGTTCTTTGATGGAGTACGG
ACADVL_ex10_rev	GCCTCTCATGGTACCTGCCA
ACADVL_ex10_FAM	/56-FAM/ACAATGGAA/ZEN/GGTTTGGCATGGCTG/3IABkFQ
ACADVL_in11_fwd	CTGGGTGATGAGGCCAAGTC
ACADVL_ex12_rev	GGCTCCCTGGTCCATGTTAG
ACADVL_in11_FAM	/56-FAM/TCCCATGTC/ZEN/CCAACTATGCAACCT/3IABkFQ/
ACADVL_ex15_fwd	TCTGGGCTTGGCAGTGCTCT
ACADVL_in15_rev	GCTCTGGCCCTAAGCCTACC
ACADVL_ex15_FAM	/56-FAM/TGCTAGGAG/ZEN/AGGCAGGCAAACAG/3IABkFQ/
ACADVL_ex20_fwd	TGGAGTGGGCACCGTAACTG
ACADVL_ex20_rev_UTR	GGCCGGGAGTATTCAGAAGC
ACADVL_ex20_FAM	/56-FAM/TGTGGTCAC/ZEN/CAGCAACCCACTT/3IABkFQ/
Hs_RPP30_in1_fwd	TTCCTAGCGCGGGAAACTCG
Hs_RPP30_in1_rev	TGCAAATCCCTCGCCCTCGT
Hs_RPP30_in1_HEX	/5HEX/TCCTGCAAT/ZEN/GAGGGAACTGAGGC/3IABkFQ/

Amplicon primer and probe sets were selected based on their ability to uniquely amplify and detect ACADVL sequences within and external to the targeted deletion region from genomic DNA. Primer and probe set for reference RPP30 was previously reported [139]. The primer ACADVL_ex10_rev and ACADVL_ex20_rev_UTR were previously reported or modified from Watanabe et al., 2000 [179].

Supplementary Table S8. Oligonucleotide sequence of RT-PCR primers used to detect *ACADVL* cDNA.

Oligo Name	Sequence (5′ to 3′)
ACADVL_ex15_fwd	TCTGGGCTTGGCAGTGCTCT
ACADVL_ex18_rev_2	CCACCATGGCATAGAGGTCG
GAPDH_ex7_fwd	TGGCATTGCCCTCAACGACC
GAPDH_ex8_rev	TACTCCTTGGAGGCCATGTGG

The above primers were used to detect ACADVL mRNA expression in HEK293T null cell line A1-07 transiently transfected with a pCMV-ACADVL plasmid vector.

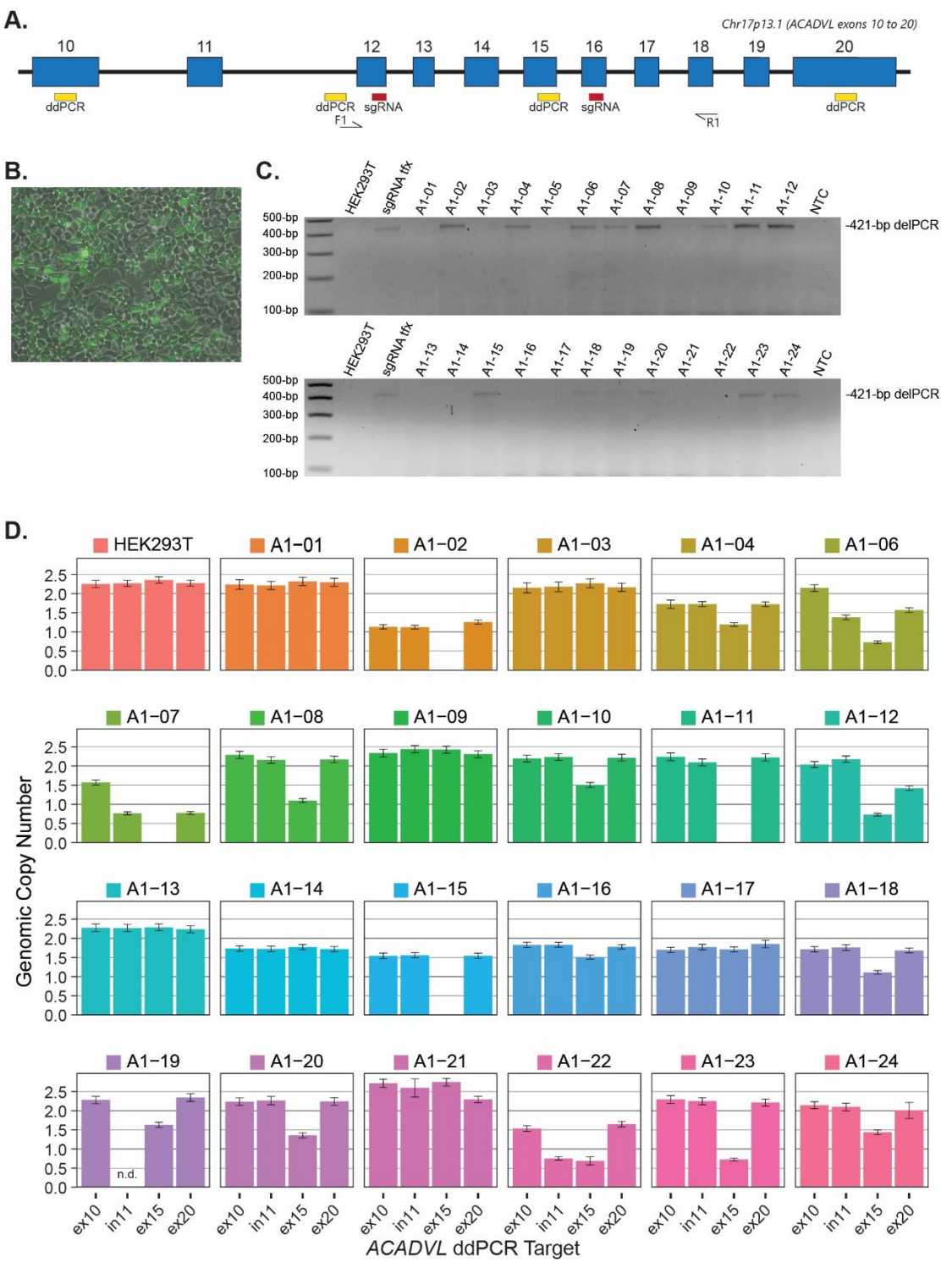

Supplementary Figure S8. Generation of ACADVL null HEK293T lines by CRISPR-Cas9 genome-editing and clonal screening.

(A) Schematic of dual sgRNA CRISPR-Cas9 targeting ACADVL. Key: Blue box, *ACADVL* exons with intervening introns; red rectangles, sgRNA sites; yellow rectangles, ddPCR amplicons and directional arrows, genotyping primers. (B) Bulk transfected HEK293T cells with the two pX458 CRISPR-Cas9 plasmids prior to flow sorting GFP(+) single cells for clonal isolation. (C) Deletion breakpoint PCR assay detects *ACADVL* exon12-16 deletions in 14 out of 24 clonal lines screened. (D) Genomic copy number (CN) of ACADVL exon 10, intron 11, exon 15 and exon 20 as quantified by ddPCR with normalization to the RPP30 locus colored by sample. Notably the parental HEK293T is near diploid (CN=2) for ACADVL across the gene whereas clonal lines show variation in CN for ACADVL normalized to RPP30 with loss of exon 15 observed in the same clonal lines in which deletion-breakpoint PCR bands were detected in Figure S1B. Ultimately, 4 clonal line showed complete loss of the targeted exon 15. A1-02 exhibited deletion of exon 15 with a haploid number (CN=1) across the untargeted region; A1-07 and A1-15 showed deletion of exon 15 with likely 3N copies of RPP30 leading to CN=1.5 for untargeted regions, with A1-07 likely having one deletion allele extending both into intron 11 proximally and through exon 20 distally; and A1-15 with an expected diploid ACADVL deletion pattern with observed CN of 2N at the untargeted regions and 0N at exon 15.

Appendix C Supplemental Information Chapter 4

Supplementary Table S9. Oligonucleotide sequence of primers used in qPCR experiments and corresponding Primer Bank ID. Forward and reverse primer sets listed were obtained from Primer Bank.

Gene	Primer Bank ID	Forward	Reverse	Forward TM	Reverse TM	Product Size
ACADVL	764964473c1	ACAGATCAGGTGTTCCCATACC	CTTGGCGGGATCGTTCACTT	61.2	62.5	114
HADHA	105990523c2	CTGCCCAAAATGGTGGGTGT	GGAGGTTTTAGTCCTGGTCCC	63	61.5	134
HADHB	105990524c1	CTGTCCAGACCAAAACGAAGAA	CGATGCAACAAACCCGTAAGC	60.4	62.4	160
ETFDH	119703745c1	TACTGTGCCTCGAATTACTACCC	ACAGCCAACTGTTTTAGACGAA	61.2	60.1	165
UQCRC2	50592987c1	TTCAGCAATTTAGGAACCACCC	GGTCACACTTAATTTGCCACCAA	60.5	61.5	120
NDUFS2	260898742c2	GCTGTTATGTACCCAAGCAAAGA	TCCCCACTCAATTCCATCACT	60.8	60.5	164
TOMM20	208609996c1	GGTACTGCATCTACTTCGACCG	TGGTCTACGCCCTTCTCATATTC	62.1	61.2	220

A

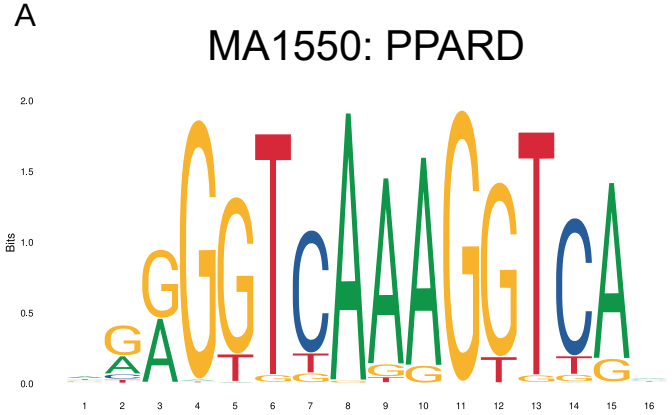
MA1550: PPARD
Bits
2.0
1.5
1.0
0.5
0.0
1 2 3 4 5 6 7 8 9 10 11 12 13 14 15 16

B

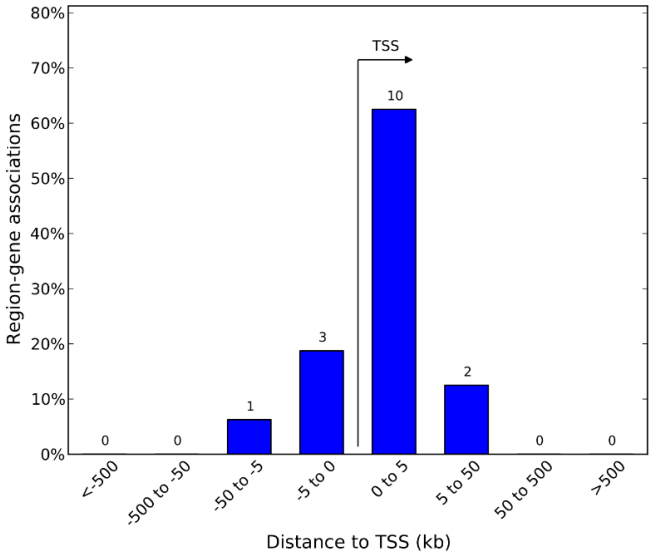
Region-gene associations
80%
70%
60%
50%
40%
30%
20%
10%
0%
TSS
0
0
1
3
10
2
0
0
<-500
-500 to -50
-50 to -5
-5 to 0
0 to 5
5 to 50
50 to 500
>500
Distance to TSS (kb)

C

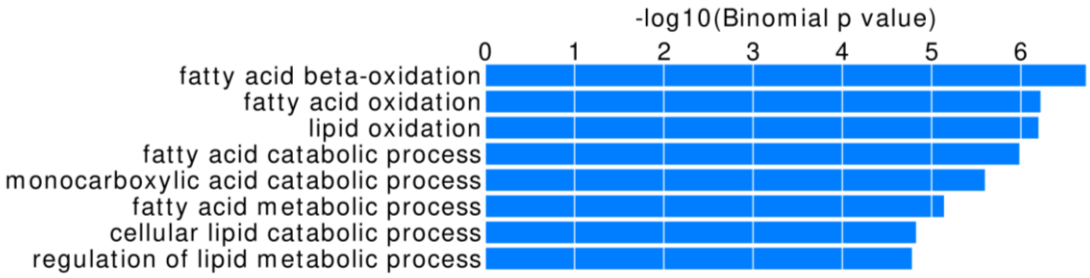
Gene Ontology
-log10(Binomial p value)
0 1 2 3 4 5 6
fatty acid beta-oxidation
fatty acid oxidation
lipid oxidation
fatty acid catabolic process
monocarboxylic acid catabolic process
fatty acid metabolic process
cellular lipid catabolic process
regulation of lipid metabolic process

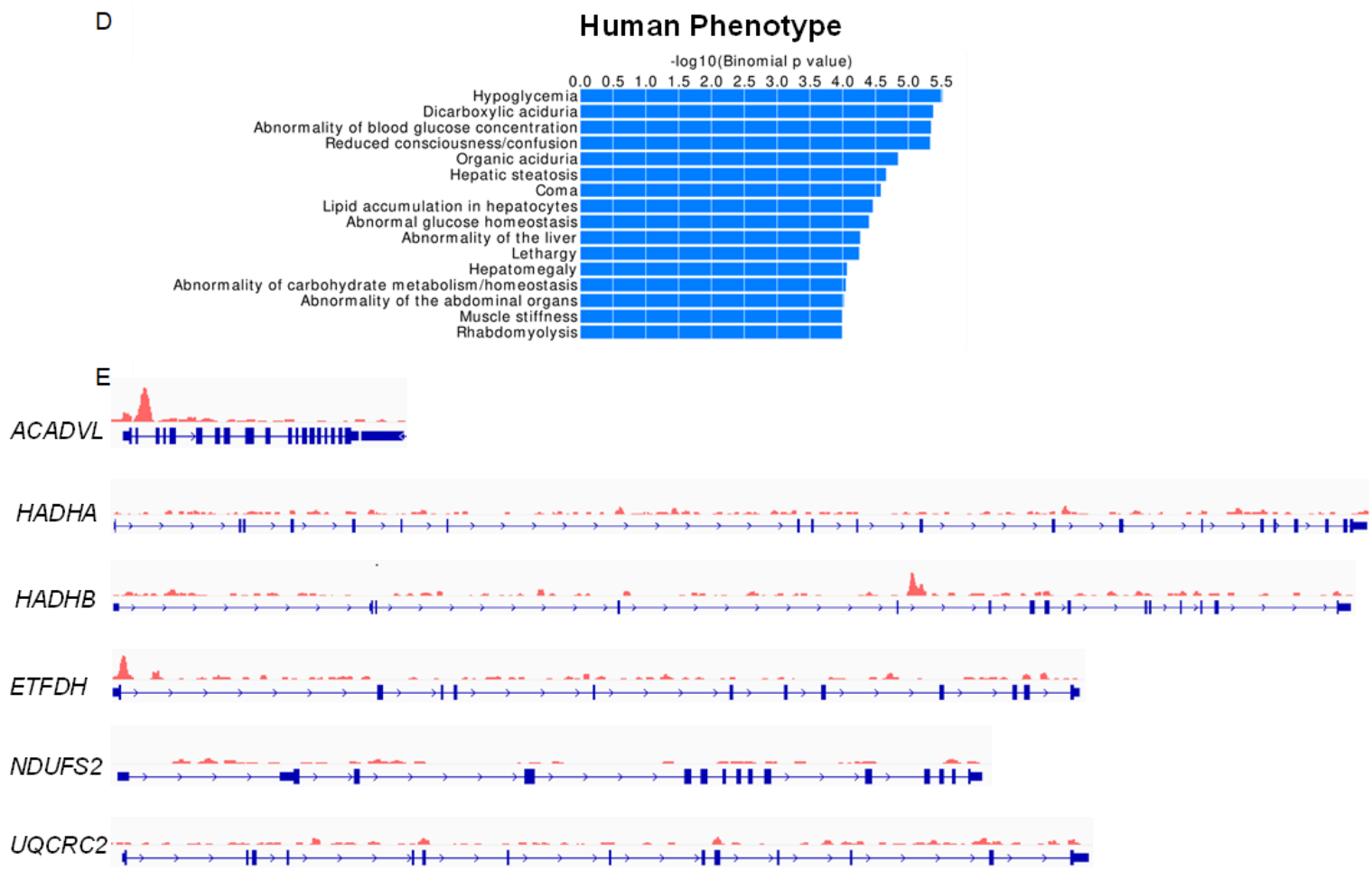

Supplementary Figure S9. ChIPseq analysis for PPARdelta utilizing HUVEC cells.

MACS2 analysis of PPARδ ChIPseq identified a localized intergenic region with a consensus binding motif (A). PPARD is a primary DNA enhancer 5kb downstream of the transcription start site (B). The fatty acid metabolism pathway is enriched by PPARδ target genes (C) and target genes (D) are implicated in FAO disorder phenotypes. *ETFDH* and *UQCRC2* lack the PPARδ binding site (E).

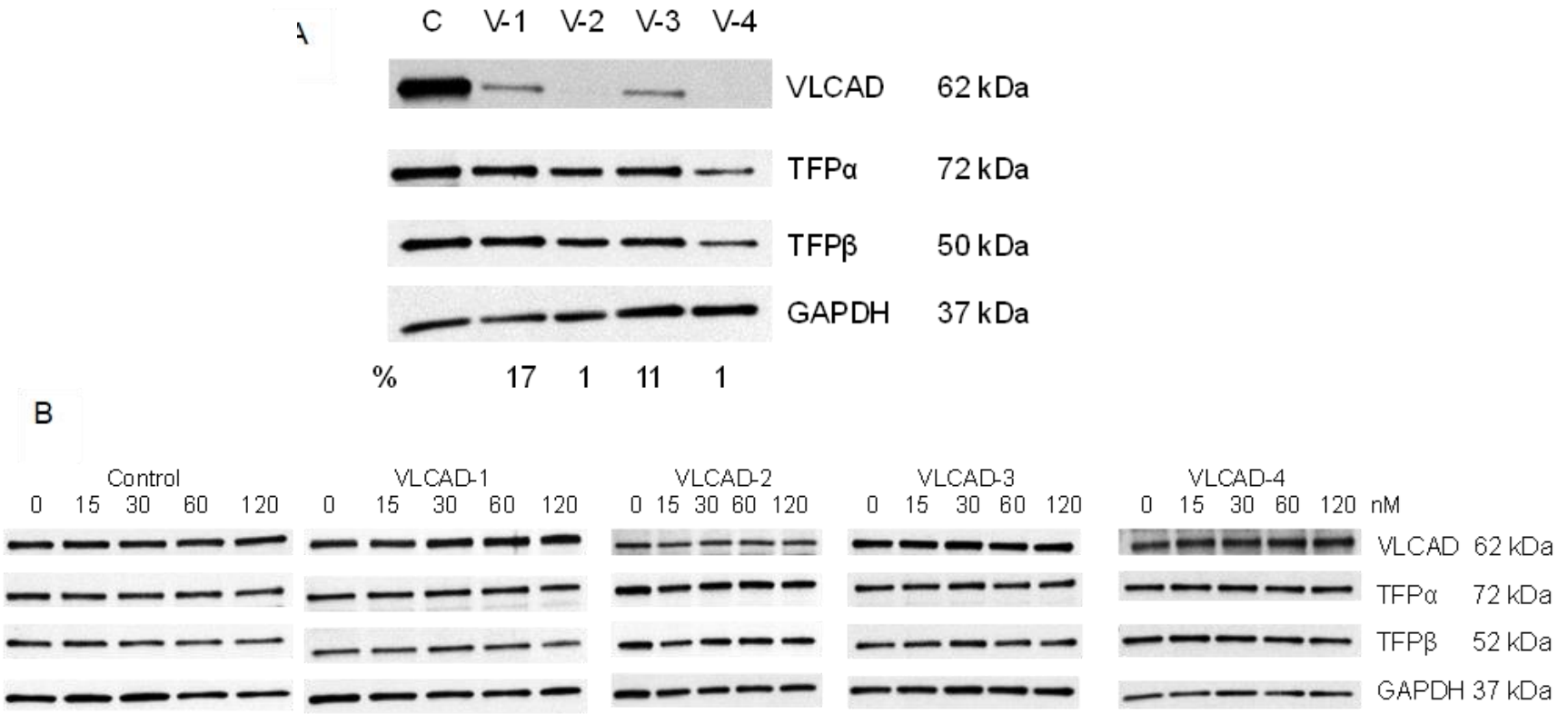

Supplementary Figure S10. Western blot of control and VLCADD fibroblasts treated with REN001.

Control and four VLCADD fibroblasts blotted for VLCAD, TFPα, TFPβ, and GAPDH (A). Fibroblasts were treated with 0, 15, 30, 60, and 120 nM of REN001 for 48 hours and harvested (B). 25 µg of protein was loaded into each well and membranes were probed for VLCAD, TFPα, TFPβ, and GAPDH as a loading control. Overexposures were taken of VLCADD cell lines to better capture the bands and to quantify. Blots were repeated 3 times. Band intensity was quantified using ImageLab (BioRad).

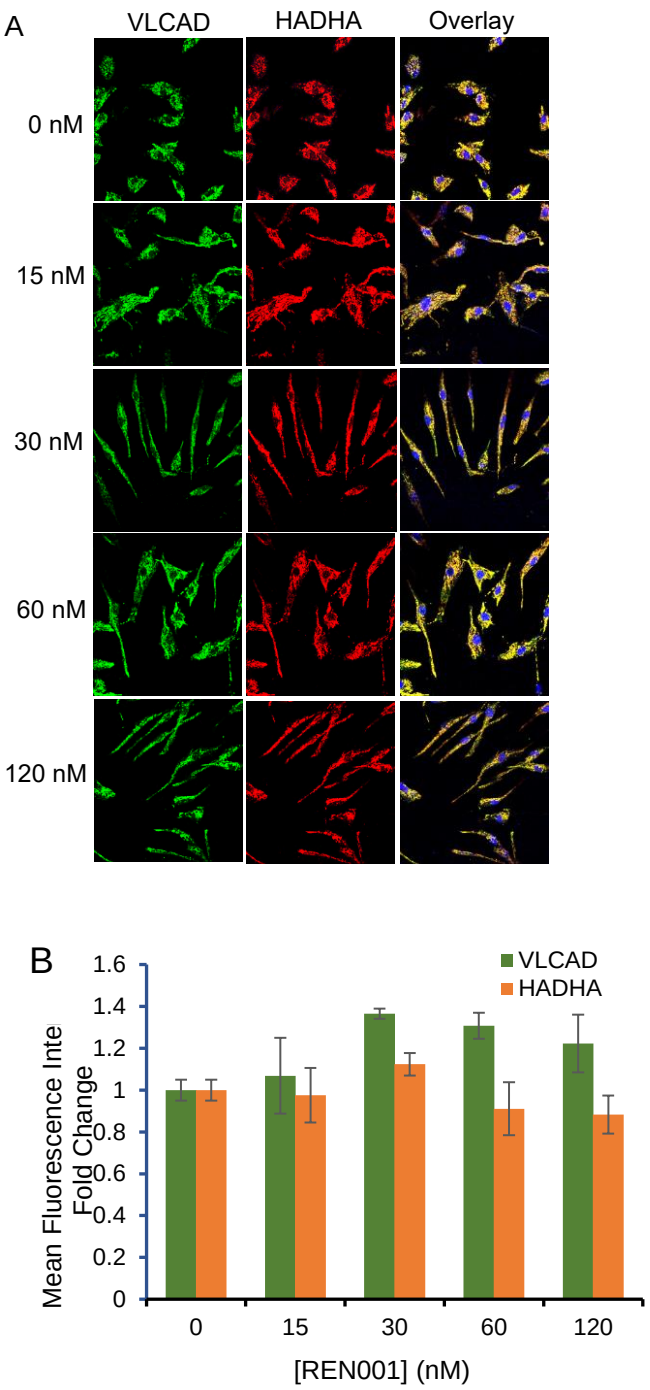

Supplementary Figure S11. Immunofluorescence and quantification of control fibroblasts treated with REN001.

Control fibroblasts were treated with REN001 in complete DMEM for 48 hours. Treated fibroblasts were fixed and stained with VLCAD (green) and HADHA (red) antibodies. Nuclei were stained with Dapi. Quantification was performed via ImageJ (B). No statistical difference was detected.

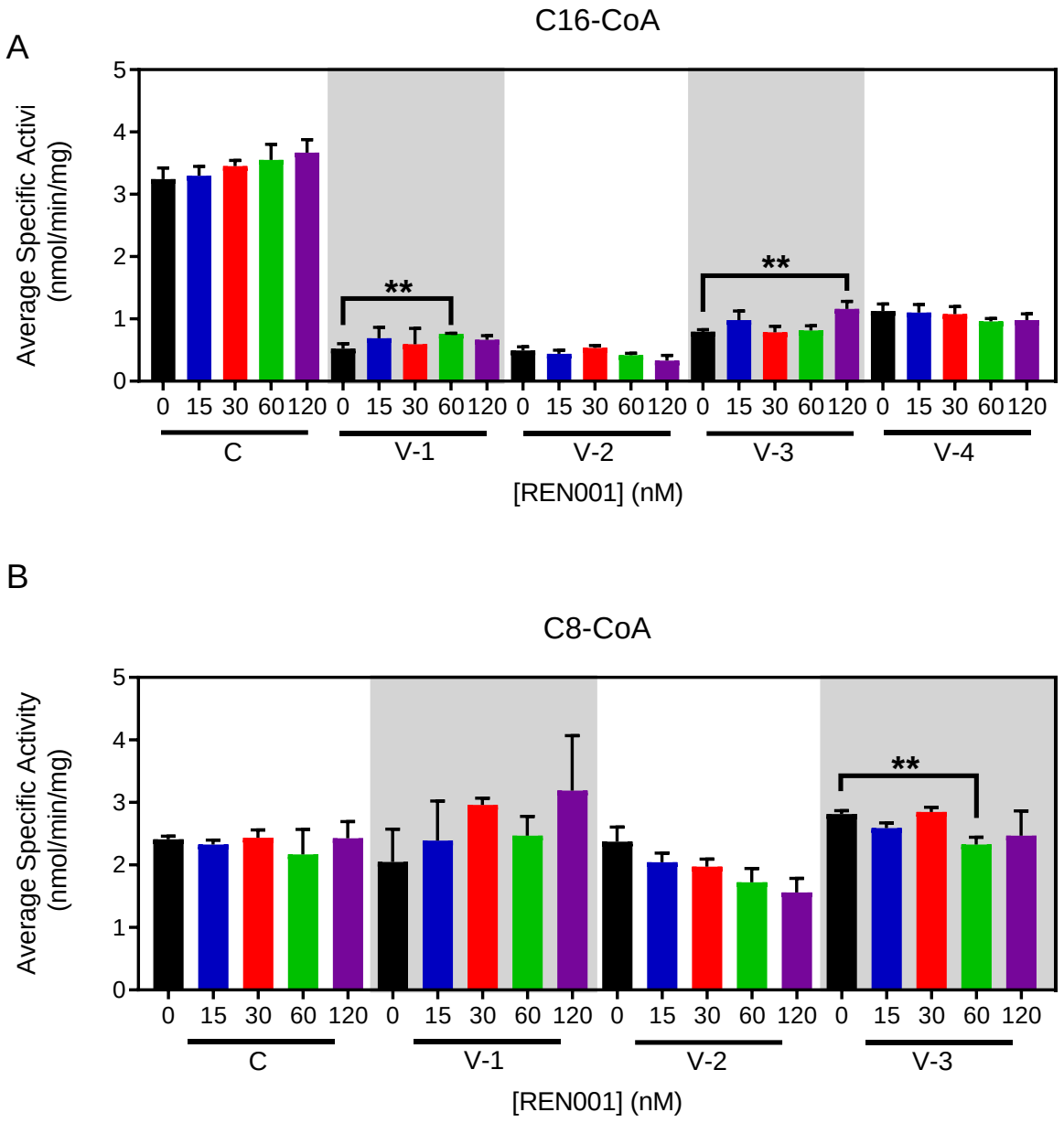

Supplementary Figure S12. Evaluation of VLCAD and MCAD enzyme activity in VLCADD whole cell lysates treated with REN001.

Activity was measured using C16-CoA as substrate (A). Bars represent means and standard deviations in triplicate assays. Activity was measured using C8-CoA as the substrate (B). V-4 (VLCAD-4) was not measured for MCAD activity due to minimal sample. Bars represent mean and standard deviations in duplicate assays. *$p < 0.05$, **$p < 0.01$, compared to each cell lines own 0 nM treatment (*t* test for unpaired samples).

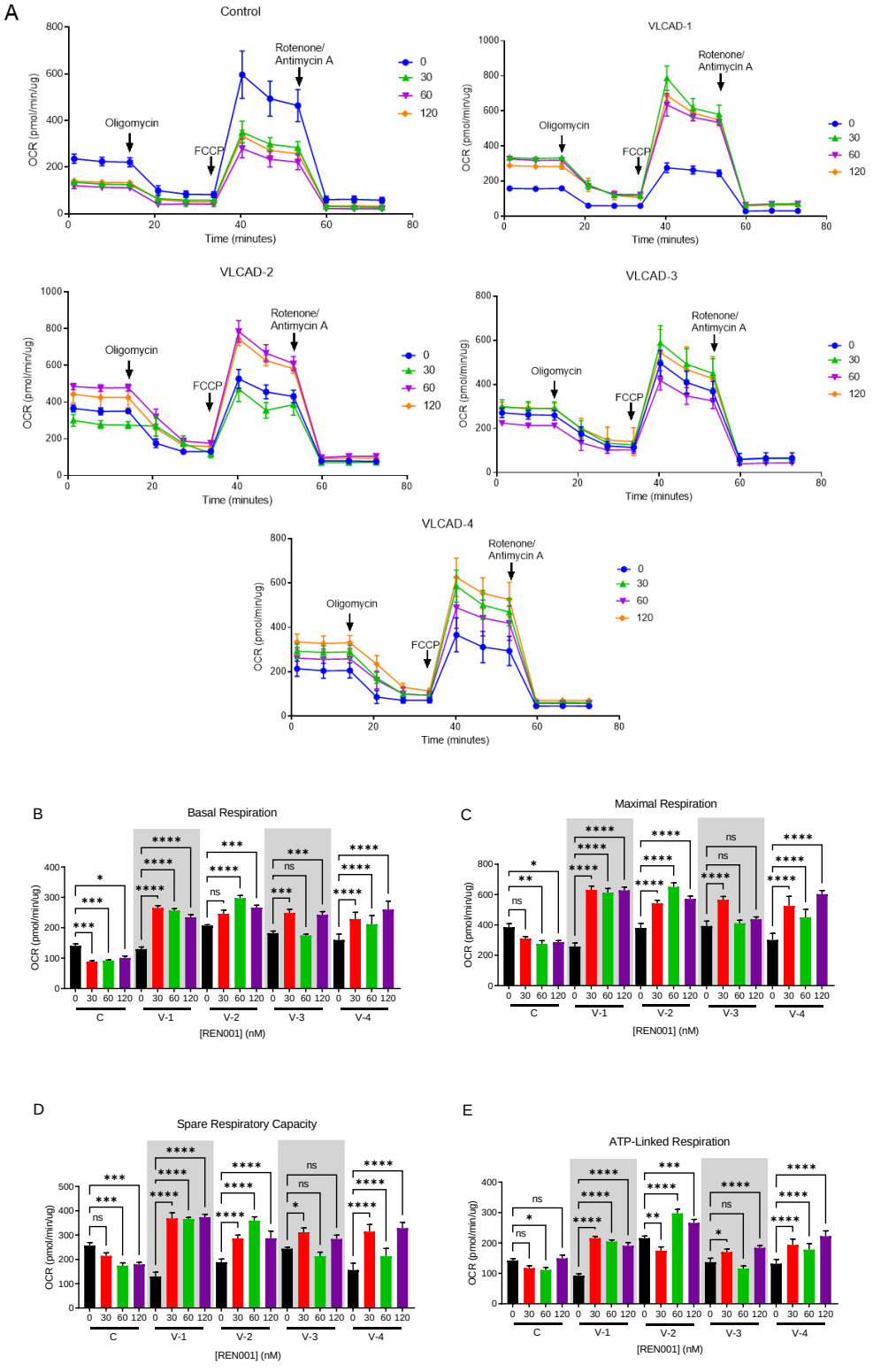

Supplementary Figure S13. Oxygen consumption rate of control and VLCAD deficient cell lines treated with REN001.

Oxygen consumption rate (OCR) was measured in the resting state (basal respiration) followed by injection of oligomycin (ATP synthase inhibitor) that reduces OCR, representing ATP turnover. Subsequent inject of FCCP dissipates the proton gradient and allows maximum respiration. Finally, rotenone and antimycin A are added to completely disable the electron transport chain, inhibiting the total mitochondrial respiration. The remaining OCR represents non-mitochondrial respiration (A). Control and VLCADD cell lines were treated with REN001 for 48 hr. Basal respiration (B), maximal respiration (C), spare respiratory capacity (D), and ATP production (E). Bars represent mean and standard deviations of 6-8 wells per parameter. *p < 0.05, **p < 0.01, ***p <0.001, ****p < 0.0001, compared to each cell lines own 0 nM treatment (*t* test for unpaired samples).

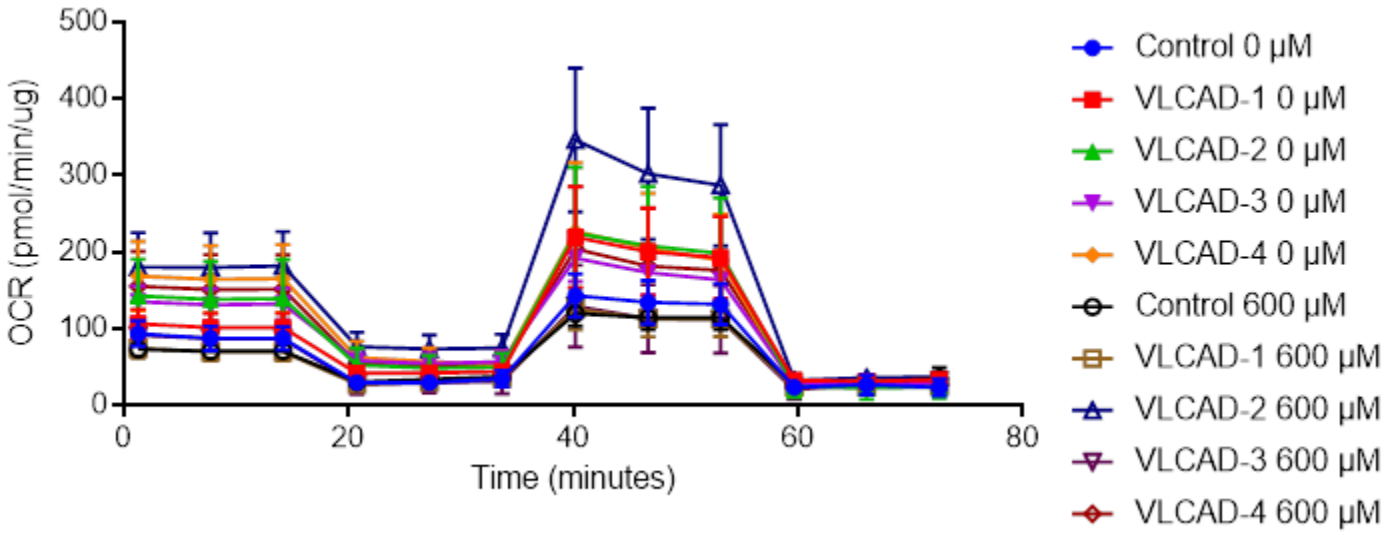

Supplementary Figure S14. Oxygen consumption rate of control and VLCADD cell lines with bezafibrate.

Oxygen consumption rate (OCR) was measured in the resting state (basal respiration) followed by injection of oligomycin (ATP synthase inhibitor) that reduces OCR, representing ATP turnover. Subsequent inject of FCCP dissipates the proton gradient and allows maximum respiration. Finally, rotenone and antimycin A are added to completely disable the electron transport chain, inhibiting the total mitochondrial respiration. The remaining OCR represents non-mitochondrial respiration (A). Control and VLCADD cell lines were treated with bezafibrate for 48 hr.

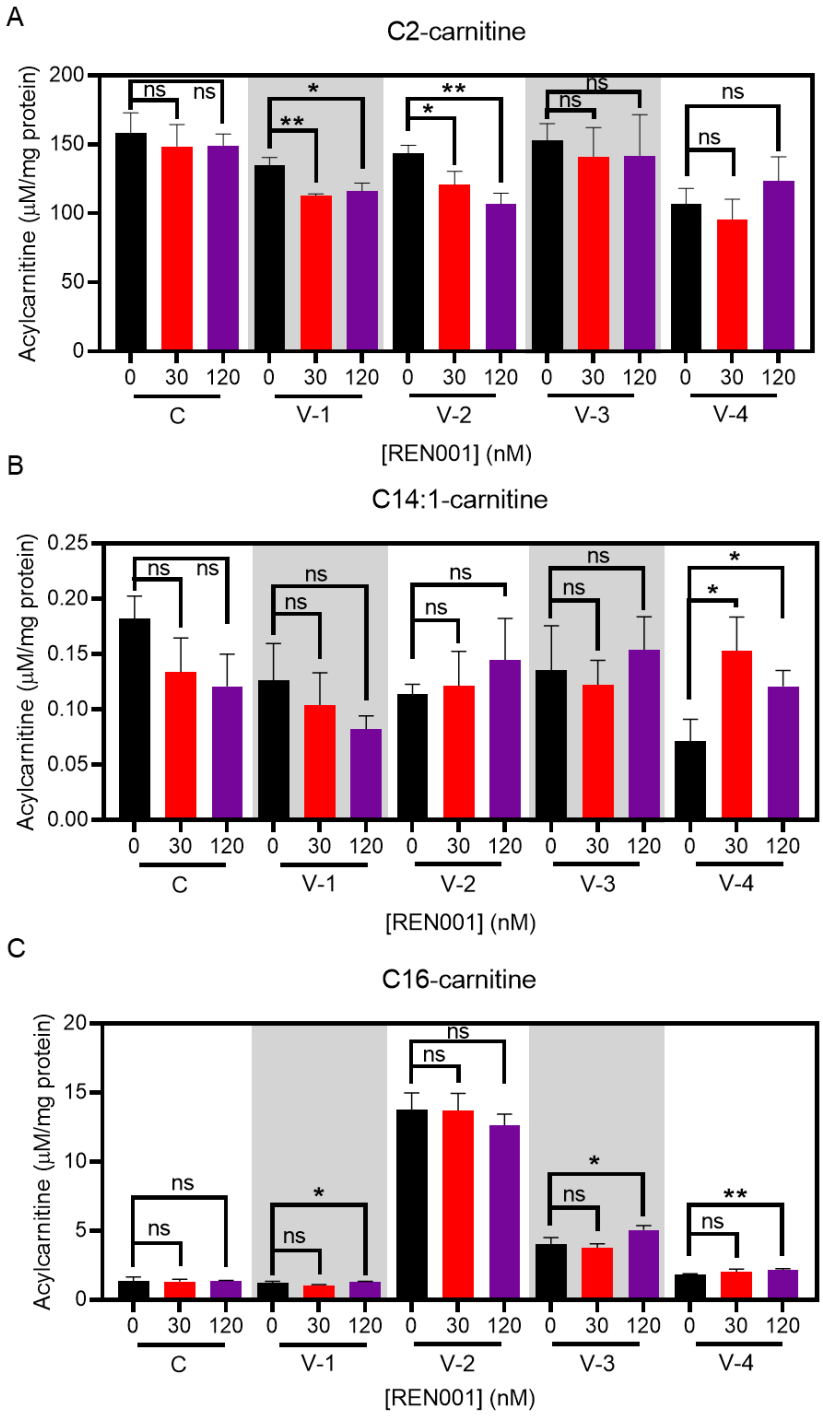

Supplementary Figure S15. Acylcarnitine profiling of control and VLCADD fibroblasts treated with REN001.

Media was collected after 72 hr incubation and analyzed via tandem mass spectrometry. Acetylcarnitine (C2-carnitine) (A), C14:0-carnitine (B), and palmitoylcarnitine (C16-carnitine) (C). Bars represent mean and standard deviations in triplicate assays. *$p < 0.05$, **$p < 0.01$, ns = not statistically significant, compared to each cell lines own 0 nM treatment (*t* test for unpaired samples).

Bibliography

1. Berg, J.M., et al., *Biochemistry*. Eighth edition. ed. 1 volume (various pagings).
2. Manoli, I. and C.P. Venditti, *Disorders of branched chain amino acid metabolism.* Transl Sci Rare Dis, 2016. **1**(2): p. 91-110.
3. Holecek, M., *Branched-chain amino acids in health and disease: metabolism, alterations in blood plasma, and as supplements.* Nutr Metab (Lond), 2018. **15**: p. 33.
4. McCalley, S., *Elucidating the mitochondrial architecture of branched-chain amino acid metabolism enzymes: implications for treatment*. 2018, University of Pittsburgh: D-Scholarship. p. 93.
5. Houten, S.M. and R.J. Wanders, *A general introduction to the biochemistry of mitochondrial fatty acid beta-oxidation.* J Inherit Metab Dis, 2010. **33**(5): p. 469-77.
6. Fillmore, N., Alrob, O. A., Lopaschuk, G. D., *Fatty Acid beta-Oxidation*. 2014, American Oil Chemistry Society: AOCS Lipid Library.
7. Talley, J.T. and S.S. Mohiuddin, *Biochemstry, Fatty Acid Oxidation,* in *StatPearls*. 2020: Treasure Island (FL).
8. Wang, Y., et al., *Mitochondrial fatty acid oxidation and the electron transport chain comprise a multifunctional mitochondrial protein complex.* J Biol Chem, 2019. **294**(33): p. 12380-12391.
9. Ghisla, S. and C. Thorpe, *Acyl-CoA dehydrogenases. A mechanistic overview.* Eur J Biochem, 2004. **271**(3): p. 494-508.
10. Kim, J.J. and R. Miura, *Acyl-CoA dehydrogenases and acyl-CoA oxidases. Structural basis for mechanistic similarities and differences.* Eur J Biochem, 2004. **271**(3): p. 483-93.
11. Nasser, I., et al., *Thermal unfolding of medium-chain acyl-CoA dehydrogenase and iso(3)valeryl-CoA dehydrogenase: study of the effect of genetic defects on enzyme stability.* Biochim Biophys Acta, 2004. **1690**(1): p. 22-32.
12. Kim, J.J., M. Wang, and R. Paschke, *Crystal structures of medium-chain acyl-CoA dehydrogenase from pig liver mitochondria with and without substrate.* Proc Natl Acad Sci U S A, 1993. **90**(16): p. 7523-7.
13. Peterson, K.M., K.V. Gopalan, and D.K. Srivastava, *Influence of alpha-CH-->NH substitution in C8-CoA on the kinetics of association and dissociation of ligands with medium chain acyl-CoA dehydrogenase.* Biochemistry, 2000. **39**(41): p. 12659-70.
14. Mohsen, A.W. and J. Vockley, *Identification of the active site catalytic residue in human isovaleryl-CoA dehydrogenase.* Biochemistry, 1995. **34**(32): p. 10146-52.
15. Tiffany, K.A., et al., *Structure of human isovaleryl-CoA dehydrogenase at 2.6 A resolution: structural basis for substrate specificity.* Biochemistry, 1997. **36**(28): p. 8455-64.
16. McAndrew, R.P., et al., *Structural basis for substrate fatty acyl chain specificity: crystal structure of human very-long-chain acyl-CoA dehydrogenase.* J Biol Chem, 2008. **283**(14): p. 9435-43.
17. Zhang, J., et al., *Cloning and functional characterization of ACAD-9, a novel member of human acyl-CoA dehydrogenase family.* Biochem Biophys Res Commun, 2002. **297**(4): p. 1033-42.

18. Ensenauer, R., et al., *Human acyl-CoA dehydrogenase-9 plays a novel role in the mitochondrial beta-oxidation of unsaturated fatty acids.* J Biol Chem, 2005. **280**(37): p. 32309-16.
19. Vockley, J., et al., *Mammalian branched-chain acyl-CoA dehydrogenases: molecular cloning and characterization of recombinant enzymes.* Methods Enzymol, 2000. **324**: p. 241-58.
20. Mohsen, A.W., et al., *Characterization of molecular defects in isovaleryl-CoA dehydrogenase in patients with isovaleric acidemia.* Biochemistry, 1998. **37**(28): p. 10325-35.
21. Tanaka, K., et al., *Isovaleric acidemia: a new genetic defect of leucine metabolism.* Proc Natl Acad Sci U S A, 1966. **56**(1): p. 236-42.
22. Online, M.I.o.M., OMIM *Isovaleric Acidemia, IVA #243500*. OMIM, Mendelian Inheritance of Man, OMIM.
23. Vockley, J., et al., *Branched Chain Organic Acidurias*, in *The Online Metabolic and Molecular Bases of Inherited Disease*, D. Valle, et al., Editors. 2019, McGraw-Hill Education: New York, NY.
24. Moorthie, S., et al., *Systematic review and meta-analysis to estimate the birth prevalence of five inherited metabolic diseases.* J Inherit Metab Dis, 2014. **37**(6): p. 889-98.
25. Ensenauer, R., et al., *A common mutation is associated with a mild, potentially asymptomatic phenotype in patients with isovaleric acidemia diagnosed by newborn screening.* Am J Hum Genet, 2004. **75**(6): p. 1136-42.
26. Tanaka, K., *Isovaleric acidemia: personal history, clinical survey and study of the molecular basis.* Prog Clin Biol Res, 1990. **321**: p. 273-90.
27. Kanungo, S., et al., *Newborn screening and changing face of inborn errors of metabolism in the United States.* Ann Transl Med, 2018. **6**(24): p. 468.
28. Guthrie, R., *Screening for phenylketonuria.* Triangle, 1969. **9**(3): p. 104-9.
29. American College of Medical Genetics Newborn Screening Expert, G., *Newborn screening: toward a uniform screening panel and system--executive summary.* Pediatrics, 2006. **117**(5 Pt 2): p. S296-307.
30. McCandless, S.E. and E.J. Wright, *Mandatory newborn screening in the United States: History, current status, and existential challenges.* Birth Defects Res, 2020. **112**(4): p. 350-366.
31. Vockley, J. and R. Ensenauer, *Isovaleric acidemia: new aspects of genetic and phenotypic heterogeneity.* Am J Med Genet C Semin Med Genet, 2006. **142C**(2): p. 95-103.
32. Oglesbee, D., et al., *Second-tier test for quantification of alloisoleucine and branched-chain amino acids in dried blood spots to improve newborn screening for maple syrup urine disease (MSUD).* Clin Chem, 2008. **54**(3): p. 542-9.
33. McHugh, D., et al., *Clinical validation of cutoff target ranges in newborn screening of metabolic disorders by tandem mass spectrometry: a worldwide collaborative project.* Genet Med, 2011. **13**(3): p. 230-54.
34. Ensenauer, R., et al., *Newborn screening for isovaleric acidemia using tandem mass spectrometry: data from 1.6 million newborns.* Clin Chem, 2011. **57**(4): p. 623-6.
35. Levy, H.L., et al., *Isovaleric acidemia: results of family study and dietary treatment.* Pediatrics, 1973. **52**(1): p. 83-94.
36. Lott, I.T., A.M. Erickson, and H.L. Levy, *Dietary treatment of an infant with isovaleric acidemia.* Pediatrics, 1972. **49**(4): p. 616-8.

37. Krieger, I. and K. Tanaka, *Therapeutic effects of glycine in isovaleric acidemia.* Pediatr Res, 1976. **10**(1): p. 25-9.
38. Zaki, O.K., et al., *Genotype-phenotype correlation in patients with isovaleric acidaemia: comparative structural modelling and computational analysis of novel variants.* Hum Mol Genet, 2017. **26**(16): p. 3105-3115.
39. Vockley, J., et al., *Exon skipping in IVD RNA processing in isovaleric acidemia caused by point mutations in the coding region of the IVD gene.* Am J Hum Genet, 2000. **66**(2): p. 356-67.
40. Lee, Y.W., et al., *Different spectrum of mutations of isovaleryl-CoA dehydrogenase (IVD) gene in Korean patients with isovaleric acidemia.* Mol Genet Metab, 2007. **92**(1-2): p. 71-7.
41. Leslie, N.D., et al., *Very Long-Chain Acyl-Coenzyme A Dehydrogenase Deficiency*, in *GeneReviews((R))*, M.P. Adam, et al., Editors. 1993: Seattle (WA).
42. Andresen, B.S., et al., *Clear correlation of genotype with disease phenotype in very-long-chain acyl-CoA dehydrogenase deficiency.* Am J Hum Genet, 1999. **64**(2): p. 479-94.
43. Wood, J.C., et al., *Diagnosis of very long chain acyl-dehydrogenase deficiency from an infant's newborn screening card.* Pediatrics, 2001. **108**(1): p. E19.
44. Solis, J.O. and R.H. Singh, *Management of fatty acid oxidation disorders: a survey of current treatment strategies.* J Am Diet Assoc, 2002. **102**(12): p. 1800-3.
45. Behrend, A.M., et al., *Substrate oxidation and cardiac performance during exercise in disorders of long chain fatty acid oxidation.* Mol Genet Metab, 2012. **105**(1): p. 110-5.
46. Gillingham, M.B., et al., *Triheptanoin versus trioctanoin for long-chain fatty acid oxidation disorders: a double blinded, randomized controlled trial.* J Inherit Metab Dis, 2017. **40**(6): p. 831-843.
47. Vockley, J., et al., *Triheptanoin treatment in patients with pediatric cardiomyopathy associated with long chain-fatty acid oxidation disorders.* Mol Genet Metab, 2016. **119**(3): p. 223-231.
48. Roe, C.R. and F. Mochel, *Anaplerotic diet therapy in inherited metabolic disease: therapeutic potential.* J Inherit Metab Dis, 2006. **29**(2-3): p. 332-40.
49. Deng, S., et al., *Interrelations between C4 ketogenesis, C5 ketogenesis, and anaplerosis in the perfused rat liver.* J Biol Chem, 2009. **284**(41): p. 27799-27807.
50. Roe, C.R. and H. Brunengraber, *Anaplerotic treatment of long-chain fat oxidation disorders with triheptanoin: Review of 15 years Experience.* Mol Genet Metab, 2015. **116**(4): p. 260-8.
51. Vockley, J., et al., *Long-term major clinical outcomes in patients with long chain fatty acid oxidation disorders before and after transition to triheptanoin treatment--A retrospective chart review.* Mol Genet Metab, 2015. **116**(1-2): p. 53-60.
52. Sklirou, E., et al., *Physiological Perspectives on the Use of Triheptanoin as Anaplerotic Therapy for Long Chain Fatty Acid Oxidation Disorders.* Front Genet, 2020. **11**: p. 598760.
53. Vockley, J., et al., *Effects of triheptanoin (UX007) in patients with long-chain fatty acid oxidation disorders: Results from an open-label, long-term extension study.* J Inherit Metab Dis, 2021. **44**(1): p. 253-263.
54. Vockley, J., et al., *Dietary management and major clinical events in patients with long-chain fatty acid oxidation disorders enrolled in a phase 2 triheptanoin study.* Clin Nutr ESPEN, 2021. **41**: p. 293-298.

55. Schiff, M., et al., *Molecular and cellular pathology of very-long-chain acyl-CoA dehydrogenase deficiency.* Mol Genet Metab, 2013. **109**(1): p. 21-7.
56. Seminotti, B., et al., *Mitochondrial energetics is impaired in very long-chain acyl-CoA dehydrogenase deficiency and can be rescued by treatment with mitochondria-targeted electron scavengers.* Hum Mol Genet, 2019. **28**(6): p. 928-941.
57. Marsden, D., C.L. Bedrosian, and J. Vockley, *Impact of newborn screening on the reported incidence and clinical outcomes associated with medium- and long-chain fatty acid oxidation disorders.* Genet Med, 2021. **23**(5): p. 816-829.
58. Goetzman, E.S., et al., *Expression and characterization of mutations in human very long-chain acyl-CoA dehydrogenase using a prokaryotic system.* Mol Genet Metab, 2007. **91**(2): p. 138-47.
59. Gobin-Limballe, S., et al., *Genetic basis for correction of very-long-chain acyl-coenzyme A dehydrogenase deficiency by bezafibrate in patient fibroblasts: toward a genotype-based therapy.* Am J Hum Genet, 2007. **81**(6): p. 1133-43.
60. Tyagi, S., et al., *The peroxisome proliferator-activated receptor: A family of nuclear receptors role in various diseases.* J Adv Pharm Technol Res, 2011. **2**(4): p. 236-40.
61. Corton, J.C., J.M. Peters, and J.E. Klaunig, *The PPARalpha-dependent rodent liver tumor response is not relevant to humans: addressing misconceptions.* Arch Toxicol, 2018. **92**(1): p. 83-119.
62. Evans, R.M., G.D. Barish, and Y.X. Wang, *PPARs and the complex journey to obesity.* Nat Med, 2004. **10**(4): p. 355-61.
63. Michalik, L., et al., *International Union of Pharmacology. LXI. Peroxisome proliferator-activated receptors.* Pharmacol Rev, 2006. **58**(4): p. 726-41.
64. Poulsen, L., M. Siersbaek, and S. Mandrup, *PPARs: fatty acid sensors controlling metabolism.* Semin Cell Dev Biol, 2012. **23**(6): p. 631-9.
65. Burdick, A.D., et al., *The role of peroxisome proliferator-activated receptor-beta/delta in epithelial cell growth and differentiation.* Cell Signal, 2006. **18**(1): p. 9-20.
66. Wang, Y.X., et al., *Peroxisome-proliferator-activated receptor delta activates fat metabolism to prevent obesity.* Cell, 2003. **113**(2): p. 159-70.
67. Berger, J. and D.E. Moller, *The mechanisms of action of PPARs.* Annu Rev Med, 2002. **53**: p. 409-35.
68. Janani, C. and B.D. Ranjitha Kumari, *PPAR gamma gene--a review.* Diabetes Metab Syndr, 2015. **9**(1): p. 46-50.
69. Tanaka, T., et al., *Activation of peroxisome proliferator-activated receptor delta induces fatty acid beta-oxidation in skeletal muscle and attenuates metabolic syndrome.* Proc Natl Acad Sci U S A, 2003. **100**(26): p. 15924-9.
70. Fredenrich, A. and P.A. Grimaldi, *PPAR delta: an uncompletely known nuclear receptor.* Diabetes Metab, 2005. **31**(1): p. 23-7.
71. Forman, B.M., J. Chen, and R.M. Evans, *Hypolipidemic drugs, polyunsaturated fatty acids, and eicosanoids are ligands for peroxisome proliferator-activated receptors alpha and delta.* Proc Natl Acad Sci U S A, 1997. **94**(9): p. 4312-7.
72. Schmidt, A., et al., *Identification of a new member of the steroid hormone receptor superfamily that is activated by a peroxisome proliferator and fatty acids.* Mol Endocrinol, 1992. **6**(10): p. 1634-41.

73. Gervois, P., J.C. Fruchart, and B. Staels, *Drug Insight: mechanisms of action and therapeutic applications for agonists of peroxisome proliferator-activated receptors.* Nat Clin Pract Endocrinol Metab, 2007. **3**(2): p. 145-56.
74. Riserus, U., et al., *Activation of peroxisome proliferator-activated receptor (PPAR)delta promotes reversal of multiple metabolic abnormalities, reduces oxidative stress, and increases fatty acid oxidation in moderately obese men.* Diabetes, 2008. **57**(2): p. 332-9.
75. Oliver, W.R., Jr., et al., *A selective peroxisome proliferator-activated receptor delta agonist promotes reverse cholesterol transport.* Proc Natl Acad Sci U S A, 2001. **98**(9): p. 5306-11.
76. Feng, L., et al., *Bavachinin, as a novel natural pan-PPAR agonist, exhibits unique synergistic effects with synthetic PPAR-gamma and PPAR-alpha agonists on carbohydrate and lipid metabolism in db/db and diet-induced obese mice.* Diabetologia, 2016. **59**(6): p. 1276-86.
77. Misawa, K., et al., *Ginger extract prevents high-fat diet-induced obesity in mice via activation of the peroxisome proliferator-activated receptor delta pathway.* J Nutr Biochem, 2015. **26**(10): p. 1058-67.
78. Information, N.C.f.B., *Bezafibrate, CID=39042*. 2019: PubChem Database.
79. Djouadi, F., et al., *Bezafibrate increases very-long-chain acyl-CoA dehydrogenase protein and mRNA expression in deficient fibroblasts and is a potential therapy for fatty acid oxidation disorders.* Hum Mol Genet, 2005. **14**(18): p. 2695-703.
80. Djouadi, F., et al., *Peroxisome proliferator activated receptor delta (PPARdelta) agonist but not PPARalpha corrects carnitine palmitoyl transferase 2 deficiency in human muscle cells.* J Clin Endocrinol Metab, 2005. **90**(3): p. 1791-7.
81. Djouadi, F., et al., *Mitochondrial trifunctional protein deficiency in human cultured fibroblasts: effects of bezafibrate.* J Inherit Metab Dis, 2016. **39**(1): p. 47-58.
82. Orngreen, M.C., et al., *Bezafibrate in skeletal muscle fatty acid oxidation disorders: a randomized clinical trial.* Neurology, 2014.
83. Blanchard, P.G., et al., *PPARgamma is a major regulator of branched-chain amino acid blood levels and catabolism in white and brown adipose tissues.* Metabolism, 2018. **89**: p. 27-38.
84. Fabie, N.A.V., K.B. Pappas, and G.L. Feldman, *The Current State of Newborn Screening in the United States.* Pediatr Clin North Am, 2019. **66**(2): p. 369-386.
85. Fingerhut, R. and B. Olgemoller, *Newborn screening for inborn errors of metabolism and endocrinopathies: an update.* Anal Bioanal Chem, 2009. **393**(5): p. 1481-97.
86. Therrell, B.L., Jr., et al., *Inborn errors of metabolism identified via newborn screening: Ten-year incidence data and costs of nutritional interventions for research agenda planning.* Mol Genet Metab, 2014. **113**(1-2): p. 14-26.
87. Regier, D.S. and C.L. Greene, *Phenylalanine Hydroxylase Deficiency*, in *GeneReviews((R))*, M.P. Adam, et al., Editors. 1993: Seattle (WA).
88. Bickel, H., J. Gerrard, and E.M. Hickmans, *Influence of phenylalanine intake on phenylketonuria.* Lancet, 1953. **265**(6790): p. 812-3.
89. Blau, N., F.J. van Spronsen, and H.L. Levy, *Phenylketonuria.* Lancet, 2010. **376**(9750): p. 1417-27.
90. Levy, H.L., *Robert Guthrie and the Trials and Tribulations of Newborn Screening.* Int J Neonatal Screen, 2021. **7**(1).
91. Pitt, J.J., *Newborn screening.* Clin Biochem Rev, 2010. **31**(2): p. 57-68.

92. Narravula, A., et al., *Variants of uncertain significance in newborn screening disorders: implications for large-scale genomic sequencing.* Genet Med, 2017. **19**(1): p. 77-82.
93. Richards, S., et al., *Standards and guidelines for the interpretation of sequence variants: a joint consensus recommendation of the American College of Medical Genetics and Genomics and the Association for Molecular Pathology.* Genet Med, 2015. **17**(5): p. 405-24.
94. Wilcken, B., *Medicine. Newborn screening: gaps in the evidence.* Science, 2013. **342**(6155): p. 197-8.
95. Sherry, S.T., M. Ward, and K. Sirotkin, *dbSNP-database for single nucleotide polymorphisms and other classes of minor genetic variation.* Genome Res, 1999. **9**(8): p. 677-9.
96. Sherry, S.T., et al., *dbSNP: the NCBI database of genetic variation.* Nucleic Acids Res, 2001. **29**(1): p. 308-11.
97. Maglott, D., et al., *Entrez Gene: gene-centered information at NCBI.* Nucleic Acids Res, 2011. **39**(Database issue): p. D52-7.
98. Maglott, D., et al., *Entrez Gene: gene-centered information at NCBI.* Nucleic Acids Res, 2005. **33**(Database issue): p. D54-8.
99. Kent, W.J., et al., *The human genome browser at UCSC.* Genome Res, 2002. **12**(6): p. 996-1006.
100. Lee, C.M., et al., *UCSC Genome Browser enters 20th year.* Nucleic Acids Res, 2020. **48**(D1): p. D756-D761.
101. Lee, B.T., et al., *The UCSC Genome Browser database: 2022 update.* Nucleic Acids Res, 2022. **50**(D1): p. D1115-D1122.
102. Landrum, M.J., et al., *ClinVar: public archive of relationships among sequence variation and human phenotype.* Nucleic Acids Res, 2014. **42**(Database issue): p. D980-5.
103. Landrum, M.J., et al., *ClinVar: improving access to variant interpretations and supporting evidence.* Nucleic Acids Res, 2018. **46**(D1): p. D1062-D1067.
104. Landrum, M.J., et al., *ClinVar: improvements to accessing data.* Nucleic Acids Res, 2020. **48**(D1): p. D835-D844.
105. Ran, F.A., et al., *Genome engineering using the CRISPR-Cas9 system.* Nat Protoc, 2013. **8**(11): p. 2281-2308.
106. Yoshimi, K., et al., *ssODN-mediated knock-in with CRISPR-Cas for large genomic regions in zygotes.* Nat Commun, 2016. **7**: p. 10431.
107. Ukai, H., H. Kiyonari, and H.R. Ueda, *Production of knock-in mice in a single generation from embryonic stem cells.* Nat Protoc, 2017. **12**(12): p. 2513-2530.
108. Agana, M., et al., *Common metabolic disorder (inborn errors of metabolism) concerns in primary care practice.* Ann Transl Med, 2018. **6**(24): p. 469.
109. Villani, G.R., et al., *"Classical organic acidurias": diagnosis and pathogenesis.* Clin Exp Med, 2017. **17**(3): p. 305-323.
110. Wanders, R.J., et al., *Disorders of mitochondrial fatty acyl-CoA beta-oxidation.* J Inherit Metab Dis, 1999. **22**(4): p. 442-87.
111. Grunert, S.C., et al., *Clinical and neurocognitive outcome in symptomatic isovaleric acidemia.* Orphanet J Rare Dis, 2012. **7**: p. 9.
112. Berry, G.T., M. Yudkoff, and S. Segal, *Isovaleric acidemia: medical and neurodevelopmental effects of long-term therapy.* J Pediatr, 1988. **113**(1 Pt 1): p. 58-64.

113. Chinen, Y., et al., *Isovaleric acidemia: Therapeutic response to supplementation with glycine, l-carnitine, or both in combination and a 10-year follow-up case study.* Mol Genet Metab Rep, 2017. **11**: p. 2-5.
114. Mayatepek, E., T.W. Kurczynski, and C.L. Hoppel, *Long-term L-carnitine treatment in isovaleric acidemia.* Pediatr Neurol, 1991. **7**(2): p. 137-40.
115. Roe, C.R., et al., *L-carnitine therapy in isovaleric acidemia.* J Clin Invest, 1984. **74**(6): p. 2290-5.
116. Concordet, J.P. and M. Haeussler, *CRISPOR: intuitive guide selection for CRISPR/Cas9 genome editing experiments and screens.* Nucleic Acids Res, 2018. **46**(W1): p. W242-W245.
117. Frerman, F.E. and S.I. Goodman, *Fluorometric assay of acyl-CoA dehydrogenases in normal and mutant human fibroblasts.* Biochem Med, 1985. **33**(1): p. 38-44.
118. Dube, S., J. Qin, and R. Ramakrishnan, *Mathematical analysis of copy number variation in a DNA sample using digital PCR on a nanofluidic device.* PLoS One, 2008. **3**(8): p. e2876.
119. Toogood, H.S., et al., *Extensive domain motion and electron transfer in the human electron transferring flavoprotein.medium chain Acyl-CoA dehydrogenase complex.* J Biol Chem, 2004. **279**(31): p. 32904-12.
120. Parimoo, B. and K. Tanaka, *Structural organization of the human isovaleryl-CoA dehydrogenase gene.* Genomics, 1993. **15**(3): p. 582-90.
121. Matsubara, Y., et al., *Molecular cloning and nucleotide sequence of cDNAs encoding the precursors of rat long chain acyl-coenzyme A, short chain acyl-coenzyme A, and isovaleryl-coenzyme A dehydrogenases. Sequence homology of four enzymes of the acyl-CoA dehydrogenase family.* J Biol Chem, 1989. **264**(27): p. 16321-31.
122. Dickinson, M.E., et al., *High-throughput discovery of novel developmental phenotypes.* Nature, 2016. **537**(7621): p. 508-514.
123. Kraft, K., et al., *Deletions, Inversions, Duplications: Engineering of Structural Variants using CRISPR/Cas in Mice.* Cell Rep, 2015. **10**(5): p. 833-839.
124. Bylund, L., et al., *Analysis of the cytogenetic stability of the human embryonal kidney cell line 293 by cytogenetic and STR profiling approaches.* Cytogenet Genome Res, 2004. **106**(1): p. 28-32.
125. Lin, Y.C., et al., *Genome dynamics of the human embryonic kidney 293 lineage in response to cell biology manipulations.* Nat Commun, 2014. **5**: p. 4767.
126. Mohsen, A.W., B. Navarette, and J. Vockley, *Identification of Caenorhabditis elegans isovaleryl-CoA dehydrogenase and structural comparison with other acyl-CoA dehydrogenases.* Mol Genet Metab, 2001. **73**(2): p. 126-37.
127. Kormanik, K., *Identification and characterization of the biochemical and physiological functions of acyl-coa dehydrogenase 10*, in *Human Genetics*. 2014, University of Pittsburgh: d-scholarship.pitt.edu. p. 376.
128. Schiff, M., et al., *Complex I assembly function and fatty acid oxidation enzyme activity of ACAD9 both contribute to disease severity in ACAD9 deficiency.* Hum Mol Genet, 2015. **24**(11): p. 3238-47.
129. Mohsen, A.W. and J. Vockley, *High-level expression of an altered cDNA encoding human isovaleryl-CoA dehydrogenase in Escherichia coli.* Gene, 1995. **160**(2): p. 263-7.

130. Pedersen, C.B., et al., *Misfolding, degradation, and aggregation of variant proteins. The molecular pathogenesis of short chain acyl-CoA dehydrogenase (SCAD) deficiency.* J Biol Chem, 2003. **278**(48): p. 47449-58.
131. Nguyen, T.V., et al., *Identification of isobutyryl-CoA dehydrogenase and its deficiency in humans.* Mol Genet Metab, 2002. **77**(1-2): p. 68-79.
132. Schowalter, D.B., D. Matern, and J. Vockley, *In vitro correction of medium chain acyl CoA dehydrogenase deficiency with a recombinant adenoviral vector.* Mol Genet Metab, 2005. **85**(2): p. 88-95.
133. Thomas, P. and T.G. Smart, *HEK293 cell line: a vehicle for the expression of recombinant proteins.* J Pharmacol Toxicol Methods, 2005. **51**(3): p. 187-200.
134. Zhang, Y., et al., *An acyl-CoA dehydrogenase microplate activity assay using recombinant porcine electron transfer flavoprotein.* Anal Biochem, 2019. **581**: p. 113332.
135. Andersen, R.M., *Revisiting the behavioral model and access to medical care: does it matter?* J Health Soc Behav, 1995. **36**(1): p. 1-10.
136. Spiekerkoetter, U., *Mitochondrial fatty acid oxidation disorders: clinical presentation of long-chain fatty acid oxidation defects before and after newborn screening.* J Inherit Metab Dis, 2010. **33**(5): p. 527-32.
137. Hoffmann, L., et al., *VLCAD enzyme activity determinations in newborns identified by screening: a valuable tool for risk assessment.* J Inherit Metab Dis, 2012. **35**(2): p. 269-77.
138. Wilcken, B., *Fatty acid oxidation disorders: outcome and long-term prognosis.* J Inherit Metab Dis, 2010. **33**(5): p. 501-6.
139. D'Annibale, O.M., et al., *Characterization of variants of uncertain significance in isovaleryl-CoA dehydrogenase identified through newborn screening: An approach for faster analysis.* Mol Genet Metab, 2021.
140. Livak, K.J. and T.D. Schmittgen, *Analysis of relative gene expression data using real-time quantitative PCR and the 2(-Delta Delta C(T)) Method.* Methods, 2001. **25**(4): p. 402-8.
141. Wanders, R.J., et al., *2,6-Dimethylheptanoyl-CoA is a specific substrate for long-chain acyl-CoA dehydrogenase (LCAD): evidence for a major role of LCAD in branched-chain fatty acid oxidation.* Biochim Biophys Acta, 1998. **1393**(1): p. 35-40.
142. Izai, K., et al., *Novel fatty acid beta-oxidation enzymes in rat liver mitochondria. I. Purification and properties of very-long-chain acyl-coenzyme A dehydrogenase.* J Biol Chem, 1992. **267**(2): p. 1027-33.
143. Chegary, M., et al., *Mitochondrial long chain fatty acid beta-oxidation in man and mouse.* Biochim Biophys Acta, 2009. **1791**(8): p. 806-15.
144. Vockley, J., *Long-chain fatty acid oxidation disorders and current management strategies.* Am J Manag Care, 2020. **26**(7 Suppl): p. S147-S154.
145. Fedorova, L.V., et al., *Peroxisome proliferator-activated receptor delta agonist, HPP593, prevents renal necrosis under chronic ischemia.* PLoS One, 2013. **8**(5): p. e64436.
146. Yamada, K., et al., *Open-label clinical trial of bezafibrate treatment in patients with fatty acid oxidation disorders in Japan.* Mol Genet Metab Rep, 2018. **15**: p. 55-63.
147. Shiraishi, H., et al., *Open-label clinical trial of bezafibrate treatment in patients with fatty acid oxidation disorders in Japan; 2nd report QOL survey.* Mol Genet Metab Rep, 2019. **20**: p. 100496.
148. Wang, X. and B. Seed, *A PCR primer bank for quantitative gene expression analysis.* Nucleic Acids Res, 2003. **31**(24): p. e154.

149. Spandidos, A., et al., *A comprehensive collection of experimentally validated primers for Polymerase Chain Reaction quantitation of murine transcript abundance.* BMC Genomics, 2008. **9**: p. 633.
150. Wang, X., et al., *PrimerBank: a PCR primer database for quantitative gene expression analysis, 2012 update.* Nucleic Acids Res, 2012. **40**(Database issue): p. D1144-9.
151. Schneider, C.A., W.S. Rasband, and K.W. Eliceiri, *NIH Image to ImageJ: 25 years of image analysis.* Nat Methods, 2012. **9**(7): p. 671-5.
152. Leipnitz, G., et al., *Evaluation of mitochondrial bioenergetics, dynamics, endoplasmic reticulum-mitochondria crosstalk, and reactive oxygen species in fibroblasts from patients with complex I deficiency.* Sci Rep, 2018. **8**(1): p. 1165.
153. Watkins, P.A., et al., *Peroxisomal fatty acid beta-oxidation in HepG2 cells.* Arch Biochem Biophys, 1991. **289**(2): p. 329-36.
154. Okun, J.G., et al., *A method for quantitative acylcarnitine profiling in human skin fibroblasts using unlabelled palmitic acid: diagnosis of fatty acid oxidation disorders and differentiation between biochemical phenotypes of MCAD deficiency.* Biochim Biophys Acta, 2002. **1584**(2-3): p. 91-8.
155. Shen, J.J., et al., *Acylcarnitines in fibroblasts of patients with long-chain 3-hydroxyacyl-CoA dehydrogenase deficiency and other fatty acid oxidation disorders.* J Inherit Metab Dis, 2000. **23**(1): p. 27-44.
156. Smith, E.H. and D. Matern, *Acylcarnitine analysis by tandem mass spectrometry.* Curr Protoc Hum Genet, 2010. **Chapter 17**: p. Unit 17 8 1-20.
157. Fang, L., et al., *PPARgene: A Database of Experimentally Verified and Computationally Predicted PPAR Target Genes.* PPAR Res, 2016. **2016**: p. 6042162.
158. Diekman, E.F., et al., *Fatty acid oxidation flux predicts the clinical severity of VLCAD deficiency.* Genet Med, 2015. **17**(12): p. 989-94.
159. Gobin-Limballe, S., et al., *Compared effects of missense mutations in Very-Long-Chain Acyl-CoA Dehydrogenase deficiency: Combined analysis by structural, functional and pharmacological approaches.* Biochim Biophys Acta, 2010. **1802**(5): p. 478-84.
160. Gillingham, M.B., et al., *Metabolic control during exercise with and without medium-chain triglycerides (MCT) in children with long-chain 3-hydroxy acyl-CoA dehydrogenase (LCHAD) or trifunctional protein (TFP) deficiency.* Mol Genet Metab, 2006. **89**(1-2): p. 58-63.
161. Pervaiz, M.A., et al., *MCT oil-based diet reverses hypertrophic cardiomyopathy in a patient with very long chain acyl-coA dehydrogenase deficiency.* Indian J Hum Genet, 2011. **17**(1): p. 29-32.
162. Keeler, A.M., et al., *Long-term correction of very long-chain acyl-coA dehydrogenase deficiency in mice using AAV9 gene therapy.* Mol Ther, 2012. **20**(6): p. 1131-8.
163. Calleri, E., et al., *Resveratrol and its metabolites bind to PPARs.* Chembiochem, 2014. **15**(8): p. 1154-1160.
164. Storgaard, J.H., et al., *No effect of resveratrol on fatty acid oxidation or exercise capacity in patients with fatty acid oxidation disorders: a randomized clinical cross-over trial.* J Inherit Metab Dis, 2022.
165. Aoyama, T., et al., *A novel disease with deficiency of mitochondrial very-long-chain acyl-CoA dehydrogenase.* Biochem Biophys Res Commun, 1993. **191**(3): p. 1369-72.

166. Miller, M.J., et al., *Recurrent ACADVL molecular findings in individuals with a positive newborn screen for very long chain acyl-coA dehydrogenase (VLCAD) deficiency in the United States.* Mol Genet Metab, 2015. **116**(3): p. 139-45.
167. Cox, K.B., et al., *Gestational, pathologic and biochemical differences between very long-chain acyl-CoA dehydrogenase deficiency and long-chain acyl-CoA dehydrogenase deficiency in the mouse.* Hum Mol Genet, 2001. **10**(19): p. 2069-77.
168. Cox, K.B., et al., *Cardiac hypertrophy in mice with long-chain acyl-CoA dehydrogenase or very long-chain acyl-CoA dehydrogenase deficiency.* Lab Invest, 2009. **89**(12): p. 1348-54.
169. Rosano, G.L. and E.A. Ceccarelli, *Recombinant protein expression in Escherichia coli: advances and challenges.* Front Microbiol, 2014. **5**: p. 172.
170. Baneyx, F., *Recombinant protein expression in Escherichia coli.* Curr Opin Biotechnol, 1999. **10**(5): p. 411-21.
171. Jager, V.B., Konrad; Schirrmann, Thomas, *Transient Recombinant Protein Expression in Mammalian Cells*, in *Animal Cell Culture*. 2014, Springer, Cham: Cell Engineering. p. 27-64.
172. Andersen, D.C. and L. Krummen, *Recombinant protein expression for therapeutic applications.* Curr Opin Biotechnol, 2002. **13**(2): p. 117-23.
173. Assenberg, R., et al., *Advances in recombinant protein expression for use in pharmaceutical research.* Curr Opin Struct Biol, 2013. **23**(3): p. 393-402.
174. Graham, F.L., et al., *Characteristics of a human cell line transformed by DNA from human adenovirus type 5.* J Gen Virol, 1977. **36**(1): p. 59-74.
175. Rio, D.C., S.G. Clark, and R. Tjian, *A mammalian host-vector system that regulates expression and amplification of transfected genes by temperature induction.* Science, 1985. **227**(4682): p. 23-8.
176. DuBridge, R.B., et al., *Analysis of mutation in human cells by using an Epstein-Barr virus shuttle system.* Mol Cell Biol, 1987. **7**(1): p. 379-87.
177. Bertrand, C., et al., *Purification of electron transfer flavoprotein from pig liver mitochondria and its application to the diagnosis of deficiencies of acyl-CoA dehydrogenases in human fibroblasts.* Clin Chim Acta, 1992. **210**(1-2): p. 75-91.
178. Arnold, G.L., et al., *A Delphi clinical practice protocol for the management of very long chain acyl-CoA dehydrogenase deficiency.* Mol Genet Metab, 2009. **96**(3): p. 85-90.
179. Watanabe, H., et al., *Molecular basis of very long chain acyl-CoA dehydrogenase deficiency in three Israeli patients: identification of a complex mutant allele with P65L and K247Q mutations, the former being an exonic mutation causing exon 3 skipping.* Hum Mutat, 2000. **15**(5): p. 430-8.